Photochemical Generation of a Viable Oxidizing Agent and Aplication to Dye Photobleaching

Sulafa Jamal Mohammed Nassar

A PhD Thesis submitted to:

Newcastle University – School of Natural and Environmental Sciences (Chemistry)

Molecular Photonics Laboratory

January 2020

Abstract

Molecular photochemistry is a well-established branch of science that owes its origins to the pioneering studies of Alexander Schönberg in Egypt during the 1940's and 50's. The main advantage of photochemistry relies on the use of sunlight to drive "difficult" reactions, the most important being the production of molecular oxygen and chemical fuel by way of natural photosynthesis. While photovoltaic cells and systems based on inorganic semiconductors have developed enormously during the past few decades, there have been few comparable advances in molecular photochemistry. This is despite the ready availability of powerful spectroscopic and computational tools. Indeed, the mantle of "artificial photosynthesis" has been transferred from chlorophyll derivatives to silicon and its allies. In this thesis, we explore the concept of developing simple photochemical means to drive oxidative processes that might be both practical and cost-effective. Several systems are considered and subjected to experimental study.

Chapter 1 presents a general introduction to the field and illustrates both the potential and the frustration offered by molecular photochemistry. Typical excited state reactions are described in terms of simple molecular orbital diagrams. The discussion is directed towards dye photobleaching; a topic of considerable contemporary significance given the recent advances in single-molecule fluorescence and super-resolution microscopy. Ways to protect dyes against the deleterious effects of exposure to laser light are reviewed and common reactive intermediates are identified. The introduction provides background information for the subsequent research work. Experimental protocols for monitoring the course of dye photofading are introduced. This chapter is followed by an account of the experimental practices followed during our work. Chapter 2 includes a description of the methods used for data analysis.

Chapter 3 recognises the need to generate a relatively stable intermediate oxidant if a viable photobleaching strategy is to be devised. Most of the intermediates generated under illumination survive for periods of a few microseconds or less and therefore require high concentrations of substrate to ensure chemical trapping before deactivation. The approach suggested involves the photochemical production of an organic hydroperoxide that is sufficiently stable to be characterised by NMR spectroscopy. The bleaching capability of this species is assessed by

specific reference to the decolouration of indigo. The latter is a popular dye that displays exceptional stability towards sunlight.

Chapter 4 continues this theme by examining the photobleaching of methylene blue (MB) in water. This cationic dye is known to bleach quickly on exposure to visible light and we have studied the mechanism and efficacy of the bleaching reaction. The importance of light intensity and dissolved oxygen are stressed. The key discovery made here relates to the ability of high concentrations of urea to inhibit photochemical bleaching of MB. This is a surprising result that offers promise for providing protection for oxidative damage of certain dyes. The mechanism by which urea operates has been deduced by way of kinetic measurements.

Chapter 5 looks at the catalysed bleaching of a novel strapped boron dipyrromethene (BODIPY) derivative. This dye represents a new type of BODIPY dye that displays circularly polarised luminescence. Direct and catalysed photobleaching processes are compared and the importance of dissolved oxygen is assessed. The dye has a highly strained geometry imposed by the straps attached to the boron atom. Oxidation can help relieve this steric strain.

Chapter 6 takes a different perspective and enquires if chlorine dioxide can be generated by photochemical protocols. Chlorine dioxide is an important bleach but is not in common use because it is difficult to manufacture in bulk and has limited stability on storage. In principle, it should be possible to generate chlorine dioxide by photochemical means. This could provide access to a powerful antiseptic reagent in remote locations using sunlight as the only energy input. Several putative ways to produce chlorine dioxide are considered and an analytical protocol is devised for quantitative determination. It is concluded that a practical set-up could be engineered for the in-situ production of chlorine dioxide in aqueous solution.

KEY WORDS: photochemistry: oxidative stress: organic dyes: decolouration: bleaching kinetics

Acknowledgements

In the Name of Allah, the Most Gracious, the most Merciful

I would like to express my deepest and most sincere gratitude to Allah (God) for giving me the strength, patience and support to do this work.

I would like to express my deep appreciation and gratitude to my supervisor Professor Anthony Harriman for his constant support, endless advice and assistance that allowed me to successfully finish my PhD research study. I truly appreciate his understanding, tireless patience, and motivation for his assistance in writing this thesis. I would like to thank Dr. Corinne Wills for her assistance in NMR spectroscopy.

My deepest thanks to the Umm Al-Qura University as represented via Saudi Embassy for providing scholarship funds and the financial support. Many thanks are also to the Newcastle University for providing access to the necessary facilities.

My unspeakable gratefulness and appreciation to my family especially my beloved husband Malik Mirza for his unflinching support and a lot of his patience during all my PhD studies. I truly deeply indebted for him and all words of thanks do not fulfill his right. I would like to give a special thanks to my sweet sons for their support and patience. I must also thank all my great family especially my loved mother for her extraordinary care, love and constant prayers for me.

Finally, I am thankful for the help from the Molecular Photonics Laboratory members especially Roza and Hatun for their assistance and encouragement during my research.

List of publications

Some results chapters are associated with a publication in a scientific journal. Full papers are attached in the appendix.

Chapter 3: S. J. M. Nassar, D. Sirbu, A. Harriman, **2019**. Photocatalyzed Degradation of Indigo in Solution via *in-situ* Generation of an Organic Hydroperoxide. *Photochemical & Photobiological Sciences*, 18, pp. 2875-2883.

Chapter 4: S. J. M. Nassar, C. Wills, A. Harriman, **2019**. Inhibition of the Photobleaching of Methylene Blue by Association with Urea. *ChemPhotoChem*, 3, pp. 1042–1049.

Contents

Chapter 1.

Introduction

A fading rose …

1.1 Background

Photochemistry can be defined as the study of chemical processes that are initiated only by the absorption of light energy delivered in the form of a photon. Although the subject is mature and has witnessed many changes in direction, the main contemporary goal of photochemistry is the capture and storage of sunlight as chemical potential. In this respect, it should be emphasized that photochemistry is able to break and form chemical bonds, to re-arrange molecular structures and to re-locate excitation energy. The first law of photochemistry, known as the Grotthuss- Draper law,[1-4] states that light must be absorbed by a chromophore in order for a photochemical reaction to occur. This is a fundamental rule but it carries several key concepts: For example, the law introduces selectivity in as much as one compound in a complex mixture can be excited by monochromatic light at the exclusion of all other components in the mixture. This is a powerful feature that cannot be achieved in thermal chemistry. A second outcome from the law is that the rate of a photochemical reaction can be controlled by the rate of up take of photons of appropriate energy. The latter can be modulated by changing the incident light intensity and/or varying the concentration of the chromophore. When the G-D law was first formulated, little concern had been shown to two-photon absorption but this provides a further means for obtaining exquisite levels of sensitivity. The application of powerful microscopes equipped with high-intensity lasers provides a way to couple optical selectivity with spatial resolution.

A major impetus for studying photochemistry stems from the realization that we might learn more about important features of photobiology.[5] Photochemistry has developed numerous elaborate spectroscopic tools that are applicable to understanding the mechanisms inherent to natural processes, such as vision and photosynthesis. Recent discoveries in the field of green fluorescent proteins have stimulated this interest and could lead to important advances in gene therapy and imaging science.[6] While photovoltaics lies outside the normal realm of what might pass as photochemistry, the same is not true for organic light emitting diodes (OLEDs) and brings physics into the same equation. Indeed, molecular photophysics lies at the heart of modern photochemistry and few researchers attempt to separate the chemistry component from the underlying physics. The days of simply exposing a solution of a known substance to sunlight by leaving the flask on the laboratory roof have long been replaced by the need to conduct mechanistic and kinetic studies. There is, however, still a measure of excitement in watching the

colour change under direct sunlight. This brings us to the unfortunate side of photochemistry. Exposure to sunlight, especially near- UV light, causes many molecules to undergo a marked change in structure, shape and/or composition. Chemical bonds can be broken, or indeed formed, and geometries can re-arrange. Strongly fluorescent materials can become "black holes" simply by leaving in room light. Early photographs were brought about by photochemical reactions, usually in the form of electron- transfer reactions, and the concept of photopolymerisation became important in the 1970's. The latter reactions became popular in dentistry and for activating the drying of emulsion paint.[7,8] The same reactions needed to effect solar fuel formation,[9] under different circumstances, cause damage and set-up chain reactions leading to cancer. Even here, the troublesome dichotomy continues since these very same reactions are nowadays used to eradicate cancerous materials by way of photodynamic therapy. A disturbing feature of photochemistry is that industry makes little real use of the subject and, apart from photography and the manufacture of dyestuffs, there are no major industrial processes that are driven exclusively by light.

The introduction of new dyes, a cause of tremendous excitement to early impressionist painters, has revolutionized our lifestyle. New colours brighten our homes and clothes and allow both young and old to express themselves through original hair dyes. Fluorescence greatly amplifies the range of colours by adding depth and new levels of perception. Most banknotes now contain luminescent patches to defeat counterfeiters and secret writing is no longer hidden from the eye. The so-called "black light", better called UV-light, used in early forensics is now allied to fluorescent labels.[10] Most of these new materials are organic, popular opinion being that metal-based chemicals are highly toxic, and susceptible to photochemical degradation. This realization is both good and bad. The latter arises because the colour of expensive items, like a motorcar, should not fade within the lifetime of the object itself. It's fine for the Forth Bridge to be continually undergoing painting but no-one wants to keep painting their car. There is also the worry about famous paintings that slowly lose their original colour during continuous exhibitions. The good aspect of photofading is that it represents a means to replenish and restore items. It is a way to remove unwanted materials, such as plastics, and to clean water supplies.[11-13] We could, if we really wanted, use photochemistry to remove the ugly stains of chewing gum that litter our pavements.

The systematic study of the photochemical fading of dyes is not popular and has not attracted great attention. Many advanced materials have been obtained by slow engineering of the product to by-pass the fading. As an example, when questioned about the stability of his OLEDs Ifor Samuel (University of St Andrews) replied that they had a projected operational time of 40,000 hours! There are fewer attempts made to understand the underlying chemistry and kinetics as a means to control or eradicate the bleaching process. This thesis is an attempt to move into this little explored region and to look at ways to promote or hinder photobleaching of substrates. Our work is restricted to organic materials and we make no attempt to cover the complementary research involving semiconductor photocatalysts.

1.2 Autumn leaves

The North East of England has some fantastic countryside with open spaces and woodlands. It is noticeable that the leaves of the trees are a beautiful green colour in spring and (what passes for) summer. With the approach of autumn, the temperature starts to fall and the leaves can no longer synthesize chlorophyll. It is the chlorophylls, there being several similar but slightly disparate molecular forms of this essential compound, which provides the characteristic green colour. During the spring, chlorophyll is constantly degrading and being replaced but, with the colder weather, the replacement is slowly switched off. The other main pigments in the leaf are carotenoids and flavonoids and these degrade more slowly than the fragile chlorophyll molecules. The latter contain a central magnesium cation which is easily displaced from the macrocycle, causing the colour to change from green to red. Thus, the distinctive reds and browns seen in the autumn leaves arise because of the triggered disappearance of the chlorophylls. With the loss of chlorophyll, the leaf can no longer synthesize sugars and so the whole tree shuts down for the winter. Once the temperature begins to rise and days become longer, the process starts again and the new chlorophyll begins to produce sugar. The tree continues its growth.

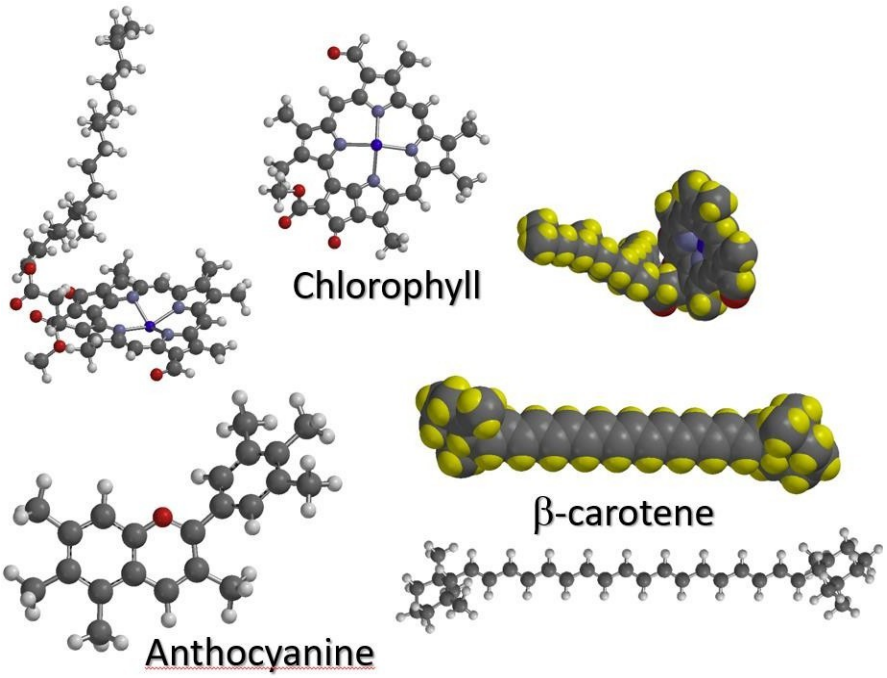

Figure 1: Representative chemical formulae for some of the most important ingredients of plant photosynthesis. Chlorophyll is shown in space-filling form and as a ball-and-stick model, with the macrocycle being shown separately. Note that the central magnesium cation does not fit properly inside the ring and is easily displaced. Also shown is β-carotene in both space-fill and ball-and-stick modes. The final structure is one form of anthocyanine.

Carotenoids also contribute orange colours. Indeed, β-carotene is an essential component of green plants and is present in high concentration.[14] This compound absorbs green and blue light but reflects red and yellow light, thereby causing its orange appearance. It is a well-known anti-oxidant.[15-25] Although the carotenoids degrade under sunlight, they do so at a much slower rate than chlorophyll. Most fallen leaves still contain measurable amounts of carotenes. An important feature of β-carotene is that the triplet-excited state is formed only in very low yield[26,27] while the triplet energy is very low. In fact, the triplet energy is below that of singlet molecular oxygen. In contrast, isolated chlorophyll forms a long-lived triplet excited state that can sensitize formation of the highly destructive singlet oxygen. Perhaps this difference is an important clue in the natural degradation process. What is important is the realization that Nature makes no attempt to stop the degradation and instead uses the downtime to replenish the tree. The degraded materials are not lost but recycled. This is a lesson we have still not learned to put into practice in artificial systems. With the onset of autumn, the sugar concentration in the leaf begins to increase because

the tree is no longer growing. This excess sugar switches on the synthesis of anthocyanine. The latter is an important compound, the synthesis of which requires exposure to sunlight. Anthocyanins are members of the flavonoid class of pigments but they are present in the leaf only during autumn and winter. [28-30] It is believed they function as a sunscreen, allowing the tree to protect its leaves from light damage and extend the amount of time before they are shed. In terms of their contribution to the colour of autumn leaves, they provide vivid red, purple, and magenta shades. Most remarkably, the colour of the anthocyanines depends strongly on pH and is affected by the acidity of tree sap, thereby enhancing the range of hues. In spring, the sap rises bringing a change in acidity and anthocyanine production ceases. This is really subtle and impressive chemistry.

1.3 Key elements of natural photosynthesis

Natural photosynthesis has been a major influence on molecular photochemistry over the past half century and, in particular, there has been tremendous effort expended on duplicating parts of the natural process with purely artificial analogues. Research has focussed on the reaction centre complex, where light-induced electron transfer occurs between carefully sited redox- active reagents, and the ancillary light-harvesting unit, where light absorption is followed by rapid electronic energy transfer to the reaction centre.[31-33] This research has gone hand-in-hand with spectroscopic studies on segments of bacterial or green plant photosynthetic organisms.[34] The natural systems exhibit very complex photophysical behaviour which utilizes the three-dimensional structure of the living systems. Artificial analogues rely heavily on synthetic chemistry to produce elaborate models with reagents carefully positioned in order to optimize rates of light-induced energy and/or electron transfer reactions. We emphasize the complexity of these artificial systems by reference to two examples, one concerned with directed electronic energy transfer (a mimic for the light-harvesting network) and the other concerned with directed electron transfer (a mimic for the reaction centre complex).[35-40]

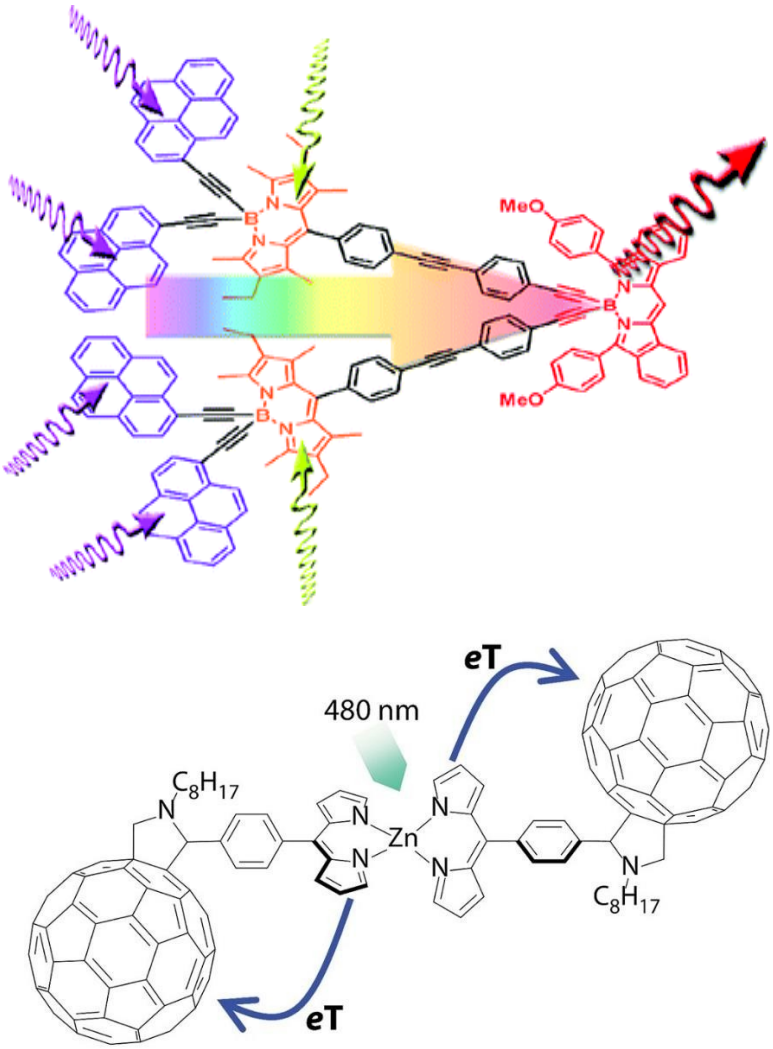

Figure 2: Examples of simple artificial molecular systems used as crude mimics for the natural process. The upper panel shows a complex molecular triad able to display vectorial electronic energy transfer along the molecular axis. See JACS 2009, 131, 13375 for details. The lower panel shows a molecular dyad used to study intramolecular electron transfer under illumination. See Org. Biol. Chem. 2004, 2, 1425 for details.

The general public recognizes that photosynthesis is the process by which plants and many types of bacteria use sunlight to convert carbon dioxide and water to sugar.[41,42] The resultant glucose can be converted into pyruvate which releases adenosine triphosphate (ATP) by cellular respiration. Oxygen is formed by green plants but not by bacteria. The overall process has inspired photochemists to seek artificial systems able to transform sunlight into chemical potential. The work has not been so successful and, in practical terms, has fallen well behind the photovoltaic

approach to energy conversion. The challenge of duplicating the photosynthetic machinery in the laboratory using molecular components has proved too difficult. However, renewed awareness about the problems caused by overproduction of carbon dioxide has re- ignited interest in molecular systems. Since the middle of the 18th century, the level of carbon dioxide in the atmosphere has been rising progressively due to largescale combustion of fossil fuels, cement production, and massive de-forestation.[43-46] Molecular photochemical systems capable of the reduction of carbon dioxide, used in conjunction with public awareness,[47,48] offer promise of controlling the output of carbon dioxide into the atmosphere. Here, we illustrate one such system.

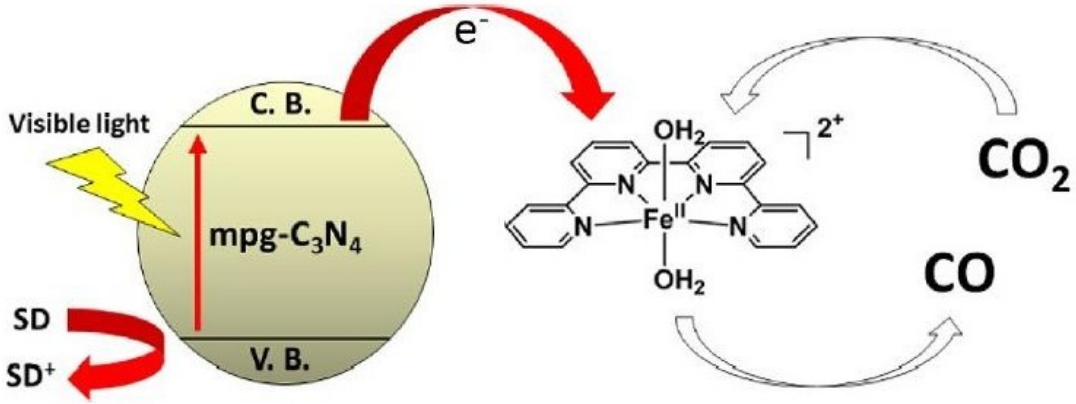

Figure 3: Simple photoredox system used to develop new catalysts able to reduce carbon dioxide to a useful product, in this case carbon monoxide. Photoreduction is performed at the expense of consuming an added sacrificial donor (i.e., triethanolamine). The sensitizer is carbon nitride particles.

One feature of natural photosynthesis should be highlighted here. This concerns the fact that plants and bacteria have evolved complex procedures for protection against long-term exposure to sunlight. All natural photosynthetic systems, and ancillary systems such as the photolyase enzyme, use light-harvesting antennae to increase the rate of photon delivery to the catalytic sites. The design of these photon collection units varies among the different species but they are all equipped with some means of self-repair. Non-photochemical quenching (NPQ) is a process whereby "excess" excitation energy reaching the oxygen-evolving unit is not used for

photochemistry,[49 -59] but is safely dissipated as local heat. There are numerous disparate types of NPQ used in plants and bacteria, often involving establishment of a pH gradient. Green plants tend to use carotenoids as anti-oxidants and deactivators of accidently formed triplet-excited states.[60] Under high photon densities, rapid energy migration around the light-harvesting network is accompanied by exciton-exciton annihiliation. This helps avoid problems with triplet formation or other deactivation pathways available to highly energetic species. Although annihilation loses excitation energy, the need to avoid triplet states is greater.

The molecular basis for NPQ is poorly understood, despite its significance. In plants and algae, NPQ occurs on different timescales and takes many forms. The most likely process that leads to rapid loss of excitation energy involves some type of conformational change that is activated under high light intensity. It is known that both zeaxanthin and relatively high pH are required for effective NPQ but exactly how this occurs is a mystery.[61-70] The main point, however, is that Nature has evolved an efficient mechanism by which to deal with high levels of excitation within the light-harvesting units. This mechanism switches the excitons from fuel production to heat so as to protect itself from whatever threat is perceived by the organism. While it is reasonable to add anti-oxidants and triplet quenchers to artificial photosystems, there have been no real attempts to include some type of NPQ. This remains for the future.

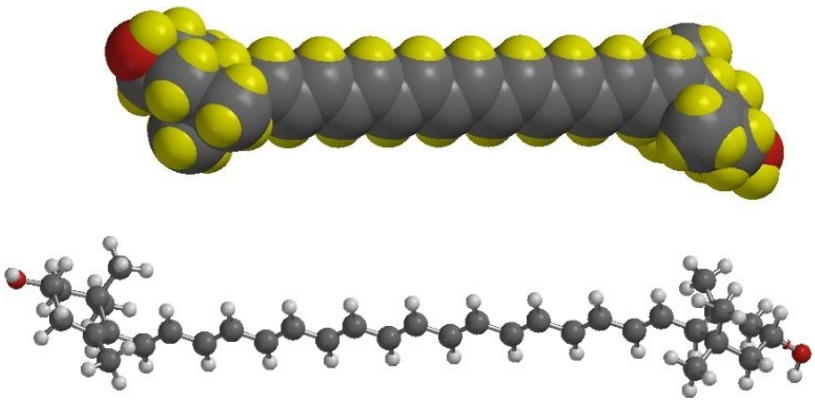

Figure 4: Molecular formula for zeaxanthin, shown as both space-filling mode and ball-and-stick. Note the close resemblance to β-carotene.

1.4 Photobleaching of dyes

For a long time, the photofading of dyes and pigments was merely a matter of inconvenience and was overcome by trial-and-error. Only light-fast dyes made it to the marketplace. Everything changed, however, with the introduction of single molecule spectroscopy and super-resolution microscopy. For such techniques, the photostability of fluorescent dyes used as labels and imaging agents[71-77] is of crucial importance for the statistical accuracy and ultimate resolution. These sophisticated instruments use high-power lasers for excitation purposes and consequently deliver an inordinately high rate of photons to the sample. Used in conjunction with scanning confocal microscopes, this leads to very high photon densities. Photostability of the fluorophore is now the most important factor in obtaining a reliable image. This realization has resulted in more detailed examination of the factors responsible for dye fading under high-power illumination. This has also resulted in the introduction of advanced experimental tools for monitoring loss of the fluorophore and both epi-illuminated microscopes with continuous wave laser excitation and fluorescence correlation spectroscopy are now commonly used for bleaching studies. A major problem with such studies concerns the low probability of photobleaching, which is in the order of 10^{-6}–10^{-7} for irradiances below 10^3 W/cm^2. Irradiances above this level can lead to increased rates of loss of the fluorophore which can only be described by photobleaching reactions from higher excited states.[78]

Although many details of fluorophore photobleaching remain unexplored, the most common route for chromophore loss involves reactions of the triplet-excited state of the dye. Upon photon absorption, the chromophore is promoted from the ground state (S_0) to the first singlet-excited state (S_1), from which it returns to S_0 through radiative (fluorescence) or nonradiative pathways (Figure 5). In most cases of interest, the fluorescence quantum yield is very high while radiationless return to the ground state is almost negligible. This would be the case for common dyes like the rhodamines and coumarins used extensively in single molecule spectroscopy.[79] In competition with fluorescence, S_1 can undergo intersystem crossing (ISC) to the first triplet-excited state (T_1). This involves loss of excitation energy but achieves a great improvement in excited-state lifetime. Typically, for the more popular dyes, fluorescence lifetimes are on the order of a few

nanoseconds while triplet lifetimes can be as high as a few milliseconds. Triplet energies, although inevitably lower than those of the corresponding excited-singlet state, remain in excess of about 1 eV, which is sufficient for initiating chemical reactions that ultimately lead to fluorophore bleaching. For example, T_1 can be quenched by molecular oxygen to produce the highly reactive species known as singlet molecular oxygen. This latter species, and other reactive oxygen species such as superoxide ions, is relatively long lived and can react with dye molecules to cause bleaching. Moreover, the long-lived T_1 state can enter into electron transfer reactions with substrates present in the reaction mixture. These might include thiols and amines that function as irreversible electron donors. Although triplet yields tend to be rather low for the majority of fluorophores used in super-resolution microscopy, most researchers opt for the singlet molecular oxygen route as being responsible for chromophore loss. We illustrate the course of reaction by way of Figure 5 given below.

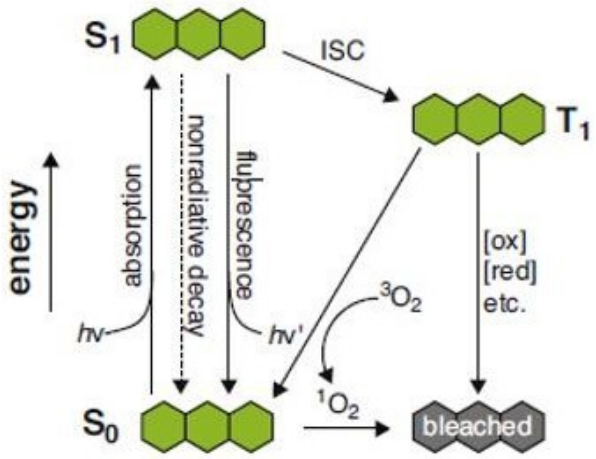

Figure 5: Example of the course of reaction by photobleaching as illustrated using anthracene. Intersystem crossing from the excited-singlet state populates the corresponding triplet-excited state in high yield. The latter reacts with molecular oxygen, by way of energy transfer, to form the highly reactive singlet molecular oxygen. This species reacts with ground state anthracene to form an endoperoxide, with subsequent loss of colour and fluorescence.

In order to follow the rate of photobleaching of an organic dye it is normal practice to record absorption spectra at various times during exposure to a suitable light source. This gives useful information with regard to the rate of loss of absorbance at any given wavelength and with respect to the rate of appearance of any coloured intermediates or products. A typical reaction

profile is illustrated below as Figure 6. Here, absorption spectra are recorded at various illumination times, allowing a plot of time vs absorbance at preferred wavelengths. From the latter plot, an idea of the reaction rate and order can be obtained by applying conventional kinetics protocols. It is important to search for any isosbestic points as these indicate product formation. The reaction can be repeated as a function of incident light intensity and after addition of certain reagents. These reagents are chosen on the basis of the expectation that they will trap certain intermediates, notably singlet molecular oxygen. Changes in light intensity or excitation wavelength might switch on new bleaching routes, leading to different reaction products (Figure 7).

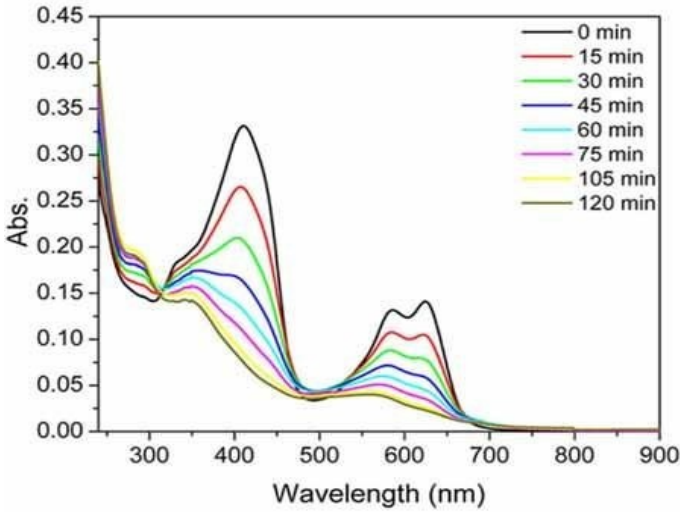

Figure 6: Example of an absorption spectrum recorded during the course of photobleaching of a dye in the presence of molecular oxygen. An isosbestic point is seen at ca. 310 nm. Spectra are recorded at regular intervals during the photoreaction.

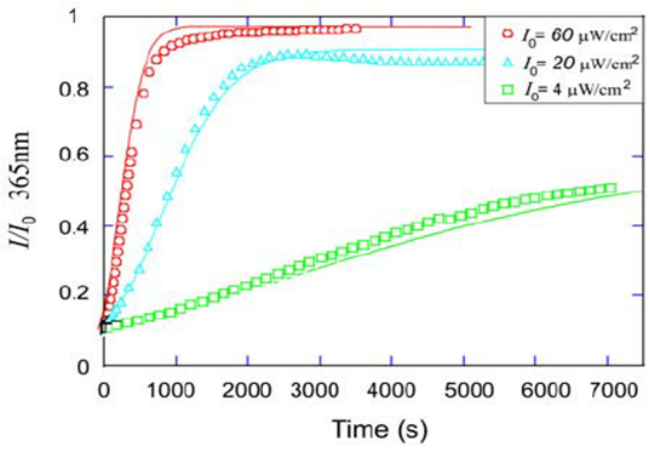

Figure 7: Kinetic profiles constructed for the photobleaching experiment with different incident light intensities.[80]

A superior way to obtain photobleaching rates is to monitor continuously at a suitable wavelength. This allows rapid collection of data concerning, for example, the effect of light intensity on the reaction rate. The advantage of this approach is that the data are more precise and allow better fitting to kinetic models. The kinetic method, however, does not help identify intermediates although, by careful selection of wavelength, it is possible to monitor the growth and subsequent loss of these transient species. This method is also suitable for the detection of autocatalysis, which occurs when one or more products promote bleaching of the chromophore. Photobleaching is especially vulnerable to the onset of autocatalysis since the initial reaction is slow and products enter the reaction mixture. With a mechanism based on singlet molecular oxygen, it is likely that organic peroxides or hydroperoxides accumulate during illumination. These reactive species might enter into the bleaching chemistry and thereby increase the rate of colour loss. For this reason, it is important to follow the reaction over long illumination times and not extrapolate to obtain reaction half-lives well beyond the exposure period.

Assuming photobleaching occurs exclusively by way of the lowest-energy triplet state it becomes feasible to minimize the effect by quenching the triplet with added reagents that catalyse radiationless decay to the ground state. Indeed, small-molecule triplet state quenchers, such as Trolox, 1,3,5,7-cyclooctatetraene (COT) and 4-nitrobenzyl alcohol have been added to the imaging media to improve levels of photostability.[81-85] However, for measureable effects these quenchers

need to be added at relatively high (e.g., mM) concentrations and, of course, it is necessary to remove oxygen from the system. The decreased oxygen pressure can be achieved by the presence of enzymatic scavenging enzymes and sealing the reaction vessel. In order to reduce the concentration of triplet quencher to a reasonable level, it has proved necessary to replace the bimolecular systems with intramolecular analogues. Here, the quencher has to be attached near to the chromophore such that only minimal diffusive motion is needed to bring the quencher into contact with the triplet state. This latter approach has been used now with several different sets of chromophore-quencher pairs and impressive levels of enhanced stability has been reported. For example, COT has been covalently linked to the cyanine dye Cy5 so as to produce a molecular dyad (Figure 8). Detailed photophysical measurements have established that the Cy5 dye transfers triplet excitation to the adjacent COT such that the triplet lifetime of the bio-label is shortened significantly, even in the presence of air. The excited singlet state energy of COT exceeds that of Cy5 so there is no corresponding quenching of the fluorescence. A pictorial representation of this system is to be found below (Figure 8).

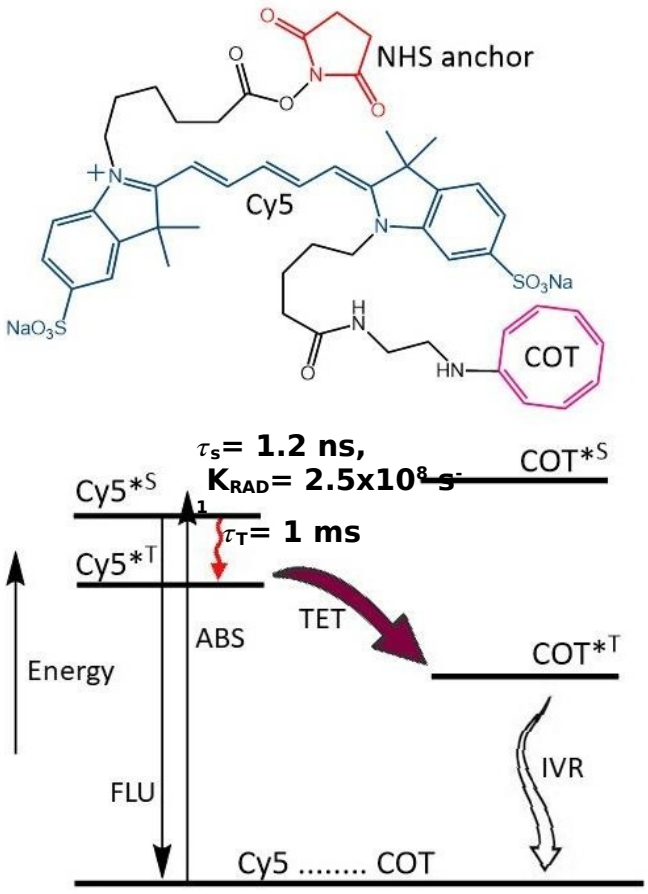

Figure 8. Molecular formula for the Cy5-COT dyad synthesized to provide extra protection against photobleaching. Below is given an energy-level diagram showing that stabilization is due to fast deactivation of the excited-triplet state via electronic energy transfer to COT. NHS is N-Hydroxysuccinimide, COT is 1,3,5,7-cyclooctatetraene, TET is triplet energy transfer and IVR is intramolecular vibration relaxation.

It is reasonable to ask if only the triplet-excited state is responsible for the photofading of dyes. Apart from the longer excited state lifetime and the capacity to sensitize singlet molecular oxygen formation, the triplet state has no advantage over the corresponding singlet-excited state in terms of being able to switch on the bleaching chemistry. In fact, the higher energy of the S_1 state could offset the longer lifetime of the T_1 state in certain cases. High light intensities could favour two-photon absorption to reach higher-lying excited states able to break bonds more easily than the relaxed states. Because probabilities of photobleaching are so low, it is simply not possible to identify a chromophore that cannot produce a triplet state in sufficient yield for this to be the

active species. As such, the triplet hypothesis persists even when there is no evidence for its involvement.

Recent years have seen tremendous advances in fluorescence imaging. It is now possible to generate high-quality images of small species within exposure times of a few seconds. The quality of the image depends on the software used to manipulate the experimental data and instrument makers are engaged in a race towards faster and more precise imaging protocols. One obvious way to speed up the process is to increase the incident laser flux and this adds further strain on the photostability of the dye. Recent advances in the development of bright and photostable fluorophores demonstrate that chemists are capable of devising sophisticated and clever ways to improve longevity of the emitters using their knowledge of molecular photophysics and advanced synthetic chemistry. However, it still remains that our understanding of the bleaching mechanisms is crude at best and most researchers simply blame the triplet sensitization of singlet oxygen as being the culprit. Anaerobic enzymes and weak electron donors are added to the matrix as a means to restrict triplet reactions and the so-called self-healing dyes are becoming popular.[86] It is only by conducting further investigations into the mechanistic and kinetic processes accompanying photobleaching that new strategies for enhancing performance will emerge.

Consideration of a typical Jablonski diagram indicates that obtaining mechanistic information is not so easy (Figure 9). We can do this with specific reference to the cyanine dye known universally as Cy5. Here, the fluorescence quantum yield in solution is about 0.3 and the excited-singlet lifetime is 1.2 ns. The radiative rate constant is therefore 2.5×10^8 s^{-1}. Light-induced isomerization occurs to form a geometrical isomer with a quantum yield of 0.3 so the rate constant for isomer formation is equal to the radiative rate constant. Intersystem crossing to the triplet state is very inefficient, with the triplet quantum yield being around 0.01 or less. The rate constant for intersystem crossing can now be established as being of the order of 8×10^6 s^{-1}. The triplet lifetime in the absence of molecular oxygen is around 1 ms and the lifetime of the photo-isomer is somewhat shorter at about 200 µs. The quantum yield for photobleaching of Cy5 is believed to be on the order of 10^{-6} for monophotonic illumination. This means that the rate constant for bleaching is about 10^3 s^{-1}.[87] In other words, for every million photons emitted as fluorescence, 10 molecules of dye are bleached. Experimental techniques are such that we can easily measure a

million photons emitted in unit time but there are no such techniques to chemically analyse 10 molecules.

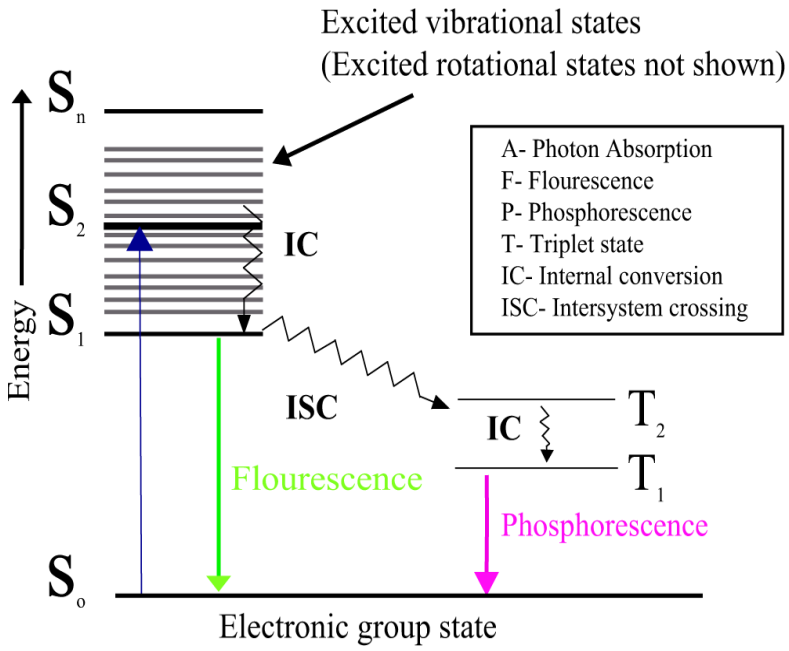

Figure 9: Modified Jablonski diagram to include photochemical bleaching of the chromophore. Note that singlet-state bleaching has to compete with fluorescence and intersystem crossing, both of which are usually fast. This is way bleaching is usually ascribed to the longer-lived triplet-excited state .[88]

1.5 Reversing the problem

It would be wrong to imagine that there is only a need to protect dyes against photobleaching and that there are no useful applications for dyes that bleach quickly. In fact, Woodford et al. have recently introduced a novel dye-based system that functions as a multi-detection dosimeter for sunlight.[89] This system uses a highly fluorescent symmetrical pyrrole-BF_2 dye embedded in plastic. During exposure to sunlight, the dye changes colour and new fluorescent species evolve. Because of the unique mixture of absorption and fluorescence profiles, this action meter can give very accurate exposure limits in terms of incident photons (Figure 10).

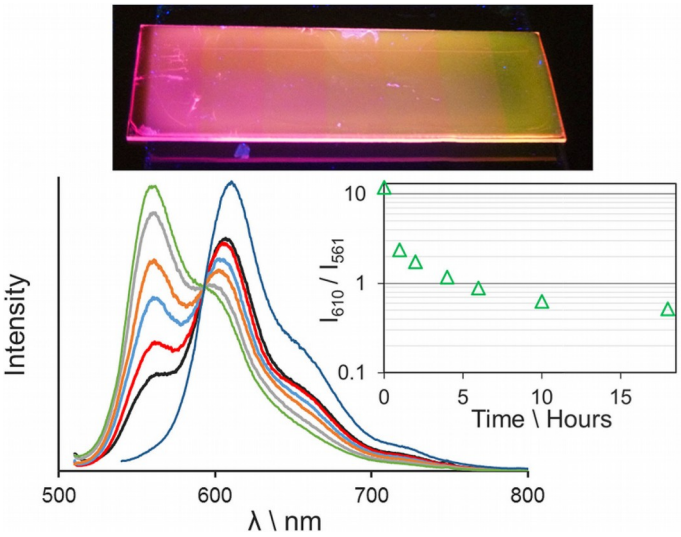

Figure 10. A thin film actinometer based on the BOPHY chromophore dispersed in PMMA. Portions of the film were exposed to sunlight for varying periods with zero illumination on the left and maximum exposure on the right. The fluorescence spectral profile is shown below the film as recorded for the different segments. The remaining panel shows the ratio of fluorescence intensities for the original sample and the exposed film. See ChemPhotoChem 2018, 2, 1046 for further details.[79]

A second useful application for dye fading involves the technique known universally as Fluorescence Recovery After Photobleaching (FRAP) which is used in biology to measure diffusion coefficients for dyes in complex media.[90 -99] The FRAP protocol involves preparing a sample with a low loading of a highly fluorescent dye immobilized in a somewhat viscous but not rigid medium.

The sample is exposed to a short burst of high-intensity light delivered from a monochromatic source, such as a high-power diode laser (Figure 11). The light beam causes rapid bleaching of a small fraction of the dye in a restricted sample volume. The sample is irradiated continuously with a weak LED that does not itself cause bleaching but promotes a tiny fraction of the dye into a fluorescent state. Fluorescence intensity is monitored in real-time with a suitable detector. As fresh dye molecules diffuse into the detection volume, there is partial recovery of the fluorescence, which is recorded and used to determine the diffusion coefficient (Figure 12). The FRAP technique has many important uses in biology and medicine, especially with lipid membranes and proteins.

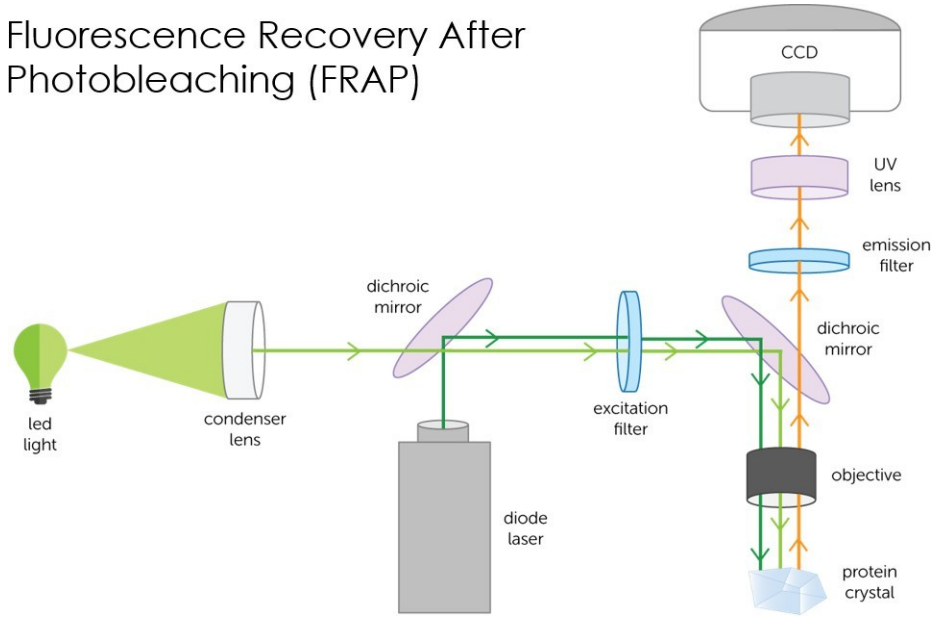

Figure 11: Experimental set-up used to measure diffusion coefficients via the FRAP technique.

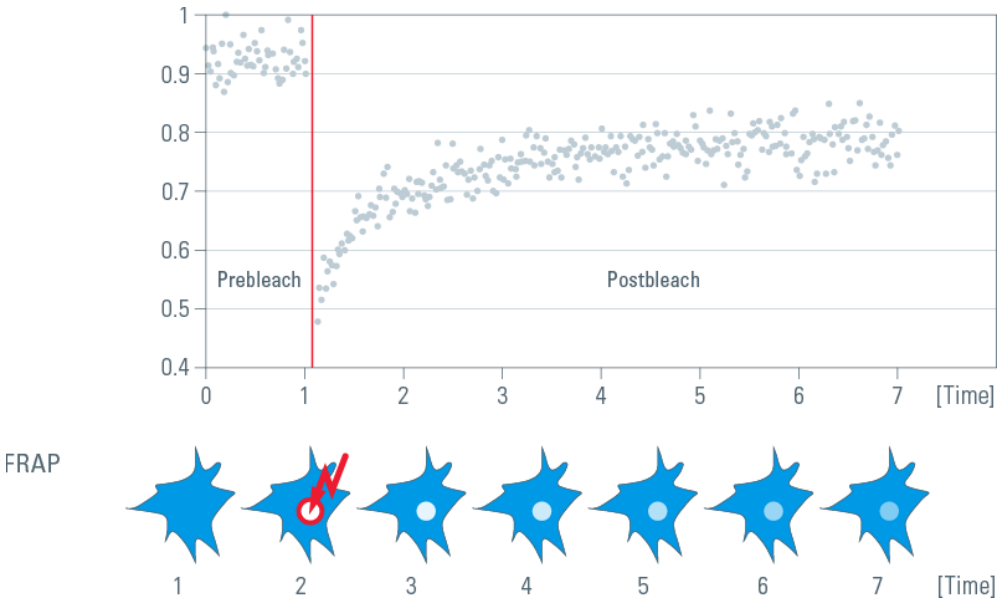

Figure 12: Typical kinetic output from a FRAP experiment. Fluorescence is monitored with a PMT or solar cell continuously during the run, using a low power LED for excitation of the sample. At a certain time, an intense laser pulse is used to bleach part of the sample, with subsequent loss of emission. With time, fresh molecules enter the zone used to monitor fluorescence so that the signal increases but not to the pre-pulse level. The rate of fluorescence recovery gives information about the actual diffusion coefficient.

Apart from the above examples, interest in the bleaching of dyes stems from a need to develop new and improved ways to treat polluted materials, such as plastic waste. Current procedures for avoiding plastic waste are based mostly on a strategy to cut down on the supply of common items such as shopping bags and wrapping. Unlike recycling of metals and glass, there is no direct financial gain in recycling plastics. In fact, the recycling of plastics is a major challenge in many cases and the situation is not made easier by the wide variety of plastics in current use. At best, plastic containers can be recycled two or three times, after addition of new monomers, before becoming unusable. For a few polymers, it is possible to convert them back into monomers, for example, PET can be treated with an alcohol and a catalyst to form a dialkyl-terephthalate. The terephthalate diester is heated with ethylene glycol to form a new polyester polymer, thus making it possible to use the pure polymer again. This, however, is an exception. At the other end of the scale, black plastic pots used by garden centres for transporting plants cannot be recycled and there is a growing mountain of such materials.

While our work does not address the issue of photodegradable plastics, we are interested in the concept of removing the dye, and especially any residual fluorescence, from materials. This would make it easier for recycling of the plastic. Under these conditions, it will not be sufficient to subject the material to visible light and some kind of photocatalyst will be required to activate the process. This is an unknown field and will require the development of new reagents and experimental protocols. The early days of photodegradable plastics saw the active ingredient, usually a benzophenone derivative, incorporated directly into the polymer prior to molding. This is a long-term strategy and it will be necessary to firstly establish viability of our approach. To do this, we need to identify a suitable, generic photocatalyst for initiating dye degradation.

1.6 Bleaching chemistry activated by light

Promotion of a molecule in the ground state to the first-allowed, excited-singlet state adds a large amount of potential energy to the system. For many of the compounds of interest to us here, this excess excitation energy is dissipated as fluorescence and heat passed on to the surrounding medium. We have more-or-less avoided compounds with high triplet yields but it is inevitable that some long-lived triplet states are formed in our systems. In principle, the excited states could be used to promote degradation of the substrate but their lifetimes are rather short. Typically, excited-singlet states possess lifetimes of a few nanoseconds while excited-triplet states rarely survive for more than a few microseconds in air-equilibrated media. High concentrations of substrate are needed to quench the excited states and the most common form of quenching involves light-induced electron transfer. This means that a suitable redox-active substrate is needed and this material must be in close proximity to the excited state. A further issue that electron transfer reactions tend to be reversible such that light-induced charge separation is followed by fast charge recombination to restore the ground-state system. There is no overall chemistry!

Work by Shilov in the 1970's showed how to circumvent rapid charge recombination by using so- called sacrificial redox agents.[100,101] Here, the added reagent undergoes fast dissociation that competes favourably with charge recombination (Figure 13). The dissociative

step must provide access to a different type of radical which will not simply replace the original radical ion. We illustrate this by the scheme below. Many mild oxidants, such as a thiol, will lose a proton upon oxidation and the resultant neutral radical no longer serves as a re-oxidizing agent. Instead, the sulphur-based radical dimerizes to give a very weak reductant. This simple strategy isolates the radical ion of the chromophore, which can transfer an electron to molecular oxygen so as to form superoxide ions. The latter can be a highly effective bleach and anti-bacterial agent. It is much longer-lived than the original excited state but has less potential energy. Corresponding schemes can be proposed for oxidation of the excited state. This is reminiscent of how certain photosynthetic cyanobacteria operate where sugar production occurs under illumination but without oxidation of water to molecular oxygen.

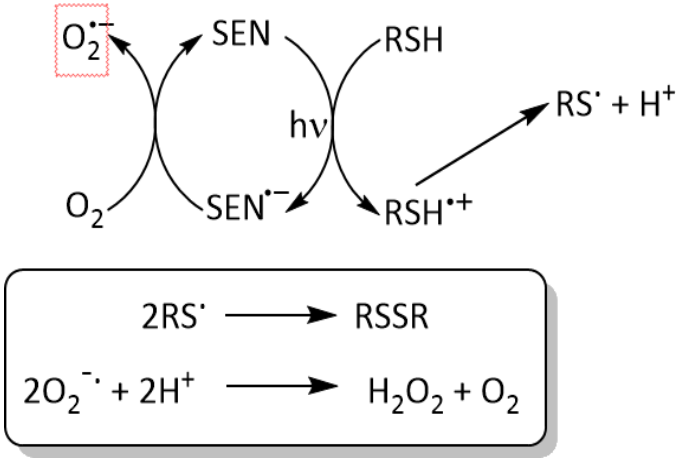

Figure 13: Typical Shilov-type photoredox reaction using a sacrificial electron donor to circumvent charge recombination. The key reaction involves fast deprotonation of the oxidized thiol to give a sulphur-centred radical. This latter species will not act as an electron acceptor but prefers to undergo dimerization or cross-coupling reactions. This provides sufficient time for molecular oxygen to oxidize the one-electron reduced form of the sensitizer (SEN) to form hydrogen peroxide.[100]

Many carbonyl compounds, such as thioxanthones, have lowest-energy triplet states of n,π* character. Such excited states resemble free radicals with the radical character located on the oxygen atom. In turn, this type of short-lived species is able to abstract a hydrogen atom from the surrounding medium and thereby initiate a chain reaction involving carbon-centred free radicals and molecular oxygen (Figure 14). The net result is the light-induced breakdown of the whole

system, which after initiation becomes a dark process. This is a serious issue with anthraquinone-based vat dyes which were popular in the 1950s as curtain dyes. The underlying chemistry was explained by Bridge and Porter[102] on the basis of one of the first applications of flash photolysis. The only real problem with this type of photocatalysis is that near-UV light is needed to access the n, π* state.

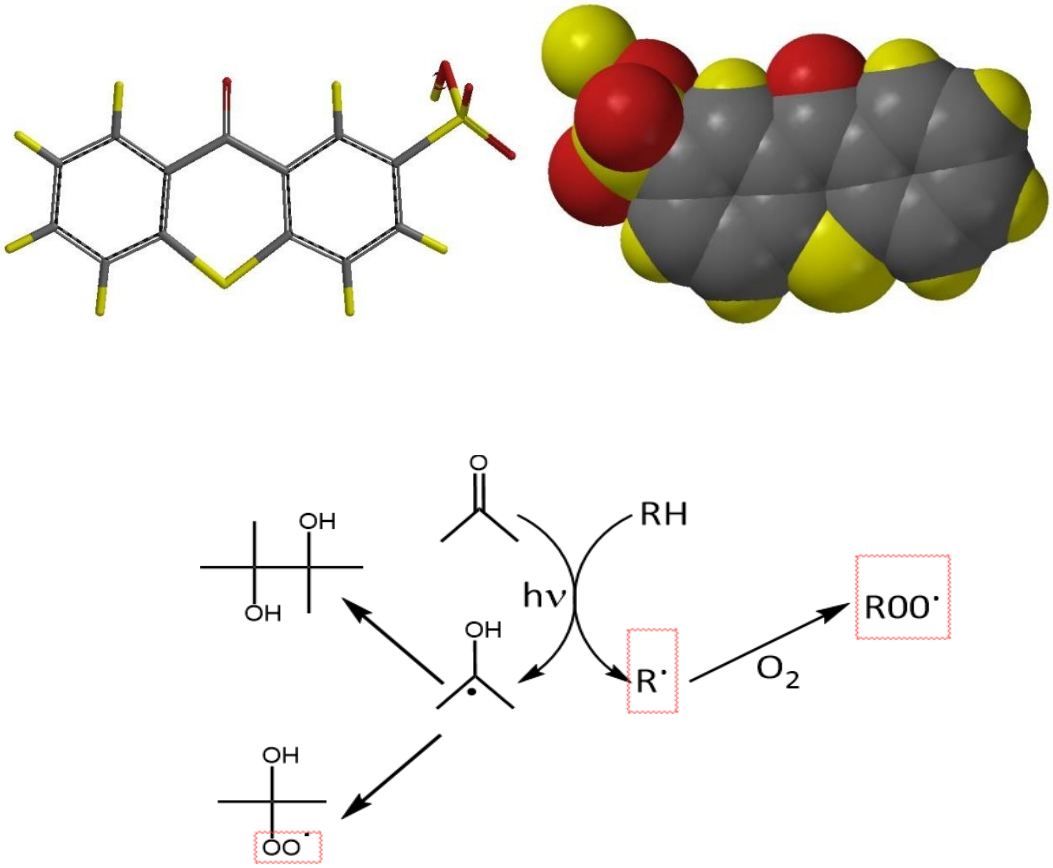

Figure 14: Molecular formula for a typical thioxanthone bearing a water-solubilizing sulphonate group, as shown in both tube mode and as a space-filling model. Also shown is a typical photochemical reaction scheme showing chain initiation by the n, π* triplet state of the thioxanthone.

Similar types of photodegradation can be initiated with certain semi-conductors such as titania. The chemistry is much the same as found with n, π* excited-triplet states but again near-UV light

is needed. There are few alternatives to this approach but recent work by Sirbu et al.[103] has described the in-situ generation of an organic hydroperoxide (Figure 15). This reaction involves a light-activated intramolecular charge-transfer reaction driven by visible light. The resultant charge-separated state undergoes charge recombination but part of the radical ion pair undergoes proton loss to stabilize the species. Electron transfer to molecular oxygen, forming superoxide ions, regenerates the chromophore in much the same way as described for the Shilov-based systems. However, now the hydroperoxyl radical formed by protonation of superoxide ions adds to the carbon-centred radical formed by proton loss by the donor function. This forms a stable organic hydroperoxide that could be fully characterized by NMR spectroscopy. This latter species is a modest oxidant and is capable of initiating chemical damage of added substrates. This is a rare example of using light to form a useful bleaching agent with a long shelf-life.

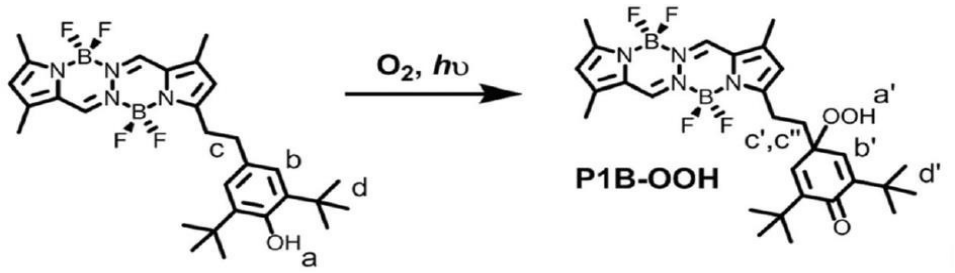

Figure 15: Overall reaction scheme proposed to explain the photochemical generation of an active hydroperoxide that can be used as a catalyst for oxidations. See Sirbu et al.[102] for further details.

1.7 Conclusions and chapter breakdown

The research reported in this thesis explores the field of light-induced degradation of organic dyes. Our interest in this subject is general and we are concerned with both enhancing and curtailing photobleaching. This type of dichotomy is common in photo-activated systems, where the primary intermediates might be quenched with added substrates or allowed to react along a destructive pathway. We intend to rely on organic molecules, taking our cue from natural photosynthesis, and make use of chemical kinetics to evaluate the reactions. There are few reports in the literature that enumerate probabilities for light-induced bleaching of a common dye. In part, this is because the rate and perhaps the mechanism depends on light intensity. We have identified the dye indigo

as a possible standard reagent for bleaching trials. Indigo is a popular dye that has been in use for more than one thousand years. Its colour is instantly recognizable. It is a small molecule that can be transformed to the colourless form, known as iso- indigo, by addition of oxygen. Indigo is very stable under illumination but does fade with time, despite only forming the triplet-excited state in very low yield. [104] In addition to looking at direct photolysis of dyes, we have studied the effects of an added photocatalyst to enhance colour loss.

During the course of our work, we began to consider new ways to produce a strong bleaching agent by way of exposure to sunlight. Most photochemical bleaches are too short-lived to operate in situations where the substrate is either slow to react or present in relatively low concentration. Our interest in this topic arises from observations of polluted water in many remote parts of the world where clean drinking water is not to be taken for granted and where there is a shortage of water for washing (Figure 16). Given the power of photochemistry, it seems reason able to expect that some type of disinfectant could be generated in situ using simple and inexpensive technology. After much consideration, we opted to develop a photochemical method for the production of chlorine dioxide in water using visible light excitation. Chlorine dioxide is a stable radical, having been largely ignored by the photochemistry community, which dissolves readily in water at neutral pH and can be removed under mild conditions.

Figure 16. Illustration of polluted water in some remote part of the world.

The outline of the thesis is as follows: Chapter 2 provides a description of the experimental procedures used throughout the work. The first description of our work related to photocatalyzed bleaching of indigo in fluid solution will be presented as Chapter 3. This work continues in Chapter 4 with specific reference to the direct photobleaching of organic dyes. Specifically this work concerns the photochemistry of methylene blue in water and introduces a novel protective mode obtained by adding urea. Chapter 5 covers the photobleaching of a strapped derivative of boron dipyrromethene dyes. The final chapter describes our work with chlorine dioxide.

1.8 References

[1] A. Albini, *Photochem. Photobiol. Sci.* **2016**, 15, 319.

[2] A. Morachevskii, Russ*. J. Appl. Chem*. **2005**, 78, 166.

[3] A. Albini, "Early Times of Photochemistry." *Photochemistry*. Springer, Berlin, **2016**. Chap. 1, p.1.

[4] C. R. Arumainayagam, R. T. Garrod, M. C. Boyer, A. K. Hay, S. T. Boa, J. S. Campbell, J. Wang, C. M. Nowak, M. R. Arumainayagama, P. J. Hodgea, *Chem. Soc. Rev.* **2019**, 48, 2293.

[5] D.Y. Nikogosy, V. S. Letoki-Iov, *Riv. Nuovo Cim.* **1983**, 8, 1978

[6] T. R. Chaudhuri, J. M. Mountz, B. E. Rogers, E. E. Partridge, K. R. Zinn, *Gynecologic Oncology.* **2001**, 3, 581.

[7] K. D. Jandt, R. W. Mills, *Dental Mater*. **2013**, 29, 605.

[8] M. Martinsen, R. F. El-Hajjar, D. W. Berzins, *Dental Mater*. **2013**, 29, 161.

[9] S. F. Sousa, B. L. Souza, C. L. Barros, A. O. Patrocinio, *Int. J. Photoener*. **2019**, 23, 24.

[10] E. N. Pollitt, J. C. Anderson, K. N. Scafide, D. Holbrook, G. D'Silva, D. J. Sheridan, *J. Forensic Nurs*. **2016**, 11, 97.

[11] J. R. Saylor, *Exp. Fluids* **1995**, 18, 445.

[12] M. Tzortziou, C. L. Osburn, P. J. Neale, *Photochem. Photobiol.* **2007**, 83, 782.

[13] M. S. Twardowski, P. L. Donaghay, *J. Geophys. Res.* **2002**, 107, 6.

[14] L. Bogacz-Radomska, J. Harasym, *Food Quality and Safety.* **2018**, 2, 69.

[15] J. Fiedor, K. Burda, *Nutrients.* **2014**, 6, 466.

[16] G. Shklar, *Oral Oncology.* **1998**, 34, 24.

[17] F. Hosseini, M. K. Gharib Naseri, M. Badavi, M. A. Ghaffari, H. Shahbazian, I. Rashidi, *Scand. J. Cin. Lab. Invest*. **2010**, 70, 259.

[18] J. J. Challem**,** *J. Orthomol. Med*. **1997,** 12, 9.

[19] T.G. Truscott, *J. Photochem. Photobiol. B* **1996**, 35, 233.

[20] A. Hässig, W. X. Liang, H. Schwabl, K. Stampfli, *Med. Hypotheses.* **1999**, 52, 479.

[21] B. Bereira, L. F. B. Rosa, D. A. Safi, M. H. G. Medeiros, R. Curit, E. J. H. Bechara, *Physiology Behavior.* **1994**, 56, 1095.

[22] H. Fickl, V. L. Van Antwerpen, G. A. Richards, D. R. Westhuyzen, N. Davies, R. V. Waltd, C. A. Merwed, R. Anderson, *Atherosclerosis.* **1996**, 124, 75.

[23] S. Cho, *J. Lifestyle Med*. **2014**, 4, 8.

[24] K. Tarwadi, V. Agte, *Int. J. Food Sci. Nutr.* **2003**, 54, 7*.*

[25] T. Wolak, E. Paran, *Vascular Pharmacol.* **2013**, 59, 63.

[26] D. J. Aberhart, *J. Am. Chem. Soc.* **1979**, 101, 3.

[27] N.-H. Jensen, R. Wilbrandt, P. B. Pagsberg, A. H. Sillesen, K. B. Hansen, *J. Am. Chem. Soc.*

1980, 102, 4.

[28] S. Gonzali, A. Mazzucato, P. Perata, *Trends Plant Sci*. **2009**, 14, 237.

[29] K. C. Garber, A. Y. Odendaal, E. E. Carlson, *J. Chem. Educ.* **2013**, 90, 755.

[30] J. B. Harborne, *J. Photochem*. **1967**, 6, 1643.

[31] R. E. Blankenship, "Molecular Mechanisms of Photosynthesis Blackwell Science.", 1st Ed., Maiden, **2002**.

[32] Y. Nakamura, N. Aratani, A. Osuka, *Chem. Soc. Rev.* **2007**, 36, 831.

[33] N. Armaroli, V. Balzani, *Angew. Chem. Int. Ed.* **2007**, 46, 52.

[34] J. M. Olson, *Biochim. Biophys. Acta.* **1980**, 594, 33.

[35] C.-W. Wan, A. Burghart, J. Chen, F. Bergström, L. B.-Å. Johansson, M. F. Wolford, T. G. Kim,

M. R. Topp, R. M. Hochstrasser, K. Burgess, *Chem. Eur. J.* **2003**, 9, 4430.

[36] A. Freer, S. Prince, K. Sauer, M. Papiz, A. Hawthornwaiteless, G. McDermott, R. J. Cogdell,

N. W. Isaacs, *Structure.* **1996**, 4, 449.

[37] C. J. Law, A. W. Roszak, J. Southall, A. T. Gardiner, N. W. Isaacs, R. J. Cogdell, *Mol. Membr. Biol.* **2004**, 21, 183.

[38] J. Janusonis, L. Valkunas, D. Rutkauskas, R. van Grondelle, *Biophys. J.* **2008**, 94, 1348.

[39] R. Ziessel, A. Harriman, *Chem. Commun.* **2011**, 47, 611.

[40] A. Helms, D. Heiler, G. McLendon, *J. Am. Chem. Soc.* **1991**, 113, 4325.

[41] M. B. Bishop, C. B. Bishop, *J. Chem. Educ.* **1967**, 64, 302.

[42] G. W. Robinson, *Annu. Rev. Phys. Chem.* **1964**, 15, 311.

[43] J. Rotmans, H. D. Boois, R, J. Swart. *Climatic Change*. **1990**, 3, 331.

[44] A. Goeppert, M. Czaun, J.-P. Jones, G. K. Prakash, G. A. Olah, *Chem. Soc. Rev.* **2014**, 43, 7995.

[45] G. Centi, S. Perathoner, *Catal. Today.* **2009**, 148, 191.

[46] E. J. Maginn, *J. Phys. Chem. Lett.* **2010**, 1, 3478.

[47] B. Kumar, M. Llorente, J. Froehlich, T. Dang, A. Sathrum, C. P. Kubiak, *Annu. Rev. Phys. Chem.* **2012**, 63, 541.

[48] L. Schmidt-Mende, J. K. Stolarczyk, S. N. Habisreutinger, *Angew. Chem. Int. Ed.* **2013**, *52*, 7372.

[49] P. Mü ller, X.-P. Li, K. K. Niyogi, *Plant Physiol.* **2001**, 125, 1558.

[50] R. G. Waiters, P. Horton, *Photosyn. Res.* **1993**, *36*, 119.

[51] K. K. Niyogi, X.-P. Li, V. Rosenberg, H.-S. Jung, *J. Exp. Bot*. **2004**, 56, 375.

[52] P. Horton, M. Wentworth, A. Ruban, *FEBS Lett.* **2005**, 579, 4201.

[53] A. Calatayud, E. Barreno, *Plant. Physiol. Biochem*. **2004**, 42, 549.

[54] C. Lu, N. Qiu, Q. Lu, B. Wang, T. Kuang, *Plant Sci*. **2002**, 163, 1063.

[55] C. Lu, J. Zhang, *J. Exp. Bot.* **1998**, 49, 1671

[56] M. Y. Gorbunov, Z. S. Kolber, M. P. Lesser, P. G. Falkowski, *Limnol. Oceanogr*. **2001**, 46, 75.

[57] L. Oceanogr. *Limnol. Oceanogr*. **2001**, 46, 75.

[58] A. Dreuw, G. R. Fleming, M. Head-Gordon, *J. Phys. Chem. B.* **2003**, 107, 6500.

[59] A. Porcar-Castell, J. Bäck, E. Juurola, P. Hari, *Funct. Plant Biol.* **2006**, *33*, 229.

[60] M. N. Merzlyak, A. E. Solovchenko, A. A. Gitelson, *Postharvest. Biol. Technol*. **2003**, *27*, 197.

[61] A. M. Gilmore, H. Y. Yamamoto, *Photosynth. Res*. **1993**, 35, 67.

[62] A. V. Ruban, P. Horton, *Aust. J. Plant Physiol.* **1995**, 22, 221.

[63] U. Schreiber, C. Neubauer, *Photosynth. Res*. **1990**, 25, 279.

[64] P. H. Lambrev, Y. Miloslavina, P. Jahns, A. R. Holzwarth, *Biochim. Biophys. Acta.* **2012**, 1817, 760.

[65] W. Bilger, O. Björkman, *Planta.* **1991**, 184, 226.

[66] Y. Miloslavina, I. Grouneva, P. H. Lambrev, B. Lepetit, R. Goss, C. Wilhelm, A. R. Holzwarth, *Biochim.*

Biophys. Acta. **2009**, 1787, 1189.

[67] R. Goss, C. Opitz, B. Lepetit, *Planta.* **2008**, 228, 999.

[68] D. L. Sutherland, C. Howard-Williams, M. H. Turnbull, P. A. Broady, R. J. Craggs,

Bioresour. Technol. **2015**, 184, 222.

[69] R. Goss, B. Lepetit, *J. Plant Physiol*. **2015,** 172, 13.

[70] N. A. Krupenina, A. A. Bulychev, *Biochim. Biophys. Acta.* **2007**, 1767, 781.

[71] S. Santra, "Fluorescent silica nanoparticles for cancer imaging." In *Cancer*

Nanotechnology, 1st Ed. Humana Press, **2010**.

[72] M. Green, *Angew. Chem. Int. Ed*. **2004**, 43, 4129.

[73] S. Rieger, R. P. Kulkarni, D. Darcy, S. F. Fraser, R. W. Köster, *Develop. Dyn.* **2005**, 234, 670.

[74] B. Miksa, *Med. Chem*. **2016**, 6, 611.

[75] Y. Koide, Y. Urano, K. Hanaoka, W. Piao, M. Kusakabe, N. Saito, T. Terai, T. Okabe, T. Nagano, *J. Am. Chem. Soc.* **2012**, 134, 5029.

[76] A. M. Smith, X. Gao, S. Nie, *Photochemistry and photobiology.* **2004**, 80, 377.

[77] K. M. Dean, A. E. Palme, *Nat. Chem. Biol*. **2014**, 10, 512.

[78] C. Eggeling, J. Widengren, R. Rigler, C. A. M. Seidel, *Anal. Chem*. **1998**, 70, 2651.

[79] L. Brand, C. Eggeling, C. Zander, K. H. Drexhage, C. A. M. Seidel, *J. Phys. Chem. A.* **1997**, 101, 4313.

[80] T. Evans, "Nonlinear Dynamics", University of Cambridge, United Kingdom, **2010**. Chap. 1, p. 366.

[81] I. Rasnik, S. A. McKinney, T. Ha, *Nature Methods.* **2006**, 3, 891.

[82] I. Gutiérrez, S. Criado, S. Bertolotti, N. A. Garcıá , *J. Photochem. Photobiol. B.* **2001**, 62, 133.

[83] J. H. van der Velde, J. J. Uusitalo, L. J. Ugen, E. M. Warszawik, A. Herrmann, S. J. Marrink, T. Cordes, *Faraday Disc.* **2015**, 184, 221.

[84] S. K. Dey, J. R. Pettersson, A. Z. Topacio, S. R. Das, L. A. Peteanu, *J. Phys. Chem. Lett*. **2018**, 9, 2259.

[85] E. Ben-Hur, S. Rywkin, I. Rosenthal, N. E. Geacintov, B. Horowitz, *Transfus*. **1995**, 35, 401.

[86] C. Joo, T. Ha, *Cold Spring Harbor Protocols*. **2012,** 10, 1530.

[87] L. A. Ernst, R. K. Gupta, R. B. Mujumdar, A. S. Waggoner, *J. Int. Soc. Anal. Cytol*. **1989**, 10, 3.

[88] S. N. Iyer, N. Behary, V. Nierstrasz, G. Guan, G. Chen, *Sci Rep*. **2019**, 9, 2045.

[89] O. J. Woodford, R. Ziessel, A. Harriman, *ChemPhotoChem*. **2018**. 2, 1046.

[90] E. V. Keuren, W. Schrof, *Macromol.* **2003**, 13, 5002.

[91] D. Champion, H. Hervet, G. Blond D. Simatos, *J. Ag. Food Chem*. **1995**, *43*, 2887.

[92] J. S. Wong, L. Hong, S. C. Bae, S. Granick, *J. Polym. Sci.* **2012**, 48, 2582.

[93] Y. G. Anissimov, X. Zhao, M. S. Roberts, A. V. Zvyagin, *Int. J. Pharm*. **2012**, 435, 93.

[94] K. C. Tseng, N. J. Turro, C. J. Durning, *Polymer.* **2000**, 41, 4751.

[95] G. Hungerford, A. Rei, M. I. C. Ferreira, C. Tregidgob, K. Suhling, *Photochem. Photobiol. Sci.* **2007**, *6*, 825.

[96] D.-W. Jeong, K. Kim, S. Lee, M. C. Choi, S. Q. Choi, *Langmuir.* **2014**, *30*, 14369.

[97] B. V. Koryakin, T. S. Dzhabiev, A. E. Shilov, *Dokl. Akad. Nauk USSR.* **1977**, 238, 620.

[98] J. Fu, C. Zhang, *Biophys Rep*. **2019**, 5, 235.

[99] N. Kourtis, N. Tavernarakis, *Bio - Protoc*. **2017**, 5, 7.

[100] A. Harriman, *Eur. J. Inorg. Chem*. **2014**, 5, 73.

[101] R. Radi, *Proc. Natl. Acad. Sci.* **2018**, 115, 5839.

[102] N. K. Bridge, G. Porter, *Mathematical and Physical Sciences*. **1958**, 244, 259.

[103] D. Sirbu, O. J. Woodford, A. C. Benniston, A. Harriman, *Photochem. Photobiol. Sci*. **2018**, 17, 750.

[104] J. K. G. Karlsson, O. J. Woodford, R. Al-Aqar, A. Harriman, *J. Phys. Chem*. A. **2017**, 121, 8569.

Chapter 2.

Experimental Methods and Procedures

Starting a reaction…

2.1 Materials

Solvents used in this work were purchased as spectroscopic grade materials and were stored under N_2 at 4 oC. Bottles were freshly opened and aliquots of solvent were removed using appropriately sized syringes. Where necessary, solvents were redistilled before use. To ensure the absence of artefacts associated with trace impurities in the solvent, samples of DMSO were purified by two different methods. Firstly, DMSO was stored overnight over freshly activated alumina before being filtered and distilled from CaH_2 under reduced pressure. Secondly, an aliquot of the purified solvent was refluxed for 4h over CaO, further dried with CaH_2 and subsequently fractionally distilled at low pressure. Water was doubly distilled and deionised as demanded for conductivity measurements. Typical conductivies were in the region of 0.05 μS cm^{-1}. Water was collected fresh from the still and used within a few hours. All solutions were protected from room light and handled in the dark. Solutions were prepared by weighing an appropriate amount of solid matter using a microbalance. The solid was transferred to a measuring flask and the correct volume of solvent added via the syringe. Before addition of the full volume of solvent, the solution was subjected to 10 seconds of ultrasound and filtered through a membrane filter. For liquid samples, the solute was added to the measuring flask using a calibrated micropipette. All solutions were prepared in duplicate or triplicate. If necessary, flask were wrapped in aluminium foil and stored at 4 ^{o}C.

Certain routine compounds were purchased from commercial sources and used as received. These include salts used to prepare buffers or as background electrolytes. Tris(2,2'-bipyridyl)ruthenium(II) dichloride was obtained from Sigma-Aldrich and used as received. The absorption spectrum was compared to literature examples.[1] Samples of indigo (Figure 1) were obtained from Sigma Aldrich Ltd. and used as received. Analysis by NMR spectroscopy in d_6-DMSO showed the purity of the dye to be about 90%.[2-4] A sample of the well-known liophillic anti-oxidant butylated-hydroxytoluene (Figure 1) was purchased from Sigma Aldrich Ltd. and subjected to column chromatography with 200-325 mesh silica gel using a mixture of diethylether/hexane 9/1 as eluent.[5]

Samples of Methylene Blue (Figure 1) were obtained from Sigma-Aldrich and subjected to Soxhlet extraction with chloroform. A minor amount of a red coloured product was removed. Analysis by ^{1}H NMR spectroscopy of the residual dye, after drying in a vacuum oven, showed the presence of small amounts of one or more impurities.[6] These were estimated to contribute less than 2% to the total dye concentration. Urea (Figure 1) was recrystallized from warm water, the temperature being held at less than 50 °C to avoid contamination with ammonium cyanate, on addition of ethanol.

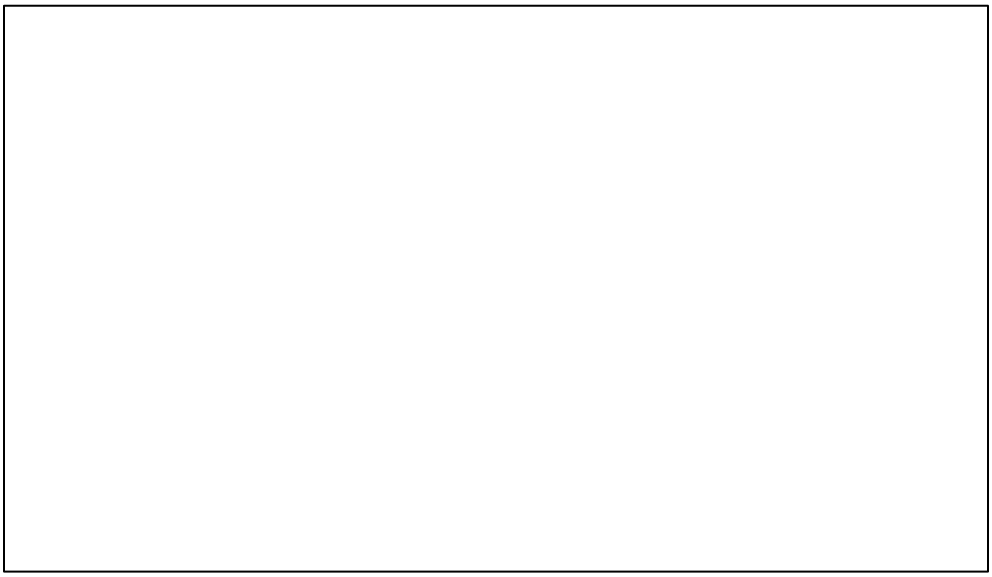

Figure 1. Chemical formulae of the common materials used in this work after purchase from commercial sources.

Other compounds used in this work were synthesized by specialist research groups at Newcastle University. These include a strapped derived of boron dipyrromethene referred to throughout this thesis as BOD (Figure 2). This compound was provided by Dr JG Knight. Synthetic details have been published in the open literature.[7] It was purified by column chromatography and analyzed by NMR spectroscopy and mass spectrometry. A second compound is a symmetrical bis-pyrrole-BF_2 complex equipped with butylated hydroxytoluene groups referred to throughout our work as CAT. The chemical formula is shown as part of Figure 2. This compound was synthesized and purified by Dr Dima Sirbu of our laboratory.[8]

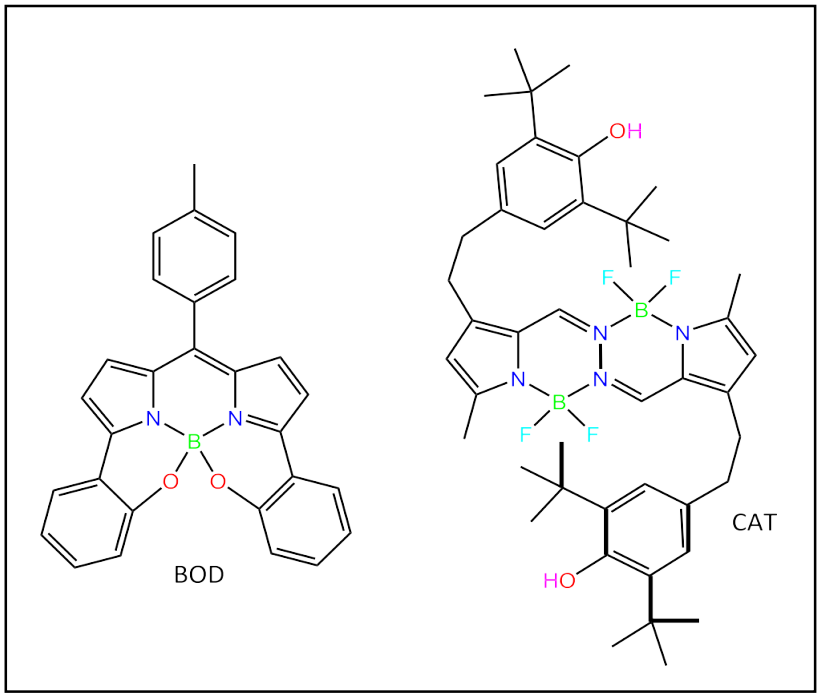

Figure 2. Chemical formulae of the specialized materials synthesized by other research groups and used for some of our studies.

Chapter 6 describes experiments carried out with chlorine dioxide. Several procedures were used to generate solutions of ClO_2. The most successful preparation involved the chemical oxidation of sodium chlorite by acetic anhydride in aqueous solution. The resultant stock solution of ClO_2 was immersed in an ice bath to minimize any loss of chlorine dioxide.[9,10] The concentration of dissolved gas was determined by iodometric titration.[11-13] In this latter procedure, chlorine dioxide was titrated with 0.05M potassium iodide solution to oxidize iodide to iodine, which is titrated with standard sodium thiosulfate ($Na_2S_2O_3$) 0.1 M solution using starch indicator. This work is described in detail in Chapter 6.

2.2 Methods

2.2.1 Absorption spectroscopy

Absorption spectra (also known as UV-Vis spectra, absorbance spectra and electronic spectra) show the change in absorbance of a sample as a function of the wavelength of the incident light beam as measured using a spectrophotometer. The intensity of light transmitted through the sample, I_{Sample}, (such as an analyte dissolved in solvent) and the intensity of light through a blank, I_{Blank}, (solvent only) are recorded and the absorbance of the sample calculated using Equation 2.1:

$$A = \log_{10} \frac{I_{Blank}}{I_{Sample}} \quad (Equation\ 2.1)$$

For most samples, the absorbance is expected to vary in a linear manner with the molar concentration of the solute; which enables the concentration of the sample to be calculated from the absorption spectrum using the Beer-Lambert Law.

Routine absorption spectra were recorded using a Hitachi U3310 dual-beam spectrophotometer. An appropriate wavelength range, between 250 and 900 nm, was selected. The slit width was usually set to 1 nm and the scan rate was usually set at 120 nm/min. The instrument resolution was set at 0.2 nm. Before replacing the solvent with the solution of interest, an automatic baseline correction was carried out with pure solvent in both optical cells. These sample cells were usually built from optical quality quartz with 1 cm path length and were cleaned with nitric acid, washed profusely with water, then with acetone and dried in the oven. The concentration of solute was adjusted such that the maximum absorbance at the peak maximum was between 0.5 and 2.0. Cells of different path length were available to ensure the required absorbance could be achieved. Microliter cells are also available for use when only small volumes of sample are available. All absorption spectral measurements were repeated several times to ensure self- consistency. The spectral data were saved to the hard disk and stored on dedicated PCs. Subsequent data analysis was carried out away from the instrument.

The Beer-Lambert law was used to relate absorbance (A_λ) at a certain wavelength to the molar absorption coefficient at that same wavelength (ε_λ).The latter term is reported in units of $M^{-1}\,cm^{-1}$.

The expression is specified in Equation 2.2 where c is the molar concentration of the solute and l is the path length in cm. In applying this simple expression it is essential to ensure that only homogeneous solutions are used and that the solute is properly dissolved. To check the latter, the solution was sonicated for a few seconds and filtered before filling the cuvette. The beam from a laser pen was directed through the solution to ensure the absence of light scattering.

$$A_\lambda = \varepsilon_\lambda cl \qquad (Equation\ 2.2)$$

Occasionally it is useful to record the corresponding transmission spectrum. More often it is appropriate to compare the absorption spectrum with the excitation spectrum recorded for fluorescent samples. Integration of the absorption band allows calculation of the oscillator strength for the transition of interest. The instrument allows the temperature of the sample to be varied between 5 and 100 ^{O}C. A separate attachment can be used to accommodate solid samples or samples of unusual shape.

2.2.2 Fluorescence spectroscopy

Fluorescence spectroscopy provides an alternative means for measuring solute concentrations in dilute solution. This is an indirect method that relies on the observation that the emission intensity is a linear function of concentration provided the solution is optically dilute. Usually, this translates to conditions where the absorbance at the excitation wavelength is less than 0.1. The linearity is lost at higher concentrations. As such, fluorescence is especially useful for studies where the chromophore is present at low concentrations. It is important to select the excitation wavelength with great care, especially for photobleaching measurements. Often, this requires the experiment to be repeated several times with different excitation wavelengths being applied each time. It is

also possible to make fluorescence measurements with solid samples and, for this purpose, a special sample holder was machined in the workshop.

Fluorescence spectra were collected using a Hitachi F-4500 fluorescence spectrophotometer, for most measurements the scan rate was kept at 60 nm/min. Additionally, the excitation and emission slit widths were kept at 2.5 for most solutions and optical filters were used to isolate any scattered light from the excitation source. Fluorescence measurements were obtained using dilute solutions, the absorbance at the excitation wavelength was between 0.05 and 0.1 in a 1 cm path length quartz cell. This was done to avoid re-absorption or inner-filter effects. The solutions were prepared using spectrophotometric grade solvents and recorded using quartz cuvettes. The cell was cleaned and dried before use and the solvent was checked for fluorescent impurities. In addition, in the case of a weak emission signal, larger slit widths (up to 10 nm) were used but this adds some suspicion when investigating the peak position. It is also noteworthy that all emission spectra were fully supported on the basis of comparing the corresponding absorption spectrum with excitation spectrum in the same solvent.

The instrument was maintained by LAT Inc. and serviced at six-monthly intervals to ensure correct calibration of the wavelength and linearity of intensity. Fluorescence and excitation spectra were automatically corrected for wavelength effects using a calibration curve stored on the instrument. This calibration curve was updated each six months. The instrument was driven by commercial software that allowed easy measurement of areas and peak maxima. Data were stored on the operating PC but copied to file for manipulation elsewhere. All emission measurements were repeated several times. Figure 3 shows an example of overlaid excitation, absorption and fluorescence spectra recorded for BOPHY (see later for a description of this compound) recorded in fluid solution. It will be noticed that there is extremely poor mirror symmetry between absorption and emission spectra.

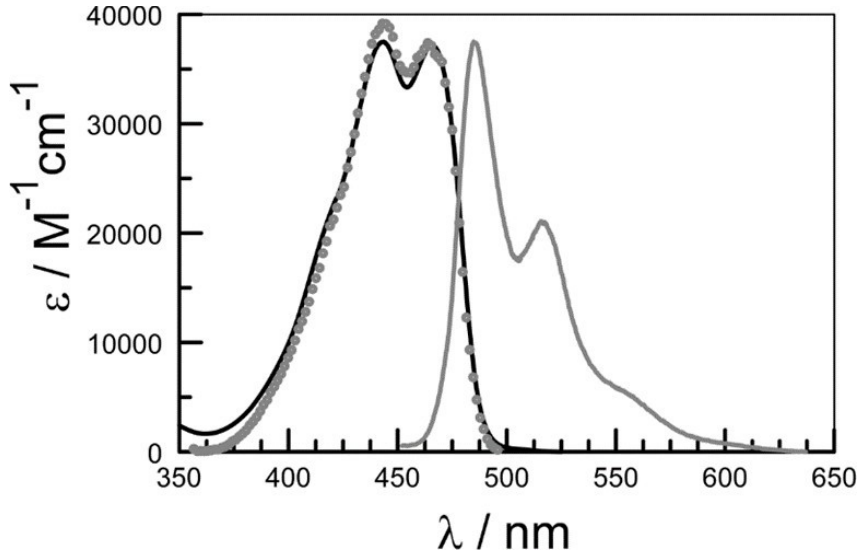

Figure 3. Normalised absorption (black curve), fluorescence (grey curve) and excitation (grey points) spectra recorded for TM-BOPHY in 2-methyltetrahydrofuran at room temperature. The excitation wavelength was 415 nm while the emission wavelength used for the excitation spectrum was 600 nm.

2.2.3 Photobleaching studies

Photobleaching (sometimes termed photofading) is the photochemical alteration of the molecular structure of a chromophore such that colour is lost.[14] The process can also be followed by fluorescence spectroscopy if the photochemical transformation leads to permanent loss of emission. Bleaching is a consequence of the breakage of covalent bonds or non-specific reactions between the chromophore and surrounding molecules. Most organic molecules are susceptible to photobleaching, especially in the presence of molecular oxygen. This is a particular problem for fluorescence microscopy and single molecule spectroscopy. In fact, the technique known as Fluorescence Recovery After Photobleaching (FRAP) uses the in-situ destruction of the fluorophore to measure diffusion coefficients. The number of excitation cycles required to achieve full bleaching of a chromophore varies enormously between compounds. It might be mentioned that natural systems use photobleaching as a simple means for recycling materials at the end of the growing season.

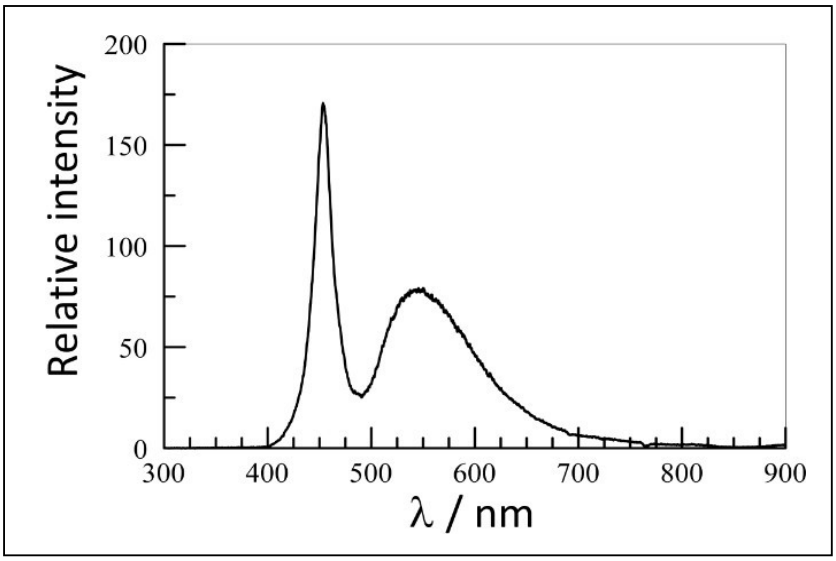

Figure 4. Output measured for one of the broadband illuminators used extensively in this work.

We used two different experimental protocols to monitor the effects of illumination. The first experiment used a white light source for excitation of the sample. Figure 4 shows a typical lamp output as a function of wavelength, note lamps could be changed in order to optimize output for a particular class of chromophore. Output from the lamp was measured by passing the beam into a corrected fluorescence spectrophotometer and recorded the spectrum with the excitation beam blocked. This set-up is intended to mimic the effects of exposure to sunlight. It does not favour selective illumination since any coloured product will also be subjected to possible photobleaching. The second experiment used high-power LEDs of particular colour to excite the sample. Here, a single chromophore can be selectively illuminated in a mixture and products can be protected against adventitious illumination. The limitation of the system is the relatively low photon flux which means that long exposure times are needed. This set up was used for measuring quantum yields for photobleaching. A typical LED output is shown as Figure 5. All of our LEDs were obtained from ThorLabs and equipped with heat sinks to avoid thermal breakdown. A variety of wavelengths is available but each LED has to be calibrated for energy output as this changes markedly between the diodes.

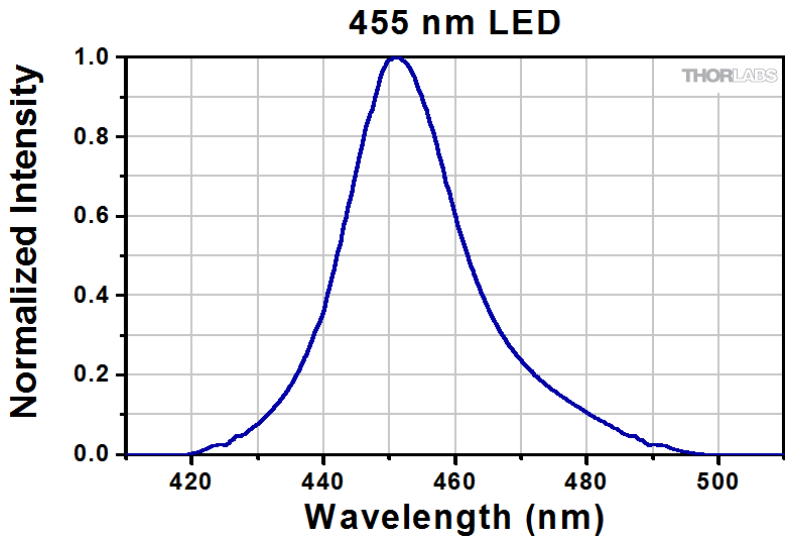

Figure 5. Typical output from the high power LEDs used to monitor the course of photobleaching of organic dyes.

The LED set-up is shown in Figure 6. Here, the high-power LED is equipped with several heat sinks to avoid overheating the lamp. Output from the LED is directed through a reflective screen to a water cooler and then to a camera objective. The latter is used to focus the light beam onto the sample cuvette which sits on a micro-stirrer. A computer controlled shutter prevents undue illumination of the sample and an iris, situated in front of the sample cell, controls the light flux incident on the sample. A quartz slide directs roughly 5% of the light beam to a photocell as a way to record day-to-day light levels. The remainder of the light beam passes through the iris and onto the sample. Part of this beam is absorbed by the dye and the rest is directed to a second photocell. Output from this detector is recorded by a data logger and sent to the controlling PC for storage. At regular intervals, the sample cell is removed for recording absorption and/or fluorescence spectra. The light intensity measured over illumination time is used to determine rates of photobleaching. Light intensity is varied by inserting neutral density filters into the beam.

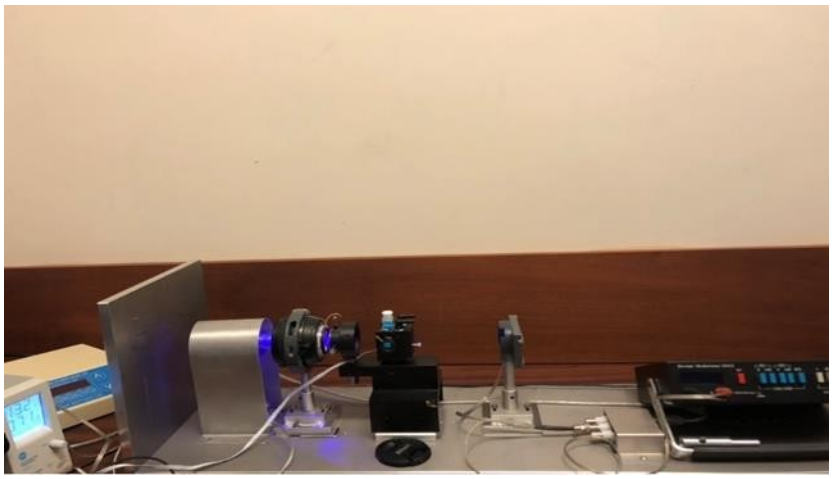

Figure 6. Photograph illustrating the monochromatic LED illuminator used for some photobleaching studies reported here.

Figure 7 shows a typical example of output from this instrumental set-up. The figure shows the stepwise bleaching of the strapped boron dipyrromethene derivative abbreviated as BOD. This system will be covered in Chapter 5. Unlike the broadband illuminator, the LED allows selective illumination of preferred chromophores within a mixture. This situation becomes important in Chapter 3 where we examine the catalyzed bleaching of indigo following selective excitation of the BOPHY-based photocatalyst CAT. Furthermore, the LED is reasonably stable with respect to light output over prolonged periods as long as the heat is dissipated quickly. This allows quantum yields for photobleaching to be measured. A further advantage of this set-up is that coloured intermediates need not be subjected to illumination during the bleaching process. This allows the loss of the primary chromophore to be compared with the accumulation of the intermediate, as happens with the example shown in Figure 7. The actual choice of LED is based on the absorption spectrum of the initial chromophore.

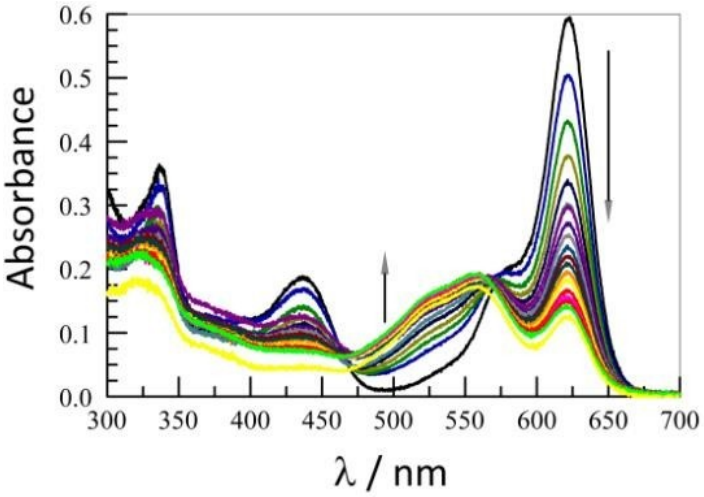

Figure 7. Illustration of the stepwise photobleaching of BOD under illumination at 620 nm in air-equilibrated DMSO solution. Absorption spectra were recorded each 30 minutes while kinetic information at 620 nm accumulates during the experiment. Note the build-up of a product absorbing at around 525 nm and the eventual stabilization of absorption in the red region. This suggests that the overall bleaching pattern is complex.

2.2.4 Measurement of the quantum yield for photobleaching

Most organic dyes tend to degrade under continuous exposure to visible light. This leads to a change in colour or, in extreme cases, to a complete loss of colour. There might be concomitant changes in fluorescence intensity and/or spectral profile. This effective light-induced change in dye concentration has serious effects for single molecule spectroscopy and for super-resolution microscopy. In order to quantify the loss of chromophore, we can think about determining a quantum yield for bleaching (Φ_B) or we can record the rate of loss of chromophore (ω). There is no consensus in the literature regarding standard chromophores that could be useful as reference compounds by which to compare bleaching rates or yields. In the case of Rhodamine 6G in air-equilibrated water, Φ_B values ranging from 2×10^{-6} to 3×10^{-5} have been reported. Furthermore, these Φ_B values depend markedly on light intensity, dye concentration, pH, O_2 pressure, temperature and the state of reaction. The latter point means that the photobleaching rate is nonlinear over time. This behaviour can result from autocatalysis, product build-up or from a change in mechanism.[15-19]

Fluorescence correlation spectroscopy (FCS)[20] is a useful technique for monitoring photobleaching. Such studies have indicated a strong dependence of photobleaching probabilities on excitation irradiance that simple mechanistic considerations cannot explain. In our work, we rely on absorption spectroscopy to monitor changes in concentration of the chromophore. In some cases, fluorescence spectroscopy provided confirmation of the results obtained from absorption spectral studies. The rate of bleaching at a fixed photon flux is determined from a plot of molar concentration against illumination time. Such plots are often exponential in nature but rarely linear. In all cases studied here, ω increased with increasing incident light intensity. The value for ω was determined as the tangent to the curve at different illumination times. A correction factor can be applied to the derived ω value for variations in the extent of light absorption, provided short illumination periods are considered. If the illumination period (Δt) is too long, the change is concentration might be too large for the correction factor to work properly. In the simplest case, we can express ω in terms of Equation 2.3:

$$\omega = I_0 \times f_A \times [dye] = I_0 \times (1 - 10^{-A}) \times [dye] \qquad (Equation\ 2.3)$$

Here, I_0 is the incident light intensity, A is the average absorbance over the wavelength range delivered by the lamp, and the coefficients α or β reflect the fact that the rate might not depend linearly on dye concentration. We express the rates of photobleaching in units of μM per unit time. As such, it is necessary to ensure that the same illumination profile is retained throughout a set of experiments. Photobleaching of a dye solution can be characterized by a quantum yield for the bleaching process (Φ_B) or in terms of a reaction probability (P_B). Indeed, it is common practice to express photochemical and photophysical behaviour in terms of a quantum yield. The quantum yield is equal to the number of molecules of dye that have been photobleached divided by the total number of photons absorbed during the same time interval (Equation 2.4).

The same quantum yield can be expressed

in terms of photophysical parameters such as the radiative (k_{RAD}) and radiationless (k_{NR}) rate constants and the excited state lifetime (τ_S):

$$\varphi_B = \frac{k_B}{k_{RAD} + k_{NR} + k_B} = k_B * \tau_s$$

This expression is suitable for chromophores that do not form the triplet-excited state in reasonable yield. It might be applicable to certain highly fluorescent dye s such as Rhodamine 6G or conventional BODIPY derivatives. Such compounds have excited-state lifetimes of around 5 ns and, allowing for Φ_B values in the range of 10-6, we reach a crude estimate for the corresponding rate constant for bleaching as being around 200 s^{-1}. This type of definition hides a multitude of competing processes, however, and it is far from obvious that photobleaching is a simple consequence of light absorption. It is more likely that bimolecular processes are involved and that impurities play an important part in the bleaching event. We have measured Φ_B values directly from Equation 2.4, which makes no reference to the reaction mechanism.

In measuring Φ_B values, we have varied the light intensity and dye concentration. Also varied are factors such as the partial pressure of dissolved O_2 and the concentration of added reagents. Yields have been determined over relatively short illumination periods and for low conversion rates. The output from the LED was recorded continuously to ensure that the rate of photon uptake remained constant during the experiment. Measurements were carried out in duplicate.

2.2.5 Electrochemistry

In searching for practical ways to produce concentrated aqueous solutions of chlorine dioxide we have considered the direct electrolysis of sodium chlorite. Ideally, this process would consist of passing direct current through molten sodium chlorite but this is not a viable option in our case. We need to identify a simple way to produce a reasonable quantity of chlorine dioxide using readily available techniques. Therefore, the simplest operation is to electrolyze an aqueous

solution using inert electrodes. For the latter, we opted to use graphite rods which were cleaned by sodium carbonate and fitted with wires attached with silver epoxy resin. The resin was coated with wax to form an insulating layer. We selected graphite as the electrode material because of the large over-potential involved in electrolysis of water to hydrogen and oxygen. Initial experiments used sodium chlorite (0.5 M) in de-ionised water containing a small amount (0.02 M) of phosphate buffer at pH 7. Cyclic voltammetry experiments made by Dr. Patrycja Stachelek in our Laboratory indicated that chlorite undergoes a fully reversible one-electron oxidation with a half-wave potential of 0.70 V vs NHE. The half-wave potential is independent of pH across the range 4<pH<10. The corresponding half-reaction can be written as:

Hypochlorous acid forms at low pH and so the pH was kept above 4 for all our experiments. In alkaline solution, chlorine dioxide is hydrolysed and so the pH must be kept below ca. 10. Chlorite can be reduced at the electrode to form chloride but this causes the pH to increase, as was measured experimentally using a microelectrode. Because of this reaction, it was necessary to change cell design and use two separate compartments as described in Chapter 6.

A further change in experimental protocol involved replacing the battery with a photovoltaic cell. We used a multiple panel Si solar cell wired in series to give an output potential of ca. 1.8 V. This was sufficient potential to drive the various electrochemical half-reactions. If required, the solar cell could be re-configured to produce 2.4 V.

Electrolysis of aqueous solutions can be treated in terms of Faraday's laws of electrolysis. In our set-up, it was possible to measure the average current flowing through the circuit under illumination with a 250 W halogen lamp. The electrical charge (expressed in coulombs) is equated to the average current in amps multiplied by the time of electrolysis in seconds. Using the Faraday constant, it is possible to relate the charge with the number of electrons passed through the cell. These must be balanced between anode and cathode compartments but give a crude idea of the amount of product formed during the photo-electrolysis process.

2.2.6 Light-driven electrochemical oxidation

A relatively new way to bring about photochemical reactions is to make use of a photovoltaic panel to produce the necessary impetus for the reaction. This can be done using a combination of silicon solar panels to generate a particular potential that can be delivered to inert electrodes. Our set-up is illustrated in Figure 8. Here, the solar panel comprises three or four individual silicon panels wired in parallel and is illuminated with a white light source. The distance between lamp and panel is varied as required. The solar panel generates a potential of 1.5 V or 2.0 V according to the number of individual panels wired into the system. Graphite electrodes are attached to the terminals of the solar panel and immersed into electrolyte solution held in the sample chamber. A variety of sample cells was designed and used for various oxidative reactions, where the nature of the catholyte was varied. This work is described in Chapter 6.

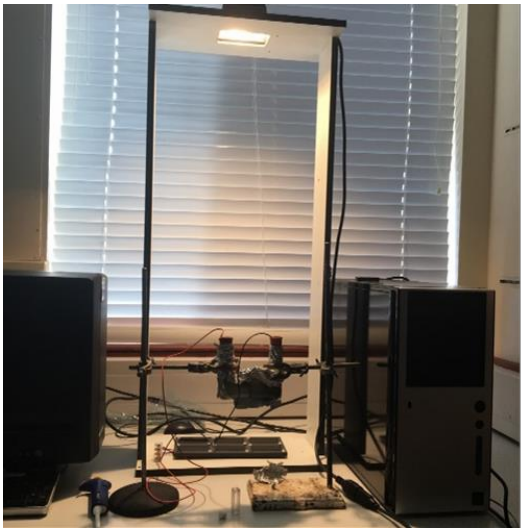

Figure 8. Photograph of the photovoltaic set-up used to drive certain oxidative reactions.

2.2.7 Laser Flash Photolysis

Transient absorption[21] spectra were recorded with several instruments. For nanosecond studies, an Applied Photophysics Ltd. LKS50 instrument was used (Figure 9). Here, the sample solution,

which had an absorbance of about 0.3 at the excitation wavelength, was placed in a quartz cuvette and was deoxygenated with a stream of N_2 gas. The sample was then excited using a frequency-doubled, tripled or quadrupled Q-switched, Nd-YAG laser giving 532 nm, 355 nm or 266 nm respectively at 4 ns pulses. A pulsed Xenon arc lamp was used as the monitoring beam. The signal was then passed through a high-radiance monochromator to a fast response transient digitizer. Regular checks were made to ensure that the laser beam, flash lamp and sample chamber were all aligned properly. Output was averaged in order to improve the signal-to-noise ratio and subsequently amplified.[22-24]

Figure 9: Laser set up used to measure transient absorption spectra.

To obtain the transient decay kinetics, a suitable monitoring wavelength must be chosen. Once the wavelength was set, the PMT voltage was altered between 0–1200 V to produce a light level in the range of 300–500 mV. Next, the time-base is selected as well as the intensity scale. The base line was corrected with 0% and 100% transmission readings and then the absorption decay profile was collected and averaged. The experimental trace can be analysed in terms of several different kinetic schemes. Transient absorption spectra are obtained by measuring decay traces at individual wavelengths. One such decay trace is analysed to give suitable time intervals that are subsequently applied to all other decay traces using the Virtual Acorn A5000 software. The resulting spectra were then splined so as to produce a smoothed transient absorption spectrum from the collected data points.

2.3 References

[1] R. D. Gerardi, N. W. Barnett, S.W. Lewis, Anal. *Chim. Acta*. **1999**, 378, 1.

[2] L. M. Abboud, R. Notario, *Pure Appl. Chem*. **1999**, 71, 645.

[3] M. M. Sousa, C. Miguel, I. Rodrigues, A. J. Parola, F. Pina, J. Mole, M. Mole, *Photochem. Photobiol. Sci.* **2008,** 7, 1353.

[4] P. W. Sadler, *J. Org. Chem*. **1956**, 21, 316.

[5] W. A. Yehye, N.A. Rahman, A. Ariffin, S. B. A. Hamid, A. A. Alhadi, F.A. Kadir, M. Yaeghoobi, *Eur. J. Med. Chem*. **2015**, 101, 295.

[6] J. R. Harbour, S. L. Issler, *J. Am. Chem. Soc*. **1982,** 104, 903.

[7] R. B. Alanoma, S. Rihn, D. C. O'Connor, F. A. Black, B. Costello, P. G. Waddell, W. Clegg, R. D. Peacock, W. Herrebout, J. G. Knight, M. J. Hall, *Chem. Eur. J*. **2016**, 22, 93.

[8] D. Sirbu, O. Woodford, A. C. Benniston, A. Harriman, *Photochem Photobiol Sci*. **2018**, 17, 750.

[9] P. W. Atkins, Physical chemistry; 6th ed.; Oxford university press: Oxford. **1998**.

[10] W. Masschelein, *Ind. Eng. Chem. Res*. **1967**, 2, 137.

[11] D. L. Sweetin, E. Sullivan, G. Gordon, *Talanta*. **1996**, 43, 103.

[12] T.-F. Tang, G. Gordon, *Environ. Sci. Technol*. **1984**, 18, 212.

[13] F. Quental, C. Elleouet, C. Madec, *Anal. Chim. Acta.* **1994**, 295, 85.

[14] C. Eggeling, J. widengren, R. Rigler, C. A. M. Seidel, *Anal. Chem***. 1998**, 70, 2651.

[15] L. Brand, C.Eggeling, C. Zander, K. H. Drexhage, C. A. M. Seidel, *J. Phys. Chem. A* **1997,** 101, 4313.

[16] C. Eggeling, L. Brand, C. A. M. Seidel, *Bioimaging.* **1997**, 5, 105.

[17] (a) T. Hirschfeld, *Appl. Opt*. **1976**, 15, 12, 3135. (b) R. A. Mathis, K. Peck, L. Stryer, *Anal. Chem*. **1990**, 62, 1786. (c) C. Enderlein, *J. Appl. Opt*. **1995**, 34, 514.

[18] R. Y. Tsien, A. Waggoner, In The Handbook of for Biological Confocal Microscopy; J. B. Pawley, Ed.; Plenum Press: New York, **1995**; pp 267.

[19] (a) D. N. Nikogosyan, *Laser Chem*. **1987**, 7, 29. (b) E. V. Khoroshilova, D. N. J. Nikogosyan, *Photochem. Photobiol. B: Biol*. **1990**, 5, 413. (c) M. Anbar, E. J. J. Hart, *J. Am. Chem. Soc.* **1964**, 86, 5633.

[20] (a) I. Rosenthal, *Opt. Commun*. **1978**, 24, 164. (b) D. Beer, Weber, *J.Opt. Commun.* **1972**, 4, 307. (c) S. A. Soper, H. L. Nutter, R. A. Keller, L. M. Davis, E. B. Shera, *Photochem. Photobiol.* **1993,** 57, 972. (d) T. Schmidt, G. J. Schultz, W. Baumgartner, H. J. Gruber, H. Schindler, *Proc. Natl. Acad. Sci. U.S.A.* **1996**, 93, 2926. (f) A. L. Huston, C. T. Reimann, *Chem. Phys*. **1991**, 149, 401.

[21] V. M. Breslin, N. A. Barbour, D.-K. Dang, S. A. Lopez, M. A. Garcia-Garibay, *Photochem. Photobiol. Sci.* **2018**, 17, 741.

[22] D. L. Andrews, A. A. Demidov, "An introduction to laser spectroscopy": 2nd Ed. Springer Science & Business Media. **2012**

[23] G. Porter, M. R. Topp, *Proc. Roy. Soc. A.* **1970**, 315, 163.

[24] R. V. Bensasson, E. J. Land, T. G. Truscott, Flash photolysis and pulse radiolysis: contributions to the chemistry of biology and medicine. Elsevier. **2013.**

Chapter 3.

Photocatalyzed Degradation of Indigo in Solution

via *in-situ* Generation of an Organic Hydroperoxide

Blue is the colour…

3.1 Summary

Indigo, an emblematic violet dye used for thousands of years to colour fabric, is resistant to fading on exposure to sunlight. Prior work has indicated that indigo is reactive towards both hydroperoxyl radicals and superoxide anions in solution. In order to promote photobleaching of indigo, we have utilised a BOPHY-based (BOPHY = aryl fused symmetrical pyrrole-BF_2 complex) chromophore known to form both superoxide ions and a stable alkyl hydroperoxide under illumination in aerated solution. Selective irradiation of the photocatalyst causes relatively fast fading of indigo, with the rate increasing gently with increasing concentration of indigo. Molecular oxygen and light are essential for bleaching to occur. One molecule of the photocatalyst can bleach more than 40 molecules of indigo. An active component of the photocatalyst is a butylated hydroxytoluene (BHT) residue which itself quenches the triplet excited state of indigo. This provides an ancillary mechanism for effecting photofading of indigo but, because the triplet is formed in very low yield, this route is not practical.

3.2 Introduction

Photochemistry has an important role to play in our attempts to remove waste products, toxins and pollutants from industrial sites, water supplies and household garbage.[1-3] There are several tried-and-tested photochemical reactions[4,5] that offer near universal treatments that could be applied on a large scale. These include photochemical hydrogen atom abstraction using an n, π* excited triplet state. This type of initiation leads to chain reactions,[6] well known in polymer chemistry,[7] but needs near-UV activation. An alternative reaction involves the sensitized generation of singlet molecular oxygen[8] via triplet energy transfer.[9] Now the energy requirements

are far less demanding than for hydrogen atom abstraction and many organic compounds are known to generate high yields of singlet oxygen in solution under visible light illumination.[10] The main difficulty in applying this process to waste removal concerns the rather short lifetime of singlet oxygen, which ranges from 4 μs in water[11] to 25 μs in N,N- dimethylformamide.[12] In situ generation of superoxide ions overcomes the kinetic limitation of singlet oxygen but is more difficult to achieve in reasonable yield.[13] Not all substrates are susceptible to attack by superoxide. Further developments in the photochemical destruction of unwanted organic residues require the introduction of a potent bleach that has a long inherent lifetime and can be regenerated during the cleansing operation. To this end, we draw attention to the recent report[14] of the photodriven formation of an aryl hydroperoxide by way of intramolecular charge transfer followed by addition of molecular oxygen.

To test the capability of this type of photocatalyst as a new bleaching reagent, we apply it to the destruction of indigo (Figure 1). The latter is a very stable violet dye with an important history.[15] Indeed, the colour of indigo was selected by Newton for describing the dispersion of light in a rainbow and it was favoured by Napoleon for his army's tunics. Originally, indigo was extracted from plants and processed to give the familiar colour always associated with blue jeans but nowadays the compound is produced synthetically from N-phenylglycine. Production of indigo is a massive industry and involves some 5,000 tonnes of dye annually.[16] Part of the great attraction of indigo dyes stems from their high stability,[17] which can be attributed to the two intramolecular hydrogen bridges formed between amino and carbonyl groups. These internal hydrogen bonds occupy positions that would otherwise be the most reactive towards nucleophilic and electrophilic attack. Indigo is highly resistant to light-induced damage by way of direct excitation.[18] This is because the excited states are deactivated rapidly by way of intramolecular proton transfer. Photoacoustic calorimetry has been used to measure properties of the triplet-excited state, as populated[19] by sensitization. This work confirmed[20] the very low inherent triplet quantum yield (i.e., $\tau_T = 0.006$) and located the triplet energy at 1.0 eV. Such properties do not favour triplet-state reactions! Given the unusually high stability reported for indigo, this compound makes an ideal target for photocatalyzed transformations. Of particular interest to this work is the

observation that the central double bond in indigo is susceptible to attack by hydroperoxyl radicals. This generic reaction, which is illustrated in Scheme 1, is likely to operate under mild conditions and should be accomplished with a range of oxidants. Certain properties of the delocalized radical formed by addition of a hydroperoxyl radical (or a hydroxyl radical) to indigo have been established by computational studies and it appears that the spin density is delocalized over most of the unsubstituted half of the molecule.[21] The fate of the radical remains unknown but might involve secondary addition of molecular oxygen at one of the many possible carbon-centred radicals. This would create a chain reaction leading to conversion of indigo to isatin. Independently, Kettle et al.[22] reported that superoxide anions attack indigo carmine (a water-soluble form of indigo prepared by treatment with concentrated sulfuric acid) to give isatin sulfonic acid. These observations suggest to us that indigo might be susceptible to bleaching by certain types of photoredox reactions. Chemical oxidation by strong oxidants, such as nitric acid, leads to formation of isatin (Figure 1).

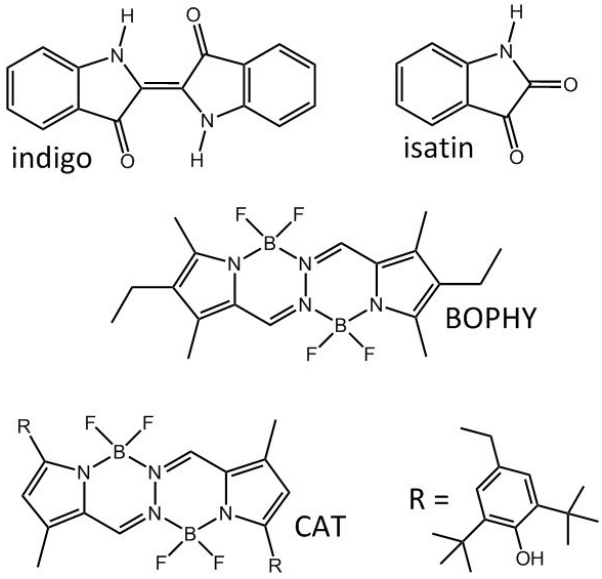

Figure 1. Chemical formulae for the main compounds discussed in the text. Note that CAT possesses two active butylated hydroxytoluene (BHT) residues per molecule of BOPHY.

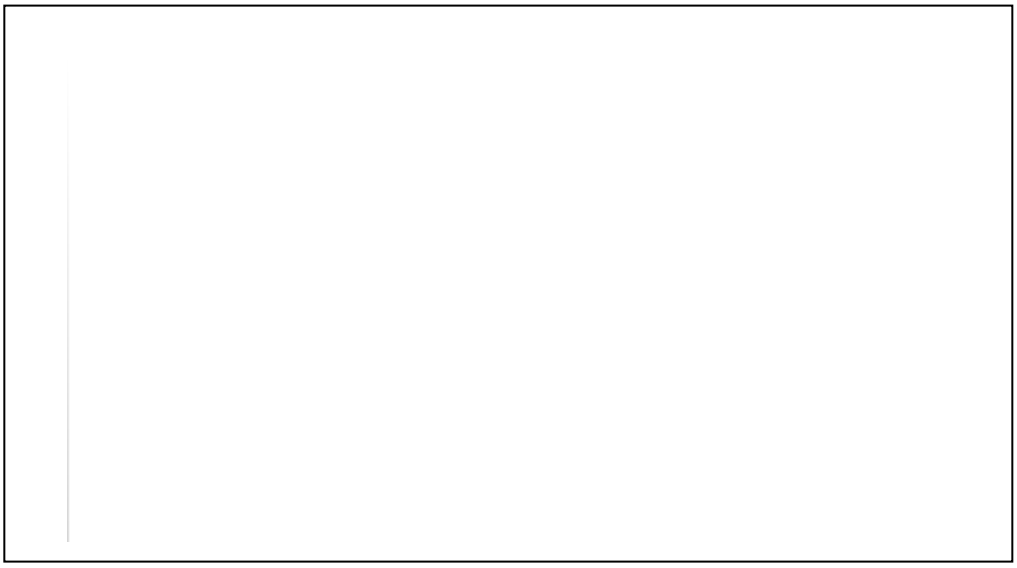

Scheme 1. Reaction between indigo and hydroperoxyl radicals to give an addition product where the spin density is delocalized around the unsubstituted half of the molecule. Re-arrangement and bond cleavage gives a molecule of isatin and a free radical. The latter can react with oxygen and indigo in a radical chain reaction to form more isatin.

Separately, previous work has established[14] that the photocatalyst, CAT (Figure 1, Scheme 2), forms an organic hydroperoxide (C-OOH) following rearrangement after light-induced intramolecular electron transfer. The key reaction here is the rapid loss of a proton from the oxidized phenol residue which helps to prevent charge recombination to recover the ground state. The corresponding BOPHY-based (BOPHY is a recognized acronym for the symmetrical fused pyrrole-BF_2 complexes introduced recently by Ziegler et al.[23] as an extension to the popular boron dipyrromethene family of fluorophores[24]) π-radical anion is re-oxidized by molecular oxygen, forming the superoxide anion which picks up the proton to generate a hydroperoxyl radical. This overall sequence forms a neutral radical resident on the phenoxyl ring which is stabilized at the bridgehead carbon centre. Subsequent addition between the two radicals leads to formation of C-OOH. It is now a straightforward matter to combine the two reactions (i.e., Schemes 1 and 2) into a single sequence.

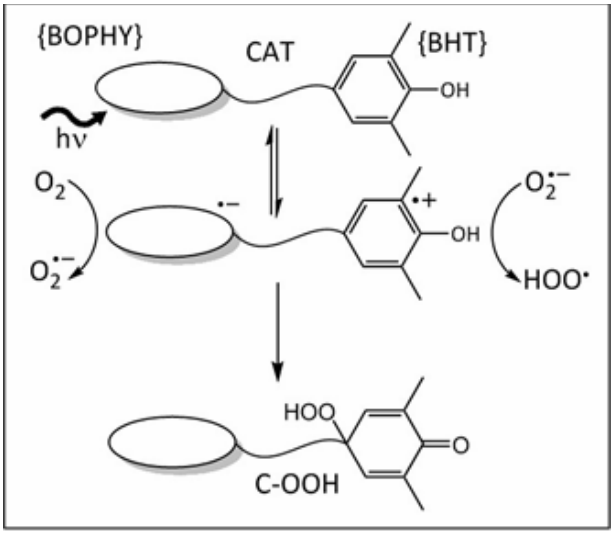

Scheme 2. Illustration of the events that follow from illumination of CAT in aerated solution. Intramolecular charge transfer leads to formation of a highly reversible charge-transfer state for which deprotonation of the oxidized phenol competes with charge recombination. Interception of the BOPHY π-radical anion by molecular oxygen is much slower but leads subsequently to formation of the hydroperoxyl radical. Addition between the two radicals leads to formation of CAT.

3.3 Photobleaching of the isolated reagents

Indigo is insoluble in water and indeed in many common organic solvents. It dissolves reasonably well in dimethylsulfoxide (DMSO), however, and this solvent was used for many of our photochemical studies. Additional experiments were made in N, N-dimethylformamide (DMF), which is a moderately good solvent for indigo. In DMSO, the solution shows a strong absorption band centred at ca. 610 nm, where the molar absorption coefficient is 22,140 M^{-1} cm^{-1}. Solutions of indigo are stable over prolonged periods when left in ambient lighting. Illumination of the air-equilibrated solution with white (λ>400 nm) light has little effect and after 250 minutes of continuous exposure there was less than 5% loss of the chromophore. On prolonged illumination (Figure 2), the chromophore slowly bleaches to give a transparent product (most likely some derivative of isatin). During the photofading process, the absorption maximum appears to undergo a modest (i.e., 3 nm) blue shift but this is difficult to follow with any real certainty (Figure 3). Photobleaching is irreversible in both DMSO and DMF solutions and requires the presence of O_2.

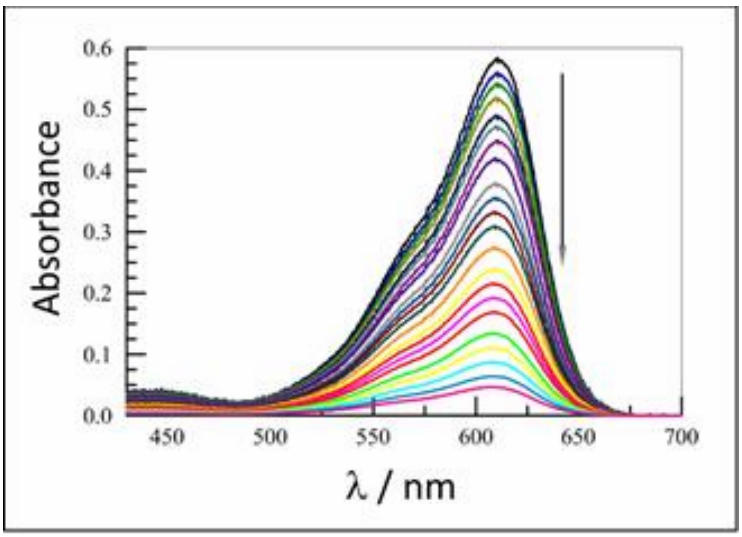

Figure 2. Stepwise bleaching of indigo in air-equilibrated DMSO under white light illumination. Spectra were recorded at various time intervals over a period of 240 hours. Note the small blue shift that accompanies bleaching of the chromophore.

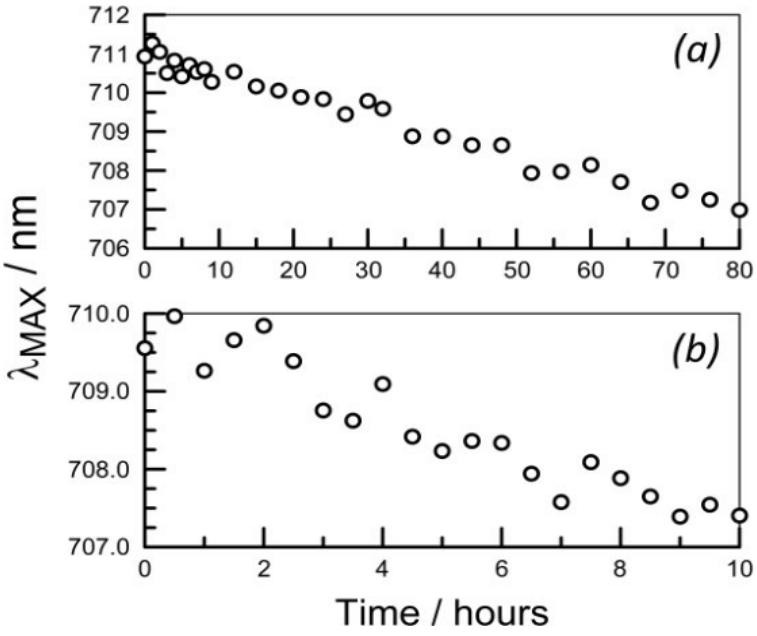

Figure 3. Progressive shift of the absorption maximum recorded for indigo in DMSO solution during illumination. (a) Direct illumination of indigo in air-equilibrated solution. (b) Indirect illumination of indigo in the presence of CAT as light absorber.

$$\frac{[indigo]}{[indigo]_0} = A_1 \exp^{-k_1 t} + A_2 \exp^{-k_2 t} \quad (1)$$

The course of reaction can be followed conveniently by absorption spectrophotometry, where bleaching appears to follow a two-step process (Figure 4). Indeed, the absorbance change at any wavelength can be well explained as the sum of two exponential processes (Equation 1). The initial step (k_1 = 0.21 ± 0.02 h-1) accounts for between 5 and 10% of the total change while the slower step (k_2 = 0.011 ± 0.002 h-1) is responsible for the more significant absorption change. Similar results were observed in DMF solution and with different samples of DMSO. Drying the solvent had no obvious effect on the rate of photobleaching. Removing molecular oxygen from the solution caused a substantial (i.e., 8-fold) decrease in the rate of bleaching.

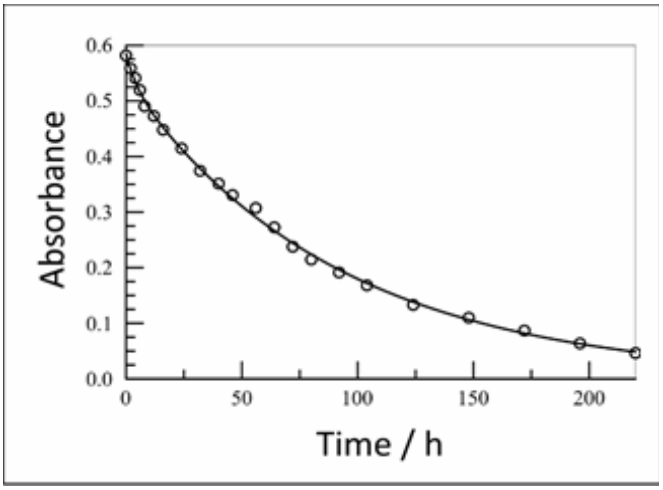

Figure 4. Kinetic plot for the absorbance change at 610 nm accompanying photobleaching of indigo in air-equilibrated DMSO. The line drawn through the data points corresponds to a fit to Equation 1.

Both steps, however, were found to speed up with increasing light intensity (Figure 5). Indeed, the average rate of chromophore bleaching increases linearly with increasing light intensity. It is this feature that causes the apparent first-order rate law (ignoring the initial loss of a few percent of indigo) since the rate of bleaching depends critically on the rate of photon uptake. The latter depends on incident light intensity and the molar concentration of chromophore. Even at high photon flux, the overall rate of loss of colour remains very slow. Adding furfuryl alcohol (2M) to the air-equilibrated solution stabilizes the chromophore against bleaching, at least over 20h of

continuous illumination. This latter substrate is considered to be a trap for singlet molecular oxygen.[25]

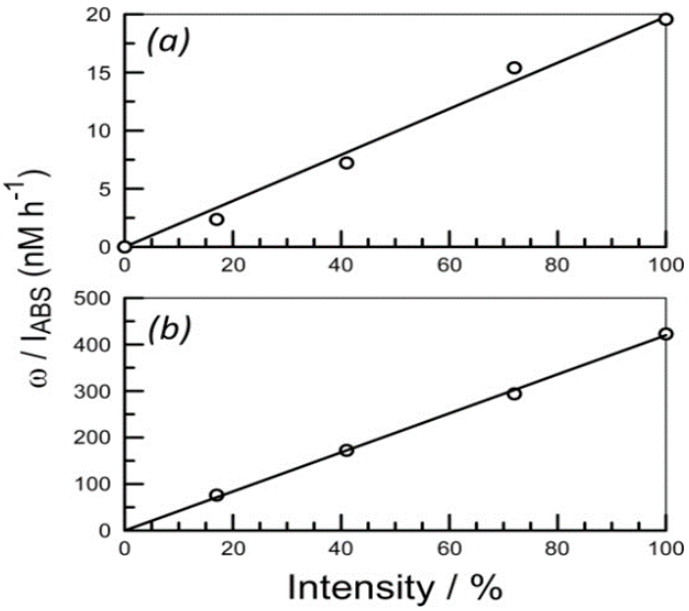

Figure 5. Effect of incident light intensity, as modulated with neutral density filters, on the rate of photobleaching of indigo in air-equilibrated DMF solution. (a) Direct illumination of indigo in air-equilibrated solution. (b) Indirect illumination of indigo in the presence of CAT as light absorber.

Under comparable conditions with respect to the rate of photon absorption, CAT undergoes[14] somewhat more efficient photobleaching when illuminated in air- equilibrated DMSO at 20 ^{0}C. Here, the absorption maximum occurs at ca. 470 nm, this being characteristic of the BOPHY chromophore,[26] where the molar absorption coefficient is 38,000 M^{-1} cm^{-1}. During photolysis of CAT with white (λ>400 nm) light, the absorption band bleaches without formation of a significant amount of a coloured intermediate. At short illumination times, the bleaching kinetics are zero-order with respect to the concentration of CAT, provided the fraction of light absorbed[27] by the chromophore is taken into account. For a typical experiment, the rate of loss of chromophore corresponds to ca. 0.45 μM h^{-1}. Over longer illumination periods, the bleaching reaction becomes auto- catalytic.[28] Our current understanding of the overall process is that photolysis in air-

equilibrated solution results in formation of the hydroperoxide, C-OOH, in modest yield.[14] This reactive species is responsible for the auto-catalysis and leads to both bleaching of the BOPHY chromophore and irreversible loss of one of the butylated hydroxytoluene residues.

It is difficult to make a direct comparison between the rates of decolouration of the two compounds because of the different reaction kinetics. However, restricting attention to the first ten hours of illumination, we can obtain consistent bleaching rates of 0.45 ± 0.06 μM h^{-1} for CAT. With the same rate of photon absorption by indigo, the average rate of bleaching is 0.011 ± 0.003 μM h^{-1}. Thus, on average, CAT bleaches some 40-fold faster than indigo in air-equilibrated DMSO.

3.4 Indirect photobleaching of Indigo

Illumination of a mixture of CAT (11 μM) and indigo (17 μM) in air-equilibrated DMF solution with an LED emitting at 425 ± 15 nm, where indigo does not absorb appreciably, was carried out for a total of 75 hours. During this period, there was considerable (i.e., ca. >90%) loss of indigo (Figure 6). Over the same period, roughly 10% of CAT was lost; most of this bleaching occurs towards the end of the reaction where the concentration of indigo has been seriously depleted. At early stages, bleaching of indigo involves very little loss of CAT. Without added indigo, some 30% of CAT bleaches over the same illumination period. Without CAT, there is no loss of indigo under these conditions. At an initial CAT concentration of 11 μM, which absorbs around 60% of the LED output, it was found that the minimum concentration of indigo needed to suppress loss of CAT was ca. 22 ± 4 μM. This is considered to be quite low and therefore consistent with the notion that the active catalyst is relatively long lived. Using such low concentrations of indigo to trap the active species, it was observed that bleaching of indigo could be roughly approximated to first-order kinetics at fixed light intensity and at a given initial concentration of CAT (Figure 6). For the specific example shown in Figure 7, the crude first-order rate constant for loss of indigo is ca. 0.011 ± 0.002 h^{-1}. This value is given simply as a measure of the bleaching efficacy and should not be considered as a “genuine” rate constant. Furthermore, it applies only to the set experimental conditions used for the experiment, especially with respect to light absorption by CAT.

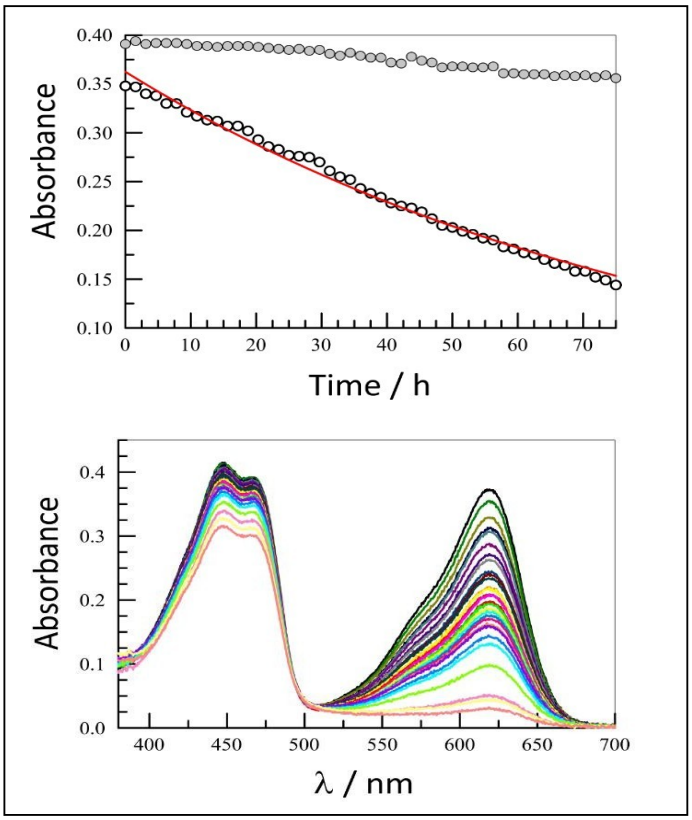

Figure 6. The lower panel provides overlaid absorption spectra following the bleaching of indigo induced by photolysis of CAT. Spectra were recorded at various times over a period of 80 hours of continuous illumination. The upper panel shows how the absorbance changes at wavelengths corresponding to CAT (grey solid circles) and indigo (open circles). The red line drawn through the latter points corresponds to the best fit to a first-order reaction.

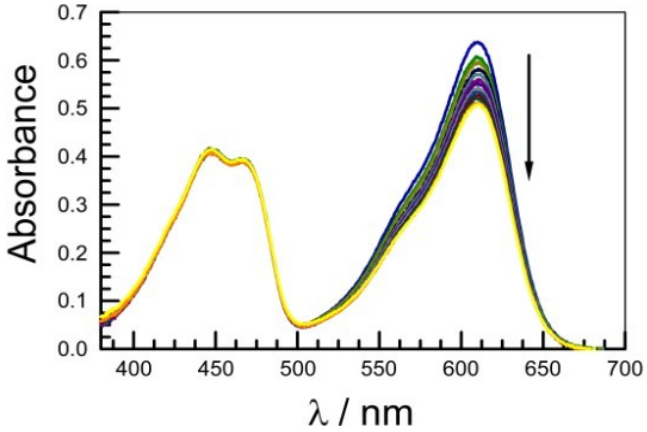

Figure 7. Typical reaction profile recorded for the indirect photobleaching of indigo using CAT as photocatalyst. The arrow indicates the course of reaction. Illumination is made at 425 nm.

The rate (ω) of catalyzed bleaching of indigo was found to depend linearly on the incident light intensity for a given concentration of CAT. The rate, in fact, correlates with the rate of photon uptake by CAT which can be modulated by light intensity and/or CAT concentration.[29] This rate remains essentially constant over 10 hours of continuous illumination but depends markedly on the initial concentration of indigo. In fact, the rate of bleaching appears to increase linearly with increasing concentration of indigo at low substrate concentrations but begins to reach a plateau at higher concentrations (Figure 8). The projected maximum rate of bleaching of indigo, as extrapolated from the plot, corresponds to ca. 1 μM per h. This behaviour can be explained in terms of indigo intercepting one of the key reaction intermediates involved in preparation of the active catalyst. Given the known chemistry, this intermediate is most likely the superoxide anion. This leads to the overall reaction sequence illustrated in Scheme 3 and requires that bleaching of indigo via CAT is considerably more effective than is direct reaction with superoxide anions. Confirmation of this latter point was obtained by the increased ω observed at higher CAT concentration for the same initial concentration of indigo, after allowance for the disparate photon uptake.

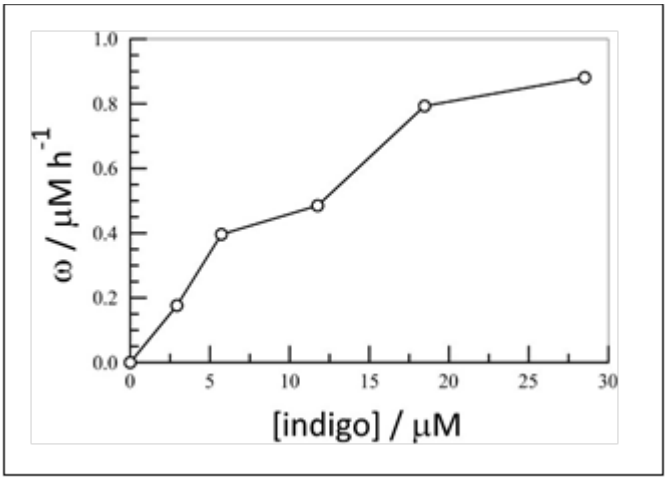

Figure 8. Effect of initial indigo concentration on the rate of bleaching of indigo following illumination of CAT (9 μM) at 425 nm.

Scheme 3 is intended to highlight the possible interference created at high concentrations of indigo. Thus, the catalytic cycle requires that the BHT group remains active following reaction with indigo. This feature is illustrated by step (d) and involves transfer of the hydroperoxyl radical from C-OOH to indigo. The resultant CAT-derived radical is the same species as formed by light- induced intramolecular charge transfer and subsequent loss of a proton (step (a)). This radical needs to undergo an addition reaction with the hydroperoxyl radical (step (c)) to form the active catalyst. The alternative is some type of inactivation that retains the BOPHY chromophore but loses the oxidative capacity of the BHT unit. The key intermediate, therefore, is the superoxide anion which is the main source of hydroperoxyl radicals (step (b)). Interception of this radical anion by indigo causes bleaching of the latter but this is not catalytic since CAT becomes inactivated. As such, the relative concentrations of indigo and CAT need careful optimization to obtain the maximum efficacy for bleaching.

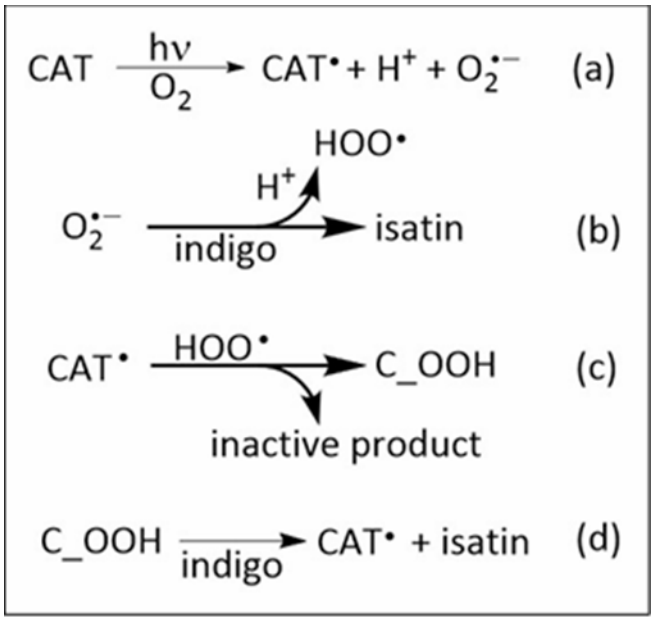

Scheme 3. Reaction sequence proposed to account for the indirect bleaching of indigo following illumination of CAT in air-equilibrated solution.

On long illumination times, it becomes possible to completely bleach indigo but with only modest consumption of CAT. The degradation of CAT occurs as the concentration of indigo decreases and is probably caused by incomplete trapping of the reactive intermediates. A product accumulates in the near-UV region, with an absorption maximum at 320 nm (Figure 9). This was not characterized but the absorption spectrum bears a reasonable resemblance to that of isatin,[30] bearing in mind the screening effect imposed by CAT. It should also be noted that isatin is photochemically active[31] and is likely to react via hydrogen atom abstraction from the solvent or one of the reagents under the conditions of the experiment. Loss of CAT could be prevented by adding extra indigo to compensate for loss of the latter during the bleaching process. In this case, the catalysed reaction could be continued for more than two weeks with less than 20% loss of CAT.

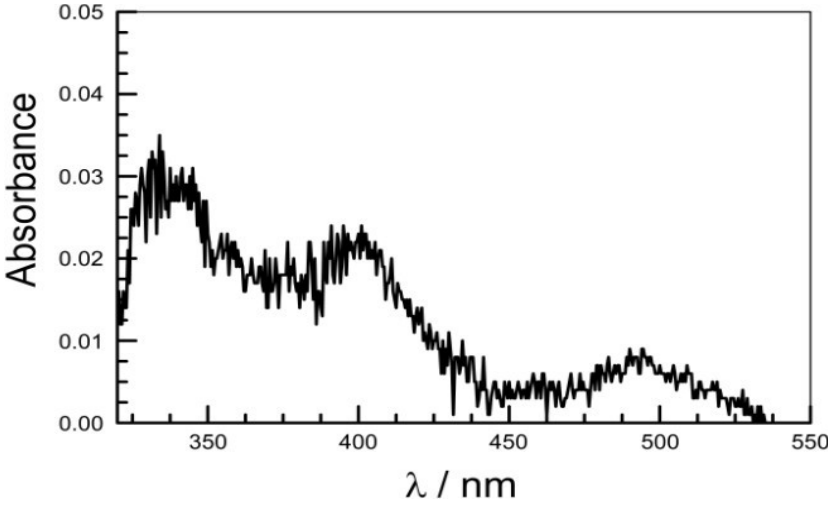

Figure 9. Absorption spectrum derived for the breakdown product derived from indirect photobleaching of indigo in air-equilibrated DMSO solution.

Under optimized conditions, with relatively low light intensity, the quantum yield for catalysed loss of indigo was determined to be ca. 2×10^{-3}. One molecule of CAT can bleach around 40 molecules of indigo in DMSO and ca. 30 molecules in DMF. Bleaching demands the presence of molecular oxygen. The decolouration of indigo occurs with sunlight as the source.

3.5 Effect of adventitious butylated hydroxytoluene (BHT)

A set of experiments was performed in order to assess the significance of covalent attachment[14] of the anti-oxidant BHT[32] to the BOPHY-based chromophore. Here, a mixture of CAT (12 μM) and indigo (18 μM) in air-equilibrated DMSO was exposed to the white-light source for a total of 10 hours. Absorbance measurements were made at frequent intervals. Under these conditions, there was essentially no loss (i.e., <3%) of CAT but indigo bleached via first-order kinetics with an effective rate constant of 0.0078 ± 0.0008 h^{-1}. Bleaching of indigo was not observed when the experiment was repeated with a 550 nm cut-off filter in front of the sample cell, indicating that the origin of the loss of indigo was C-OOH. This was confirmed by illumination of the mixture with a 550-nm short wavelength pass filter where the rate of bleaching of indigo was the same as observed without the filter. Addition of butylated hydroxytoluene (BHT) at a concentration of 1 mM resulted in a two-fold increase in the rate of bleaching of indigo but did not cause loss of CAT. Omitting CAT from this latter mixture caused the rate of bleaching to fall by roughly 50%. In the absence of CAT, but with added BHT (1 mM), placing a concentrated solution of indigo in front of the sample cell stopped the bleaching reaction. Thus, under these conditions, bleaching of indigo is initiated by BHT reacting with an excited state of the dye.

Following the work of Melo et al.,[19,20] the triplet state of indigo could be detected by transient absorption spectroscopy following excitation of a de-aerated DMF solution with a 4-ns laser pulse at 610 nm. The differential absorption signal was of low intensity (Figure 10), with a maximum at ca. 525 nm, and required multiple averages in order to obtain a convincing spectrum. The signal-to-noise, however, was sufficient to estimate a triplet lifetime of 19 ± 4 μs. This triplet lifetime was shortened to ca. 9 μs upon addition of BHT (10 mM) to the solution. The signal was too small to allow accurate derivation of the bimolecular quenching rate constant but appears to confirm that the indigo triplet is reduced by BHT in polar solvent. It might be stressed that there is a problem removing the dissolved oxygen from the viscous DMSO solvent.

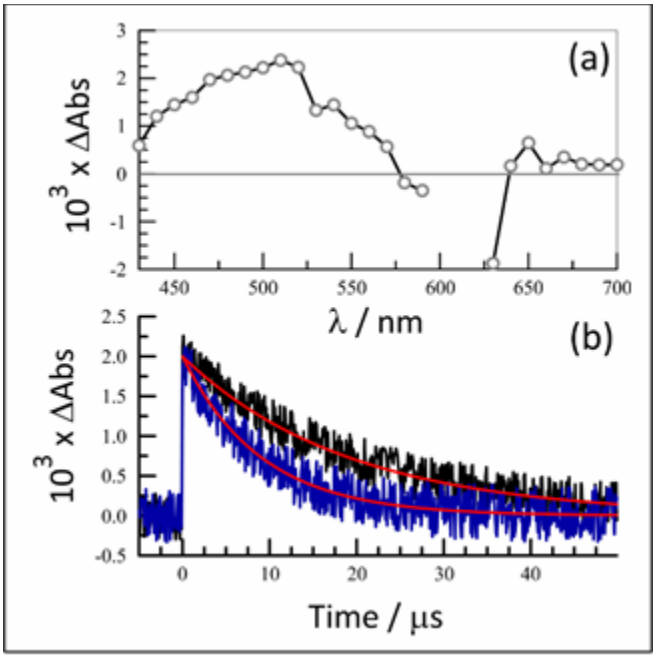

Figure 10. (a) Transient differential absorption spectrum recorded following laser excitation of indigo in de-aerated DMSO solution. The excitation wavelength was 610 nm. (b) Kinetic decay traces recorded at 525 nm in the absence (black curve) and presence (blue curve) of BHT (10mM). The red lines drawn through the data curves correspond to first-order fits of 19 and 9 μs, respectively.

Returning to the decolouration of indigo in the absence of CAT, it was observed that the rate ($_{\omega}$) of photobleaching was constant for the first 10 hours of illumination. The derived value of ω was very low but increased dramatically on addition of BHT (Figure 11). The rate continued to increase with increasing concentration of BHT but tended towards a plateau at high concentrations. This indicates that interception of the triplet state by BHT is not rate limiting under these latter conditions. Instead, the bottleneck appears to be the rate of generation of the triplet state. This is evident by the linear relationship between ω and the rate of photon uptake. The latter can be modulated by varying the incident light intensity or by changing the concentration of indigo. The overall reaction is illustrated by way of Scheme 4. At high concentrations of added BHT ([BHT] >25 mM), the bleaching kinetics become mildly auto-catalytic.[28]

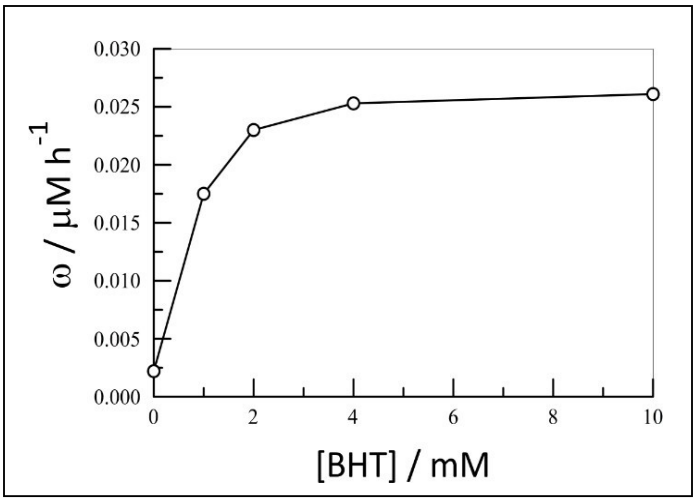

Figure 11. Effect of added BHT on the rate of photobleaching of indigo on exposure to broadband illumination.

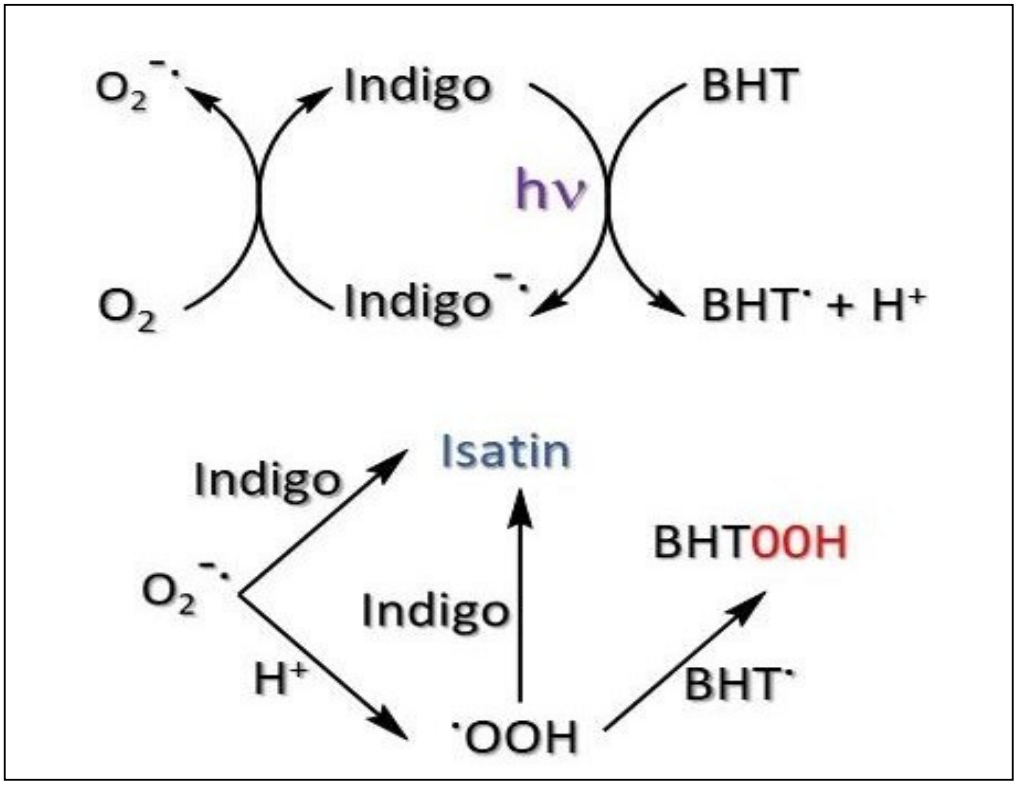

Scheme 4. Reaction sequence proposed to explain the photobleaching of indigo in the presence of added BHT but without CAT. The triplet lifetime of 19 ± 4 μs. This triplet lifetime was shortened to ca. 9 μs upon addition of BHT (10 mM) to the solution.

3.6 Conclusions

This work has introduced[14] a new type of photobleaching strategy and applied the protocol to the decolouration of the classical dye indigo in fluid solution. Useful rates of photobleaching have been observed that significantly exceed rates found by direct illumination of indigo.[17, 18] The active ingredient is believed to be an organic hydroperoxide[14] but this might change during the course of the reaction. Indeed, it is difficult to devise a reaction cycle that leads to regeneration of the hydroperoxide. There are no such difficulties, however, if the catalytic species changes to become a peroxyl radical. The end product from catalyzed degradation of indigo appears to be isatin[30, 31] but this is not recognized as being an important resource. Rather, the main purpose of the work is to introduce a means for the photochemical removal of colourants from solution. The turnover frequency and turnover number need to be increased significantly before a practical outlet can be imagined but there is considerable scope for optimisation. It remains to be seen if an effective water-soluble form of the photocatalyst can be realized. If so, this could lead to a critical advance in water treatment strategies.

An interesting side-effect concerns the comparison of intra- and intermolecular reactions in terms of the anti-oxidant. The most effective catalytic chemistry is observed with CAT which makes use of a light-induced intramolecular charge-transfer reaction to form the active species. A modified version of the reaction sequence can be obtained by illumination of indigo in the presence of excess anti-oxidant. This route avoids the expensive synthesis of CAT but leads to a much inferior reactivity that is not catalytic.

3.7 References

[1] (a) C. A. K. Gouvêa, F. Wypych, S. G. Moraes, N. Durán, N. Nagata, P. Peralta-Zamora, *Chemosphere.* **2000**, 40, 433. (b) C. Pan, Y. Zhu, *Environ. Sci. Technol.* **2010**, 44, 5570. (c) H. Wang, Y. Wu, M. Feng, W. Tu, T. Xiao, T. Xiong, H. Ang, X. Yuan, *J. W. Chew, Water Res.* **2018**, 144, 215.

[2](a) M. Y. Ghaly, G. Härtel, R. Mayer, R. Haseneder, *Waste Management*. **2001**, 21, 41. (b) C. Sirtori, A. Zapata, I. Oller, W. Gernjak, A. Agüera, S. Malato, *Water Res*. **2009**, 43, 661. (c) M. M. Ahmed, S. Chiron, *Water Res*. 2014, 48, 229. (d) A. G. Trovó, T. F. S. Silva, O. Gomes, A. E. H. Machado, W. B. Neto, P. S. Muller, D. Daniel, *Chemosphere*. **2013**, 90, 170.

[3] (a) D. E. Latch, B. L. Stender, J. L. Packer, W. A. Arnold, K. McNeill, *Environ. Sci. Technol*. **2003**, 37, 3342. (b) N. H. Ince, *Water Res*. **1999,** 33, 1080. (c) X. Tao, W. Ma, T. Zhang. *J. Zhao, Chem. Eur. J.* **2002,** 8, 1321. (d) S. Natarajan, H. C. Bajaj, R. J. Tayade*, J. Environ. Sci. (China).* **2018**, 65, 201. (e) E. Tauchert, S. Schneider, J. L. de Morais, P. Peralta-Zamora, *Chemosphere***. 2006**, 64, 1458.

[4] J. Griffiths, in Developments in the Chemistry and Technology of Organic Dyes, Editor: J. Griffiths, Blackwell, London, **1984.**

[5] M. L. Marin, L. Santos-Juanes, A. Arques, A. M. Amat, M. A*. Chem. Rev.* **2012**, 112, 1710.

[6] (a) S. J. Formosinho*, J. Chem. Soc. Faraday Trans. 2,* **1976,** 72, 1313. (b) W. M. Moore, J. T. Spence, F. A. Raymond, S. D. Colson, *J. Am. Chem. Soc*. **1963**, 85, 3367. (c) N. S. Allen, F. Catalina, P. N. Green, W. A. Green, *J. Photochem***. 1987**, 36, 99.

[7] (a) M. Hasegawa, K. Horie, *Prog. Polym. Sci***. 2001**, 26, 259. (b) T. Grossetête, A. Rivaton, J. L.

Gardette, C. E. Hoyle, M. Ziemer, D. R. Fagerburg, H. Clauberg, Polym. **2000**, 41, 3541. (c) H.-G. Heine, H.- J. Rosenkranz, H. Rudolph, Chem. Int. Ed. **1972**, 11, 974. (d) M. Oelgemöller N. Hoffmann, *Pure Appl. Chem*. **2015**, 87, 569.

[8] (a) A. A. Krasnovsky, Jr, *Membrane Cell Biol*. **1998**, 12, 665. (b) P. B. Merkel, D.R. Kearns, *J. Am. Chem. Soc*. **1972**, 94, 7244. (c) F. Wilkinson, J. G. Brummer, *J. Phys. Chem. Ref. Data.* **1981**, 10, 809. (d) H. Sies, C. Berndt D. P. Jones, Ann. Rev. Biochem. **2017**, 86, 715.

[9] C. Schweitzer, R. Schmidt, *Chem. Rev*. **2003,** 103, 1685.

[10] F. Wilkinson, W. P. Helman, A. B. Ross, *J. Phys. Chem. Ref. Data*. **1993**, 22, 113.

[11] S. Yu. Egorov, V. F. Kamalov, N. I. Koroteev, A. A. Krasnovsky Jr., B. N. Toleutaev, S. V. Zinukov, *Chem. Phys. Lett.* **1989,** 163, 421.

[12] (a) F. Wilkinson, W. P. Helman, A. B. Ross, *J. Phys. Chem. Ref. Data.* **1995,** 24, 663. (b) R. H. Young, D. Brewer, R. A. Keller, *J. Am. Chem. Soc*. **1973**, 95, 375.

[13] (a) P. Montaña, N. Pappano, N. Debattista, V. Ávila, A. Posadaz, S. G. Bertolotti, N. A. García, Can. *J. Chem*. **2003**, 81, 909. (b) R. M. Baxter, *J. H. Carey, Nature*. **1983**, 306, 575.

[14] D. Sirbu, O. J. Woodford, A. C. Benniston, A. Harriman, *Photochem. Photobiol. Sci.* **2018**, *17*, 750.

[15] (a) H. Schmidt, *Melliand Int*. **1979,** 2, 89. (b) M. M. Sousa, C. Miguel, I. Rodrigues, A. J. Parola, F. Pina, J. S. Seixas De Melo, M. *J. Melo, Photochem. Photobiol. Sci*. **2008**, *7*, 1353. (c) N. R. Krishnaswamy, C. N. Sundaresan, *Resonance.* **2012**, *17*, 1022.

[16] (a) K. G. Gilbert, D. T. Cooke, *Plant Growth Regulation*. **2001**, *34*, 57. (b) A. Pala, Ind. *J. Environ. Health.* **2001**, *43*, 128. (c) Q. Ma, Y. Qu, X. Zhang, B. Xu, J. Zhou, Chin. *J. Appl. Environ. Biol*. **2012**, *18*, 344. (d) K. K. Agarwal, *Colourage*. **2003**, *50*, 37.

[17] (a) N. Kuramoto, T. Kitao, *J. Soc. Dyers Colourists*. **1979**, *95*, 257. (b) R. Rondão, J. S. Seixas de Melo, G. Voss, *ChemPhysChem.* **2010**, *11*, 1903. (c) P. M. Dellamatrice, M. E. Silva-Stenico, L. A. B.D. Moraes,

M. F. Fiore, R. T. R. Monteiro, Braz. *J. Microbiol*. **2017**, 48, 25. (d) M. Cano, Solis, J. Diaz, A. Solis, O. Loera
M. M. Teutli, African *J. Biotechnol*. **2011**, 10, 12224. (e) J.- B. He, G.-H. Ma, J.-C. Chen, Y. Yao, Y. Wang, Electrochimica Acta. **2010**, 55, 4845. (f) F. Henesey, *J. Soc. Dyers Colourists*. **1937**, 53, 347.

[18] (a) J. Pina, D. Sarmento, M. Accoto, P. L. Gentili, L. Vaccaro, A. Galvão, J. S. Seixas De Melo, *J. Phys. Chem. B.* **2017**, *121*, 2308. (b) N. Gandra, A. T. Frank, O. Le Gendre, N. Sawwan, D. Aebisher, J. F. Liebman, K. N. Houk, A. Greer, R. Gao,
Tetrahedron. **2006**, *62*, 10771. (c) P. Novotná, J. J. Boon, J. van der Horst, V. Pacáková, *Coloration Technol.* **2003**, *19*, 121.

[19] J. S. Seixas De Melo, R. Rondão, H. D. Burrows, M. J. Melo, S. Navaratnam, R. Edge, G. Voss, *J. Phys. Chem. A.* **2006**, *110*, 13653.

[20] J. S. Seixas De Melo, H. D. Burrows, C. Serpa and L. G. Arnaut, *Chem. Int. Ed.* **2007**, *46*, 2094.

[21] C. Iuga, E. Ortíz, J. R. Alvarez-Idaboy. A. Vivier-Bunge, *J. Phys. Chem. A*. **2012**, *116*, 3643.

[22] (a) A. J. Kettle, B. M. Clark. C. C. Winterbourn, *J. Biol. Chem*. **2004**, *279*, 18521. (b) N. Kuramoto, T. Kitao, *J. Soc. Dyers Colourists*. **1982**, *98*, 159.

[23] I.-S. Tamgho, A. Hasheminasab, J. T. Engle, V. N. Nemykin, C. J. Ziegler, *J. Am. Chem. Soc*. **2014**, *136*, 5623.

[24] G. Ulrich, R. Ziessel, A. Harriman, Angew. *Chem. Int. Ed.* **2008**, *47*, 1184.

[25] M. Carchesio, L. Tonucci, N. D'Alessandro, A. Morvillo, P. D. Boccio, M. Bressan, *J. Porphyrins Phthalocyanines*. **2010**, *14*, 499.

[26] O. J. Woodford, R. Ziessel, A. Harriman, C. Wills, A. A. Alsimaree, J. G. Knight, *Spectrochim. Acta - Part A*: Mol. Biomol. Spectroscopy. **2019**, *208*, 57.

[27] J. K. G. Karlsson, O. J. Woodford, R. Al-Aqar, A. Harriman, *J. Phys. Chem. A.* **2017**, *121*, 8569.

[28] (a) E. R. Thapaliya, S. Swaminathan, B. Captain F. M. Raymo, *J. Am. Chem. Soc*. **2014**, *136*, 13798. (c) D. Bartusik, M. Minnis, G. Ghosh, A. Greer, *J. Org. Chem.* **2013**, *78*, 8537. (d) M. Galajda, G. Lente, I. Fábián, *J. Am. Chem. Soc*. **2007**, *129*, 7738.

[29] (a) M. A. H. Alamiry, A. Harriman, A. Haefele, R. Ziessel, *ChemPhysChem.* **2015**, *16*, 1867. (b) A. Harriman, P. Stachelek, A. Sutter, R. Ziessel, *Photochem. Photobiol. Sci*. **2015**, *14*, 1100.

[30] (a) M. Shahbazy, P. Pakravan, M. Kompany-Zareh, *J. Biomol. Struct. Dynamics.* **2017**, *35*, 2539. (b) S. Kashanian, M. M. Khodaei, P. Pakravan, *DNA Cell. Biol*. **2010**, *29*, 639. (c) C. M. Castevens, Theor. *Chem. Acc.* **2008**, *121*, 43. (d) V. Galasso, G. C. Pappalardo, *J. Chem. Soc. Perkin Trans.* **1976**, 2, 574. (d) P. D. Popp, Adv. *Heterocyclic Chem.* **1975**, *18(C)*, 1. (e) R. G. Ault, E. L. Hirst. R. A. Morton, *J. Chem. Soc.* **1935**, 1653. (f) W. N. Hartley, J. J. Dobbie, *J. Chem. Soc. Trans*. **1899**, *75*, 640.

[31] (a) M. T. Silva, J. C. Netto-Ferreira, *J. Photochem. Photobiol. A. Chem.* **2004**, *162*, 225. (b) G. Haucke, B. Seidel, A. Graness, *J. Photochem*. **1987**, 37, 139. (c) D.-D. Wu, M.-T. He, Q.- D. Liu,

W. Wang, J. Zhou, L. Wang, H.-K. Fun, J.-H. Xu, Y. Zhang, *Org. Biomol. Chem*. **2012**, *10*, 3626.

[32] (a) V. D. Kancheva, L. Saso, S. E. Angelova, M. C. Foti, A. Slavova-Kasakova, C. Daquino, V. Enchev, O. Firuzi, *J.*

Nechev, Biochim. **2012**, *94*, 403. (b) H. S. Black, C. M. Kleinhans, H. T. Hudson, *Photobiochem. Photobiophys*. **1980**, *1*, 119. (c) M. S. Noel-Hudson, C. de Belilovsky, N. Petit, A. Lindenbaum, *J. Wepierre, Toxicology in Vitro*. **1989**, *3*, 103.

Chapter 4.

Inhibition of the Photobleaching of Methylene Blue by Association with Urea

FIGURE: Methylene Blue Dye Reduction

Keeping the blue colour…

4.1 Summary

Methylene Blue has a long history in photochemistry and is known to undergo photofading on exposure to visible light in aqueous solution. Under aerobic conditions, photobleaching occurs by way of a two-step process involving intermediary formation of singlet oxygen. The first step is ascribed to regio-selective addition of singlet oxygen within the precursor complex. This geminate reaction ultimately leads to formation of the leuco-dye via a slower second step. Urea forms a weak ground-state complex with Methylene Blue which affects the optical properties of the dye but is not evident by NMR spectroscopy. This complex is weakly fluorescent and undergoes intersystem crossing to the triplet manifold. The presence of urea decreases the rate of photobleaching of the dye and, at high concentrations of urea, the bleaching kinetics are consistent with an equilibrium mixture of complexed and free dye. The complexed dye does not bleach on the timescale of the experiment. Such protection might arise from urea blocking access to the site where geminate addition of O_2 takes place.

4.2 Introduction

Most organic substances are susceptible to light-induced degradation in both solution and solid phases. [1] Such photochemical bleaching, which is also a feature of natural photosynthesis, [2] can restrict the usefulness of certain classes of dye as components in optical devices. However, controlled photofading can be a valuable tool in terms of removing the chromophore after completion of desired tasks, for example following photodynamic therapy. [3] Numerous disparate mechanisms have been proposed to account for dye photobleaching in particular cases, the most common being the triplet sensitization[4] of singlet molecular oxygen. Dyes that do not populate the triplet state with reasonable efficacy are not immune to photobleaching[5] and removal of molecular oxygen is not guaranteed to prevent colour loss. [6] More often than not, unique products

do not evolve during the bleaching process, especially under white light illumination, and instead a distribution of breakdown products arises. In certain cases, [7] a cascade of well- defined intermediate species develops during the reaction so that the bleaching kinetics can be considered in some detail. In general, quantum yields for photofading tend to be very low but recen t observations[7,8] of autocatalysis mean that such measurements might be misleading. The most common method by which to follow chromophore photobleaching is via the significance of light intensity and the role of molecular oxygen.[9-11]

Well accepted practices for minimizing the effects of photofading include immobilisation of the dye in solid media, [12] incorporation of UV screens[13] and removal of heat from the system. Other simple approaches to increasing the duty cycle for the dye include incorporation of anti- oxidants. [14] The emergence of super-resolution microscopy and single-molecule spectroscopy has emphasized the need for photochemically stable dyes[15] and new strategies for protecting the chromophores have been introduced over the past decade. [16] Unlike in natural photosynthesis, [17] however, these protective methods do not include in-situ repair processes and more-often-than- not involve encasing the dye in an expensive package. As more-and-more dyes enter the marketplace, new and innovative protocols are needed to circumvent the destructive bleaching events. One way to achieve this ideal, taken from natural systems, [18] is to identify and block a key intermediate or reaction cycle. This type of smart technology, which must be closely associated with the underlying mechanism responsible for light-induced damage, has rarely been applied in artificial systems.

In developing a prototypic defensive strategy against photobleaching in fluid solution, we have turned our attention to Methylene Blue. This is a very well-known photosensitizer, [19] that exhibits photo-bactericidal activity in water. In fact, Methylene Blue was first synthesized in 1876 by Caro[20] and its capability to stain biological media was recognized [21] almost immediately. The dye associates strongly with DNA[22] and has found key applications in certain types of photodynamic therapy. [23] Under illumination in aqueous solution, Methylene Blue can be used to sensitize formation of singlet molecular oxygen and/or superoxide ions. [24] Although water soluble, the dye

is prone to aggregation in aqueous solution[25] and its properties are pH sensitive. [26] Photobleaching of Methylene Blue has been studied in some detail and the role of the triplet-excited state has been recognised. [27] The dye fades relatively quickly on exposure to sunlight, even in the absence of added electron donors, and has been reported to follow two-step kinetics. [28] By way of separate studies, considerable effort has been expended on following the destruction of Methylene Blue under illumination of certain semiconductors, such as TiO_2, which function as electron donors. [29] The leuco-form of the dye, generated by addition of a hydride anion, is often cited as being the most likely candidate for any transparent product. [30]

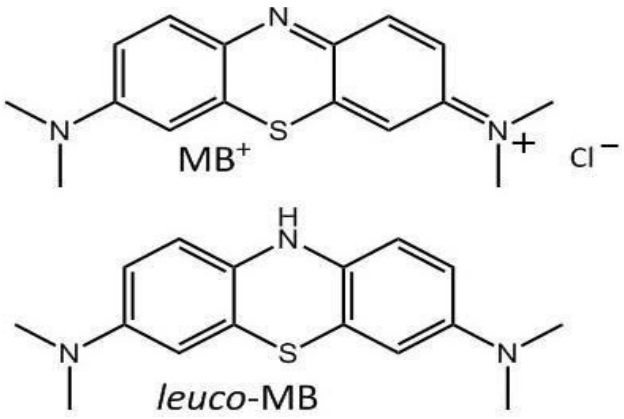

Figure 1. Molecular formulae for methylene blue and its leuco-form.

The present work seeks to develop a simple and inexpensive strategy that inhibits photochemical bleaching of Methylene Blue in aqueous solution. The intention is to extinguish the bleaching reaction by blocking access to a crucial intermediate species. To simplify the reaction, air-equilibrated solutions are used. This ensures that the triplet-excited state of the dye reacts almost exclusively with molecular oxygen. It is also appropriate to avoid high (i.e., >10 μM) concentrations of dye where aggregation[25] should be anticipated. As an inhibitor, we have selected urea because of its molecular dimensions, cheap and ready availability reagent.

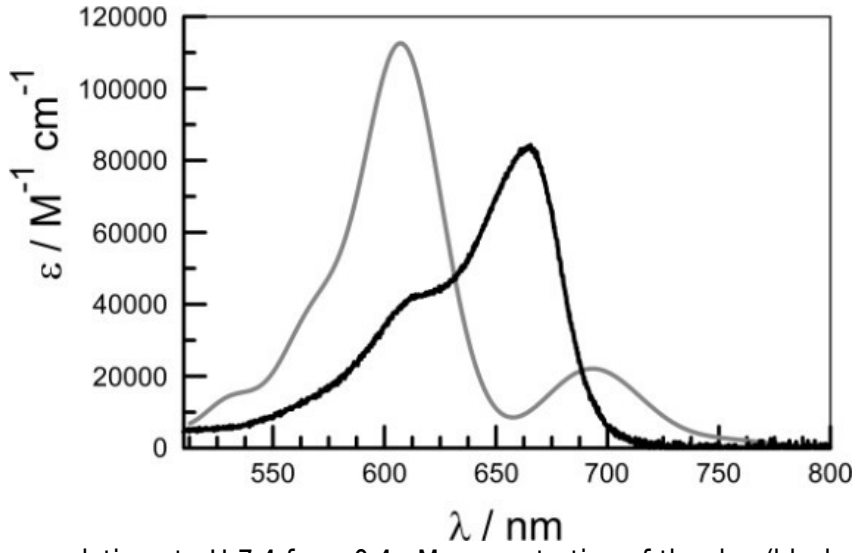

Figure 2. Absorption spectrum recorded for MB^+ in aqueous solution at pH 7.4 for a 0.4 μM concentration of the dye (black curve). The grey curve shows the corresponding absorption spectrum derived for the dimer as obtained by spectral deconstruction of spectra recorded at much higher concentration.

4.3 Properties of Methylene Blue

Methylene Blue (hereafter abbreviated as MB^+) in water at pH 7.4 exhibits a strong absorption maximum centred at 664 nm for which the molar absorption coefficient at the peak (λ_{MAX}) was determined to be 93,000 ± 7,000 M^{-1} cm^{-1} at low concentration. At higher concentrations, the absorption transition broadens and a new absorption band can be discerned with a maximum at ca. 610 nm (Figure 2). The ratio of absorbance values recorded at 664 and 610 nm can be used as a rough indication of the state of aggregation of the dye[31] (Figures 3-5).

4.4 Aggregation of Methylene Blue in water

Aggregation of MB^+ in water has been investigated over a long period of time and the literature contains many estimates of the dimerization constant measured under a variety of experimental conditions.[32] At very dilute concentrations, the absorption maximum attributable to the monomer lies at 665 nm (Figure 3). On increasing the concentration, this latter band decreases in intensity and a new band appears with a maximum at ca. 610 nm (Figure 3). Experiments were made with an optical cell having a variable path length so that the absorbance at 664 nm could be

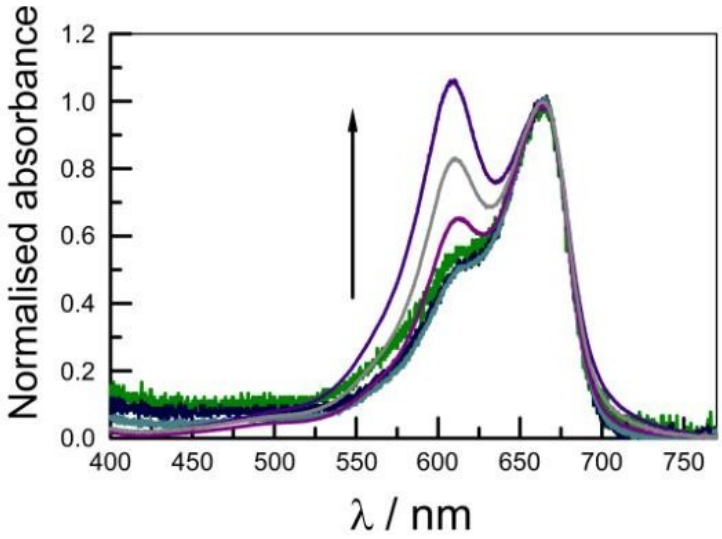

maintained at 1.0 over a wide concentration range. This clearly shows the build-up of the dimer at higher concentrations (Figure 3).

Figure 3. Absorption spectra recorded for aqueous solutions of MB^+ at different concentrations.

The arrow indicates the effect of increasing concentration. The spectra were recorded in an optical cell equipped with the capability to control the path length over an unusually wide range. This enabled the absorbance at 664 nm to be kept close to unity across the entire concentration window. Note the variation in the ratio of absorbance values recorded at 665 nm (i.e., the monomer) and 610 nm (i.e., the dimer).

Solutions of MB^+ in aqueous buffer at pH 7.4 do not follow the Beer-Lambert law (Figure 4). At wavelengths near to the absorption peak of 665 nm, the absorbance vs concentration profile shows negative deviation from linearity. Positive deviation is seen in the region where the dimer absorbs strongly. For these measurements, a variable path length optical cell was used so that the absorbance could be maintained at a reasonable value throughout the experiment. Global analysis, using 10 wavelengths selected across the entire wavelength range, allows accurate determination of the dimerization constant (K_D) under our conditions by way of iterative fitting the absorbance vs molar concentration profile at a given wavelength. Analysis was made using Equation 1, where α is the fraction of monomer at that total concentration (C_T) and A refers to observed absorbance. This analysis gives values for the molar absorption coefficient for the dimer

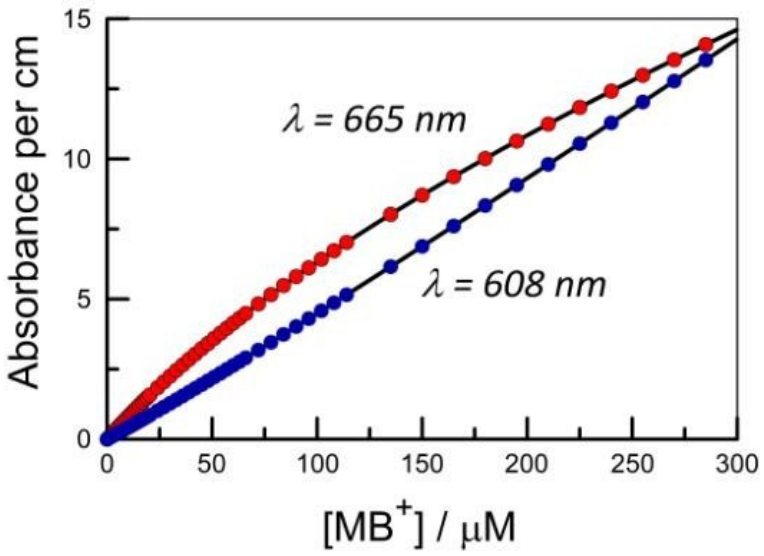

(ε_D) at that wavelength. The corresponding molar absorption coefficients for the monomer (ε_M) were determined from absorption spectra recorded for very dilute (<5 x 10^{-7} M) solutions in a long path length cell.

Figure 4. Concentrations vs absorbance plots recorded at 665 nm (red points) and 608 nm (blue points). Spectra were recorded with a variable path length cell that allowed the absorbance to be kept at a reasonable level. The solid line drawn through each set of data points corresponds to a nonlinear, least-squares fit to Equation 1. Values for the dimerization constant and molar absorption coefficient for the dimer were derived from these plots. The absorbance values have been converted to a path length of 1 cm.

According to Figure 3, the degree of aggregation of MB^+ in aqueous solution can be monitored conveniently by recording the ratio of absorbance values at 665 nm and at 610 nm. The former wavelength corresponds to the monomer and the latter wavelength is where the dimer (or aggregate) has its maximum absorption. This ratio was determined for a series of MB^+ solutions at various concentration and is illustrated below in Figure 5. It is seen that, at low concentrations, the ratio reaches an upper limit of ca. 2.05. This value is representative of the monomer absorption spectral profile. The dimer spectrum given as part of Figure 3 has a revised ratio of 0.094 and this represents the lower limit. At intermediate concentrations, the ratio falls progressively from 2.05 and, for example, reaches a value of 2.0 at a concentration of 3 μM (this being a typical MB^+ concentration used in the bleaching studies). Under the conditions used for our experiments, the dimerization constant, K_D, has a value of 2,480 M-1, as determined by fitting the absorption

spectra recorded over a wide concentration range (Figure 4). From the iterative fits, molar absorption coefficients for monomer at 665 nm and dimer at 608 nm, respectively, are found to be 84,285 M^{-1} cm^{-1} and 111,295 M^{-1} cm^{-1}. This information allows construction of a plot of ratio vs fraction of monomer (Figure 6) over the full concentration profile. Of course, changes in the solution composition, notably buffer concentration and temperature, will lead to a change in K_D. We did not explore these effects but note that there are literature reports referring to detailed studies of MB^+ aggregation in the presence [32] and absence of surfactants. [33] Our value for K_D falls at the higher end of literature values for MB^+ in water at 20 ° C, because of the relatively high ionic strength imposed by the buffer under these conditions.

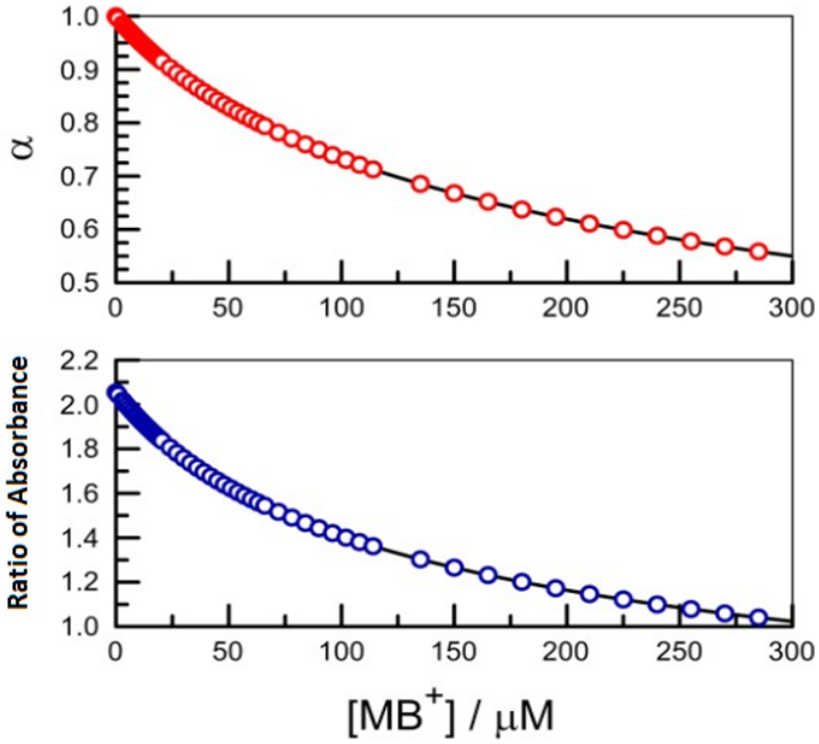

Figure 5. The upper panel shows the effect of total dye concentration on the fraction of monomer (α) present in solution, as calculated from Equation 2. The lower panel shows how total dye concentration affects

the ratio of absorbance values measured at 665 nm and at 610 nm. The latter values were obtained by way of Equation 3.

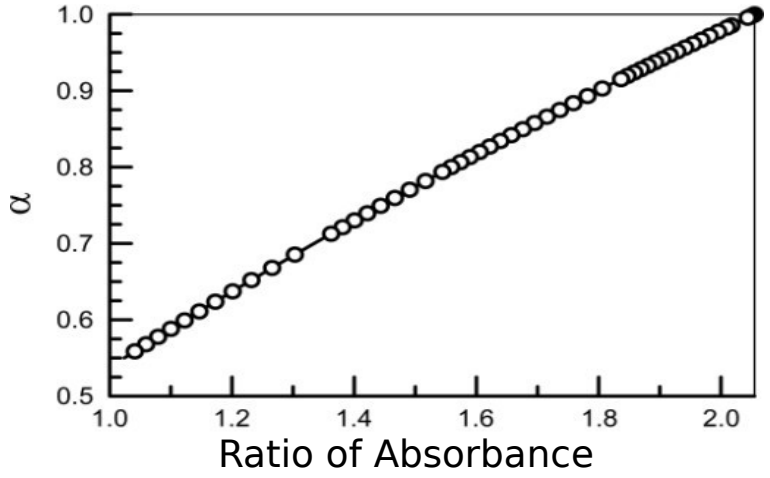

Figure 6. Relationship between the fraction of monomer (α) present in solution and the ratio of absorbance values as shown in Figure 5. This correlation has no theoretical significance but is a useful tool for determining the extent of dimerization of the dye.

$$C_T = C_M + 2C_D$$

$$A = \epsilon_M C_M + \varepsilon_D C_D$$

$$A = \varepsilon_M C_T \alpha + \varepsilon_D \left(\frac{C_T (1-\alpha)}{2} \right) (1)$$

$$K_D = \frac{C_D}{C_M^2} = \frac{1-\alpha}{2 C_T \alpha^2}$$

$$\alpha = \frac{-1+\sqrt{1+8 K_D C_T}}{4 K_D C_T} (2)$$

$$Ratio = \frac{C_T \alpha \varepsilon_M}{C_T \epsilon_D \left(\frac{1-\alpha}{2} \right)} (3)$$

From the spectral shifts, various aggregation patterns of the dyes in different media have been studied. The hypsochromically shifted H-bands (H for hypsochromic) and bathochromically shifted J bands (J for Jelly, one of the first researcher who investigated these shifts) of the aggregates have been explained in terms of molecular exciton coupling theory. From the absorption spectrum reported for the dimer in water as shown in Figure 3, the relative integrals under the relevant absorption bands for the J-type (λ_{MAX} = 695 nm) and H-type (λ_{MAX} = 607 nm) species are 12.6 and 87.4, respectively. This analysis was made by deconstructing the reduced absorption spectrum attributed for the dimer into the smallest number of Gaussian components needed to properly represent the spectrum (Figure 7). These Gaussian components were not restricted to a common half-width but values for the H and J bands, respectively, were determined during the analysis. On the basis of a head-to-tail stacked geometry for the dimer, [34] the twist angle between the transition dipole moment vectors in the stacked pair can be estimated[35] as being ca. 34^0. We were unable to resolve fluorescence attributable to the dimer, either by steady-state or time-resolved emission spectroscopy, although very weak emission from the J-band remains a possibility. Therefore, the emission shift related to the effect of urea on the fluorescence spectral profile recorded for MB^+ cannot be ascribed to the solute dissociating a dimer. In any case, under the optically dilute conditions used for fluorescence work, the extent of dimerization of MB^+ is less than 1%.

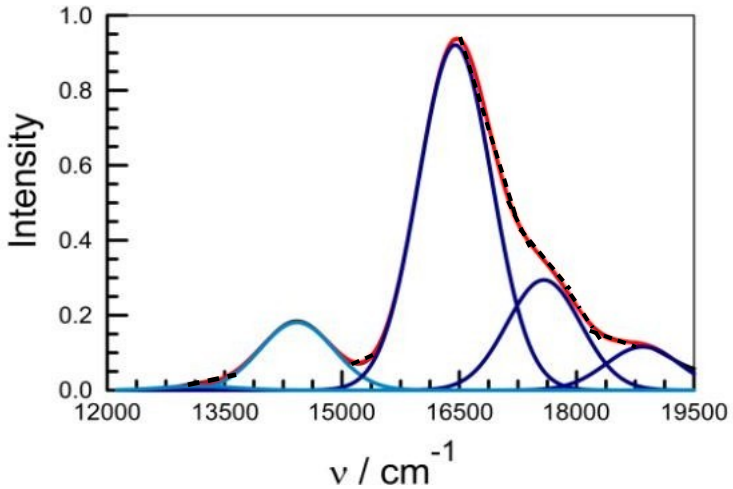

Figure 7. Deconstruction of the reduced absorption spectrum derived for the dimer into Gaussian-shaped components. The experimental spectrum is shown as a black dashed line while the red curve superimposed over this record corresponds to the sum of the Gaussian components.

Individual bands assigned to the H- and J-species are indicated in dark blue and light blue respectively. Integration of these bands allows determination of the twist angle suggested for the dimer on the basis of excitonic coupling. The energy gap between the H- and J-bands allows determination of the splitting energy, $R^2 = 0.99992470$.

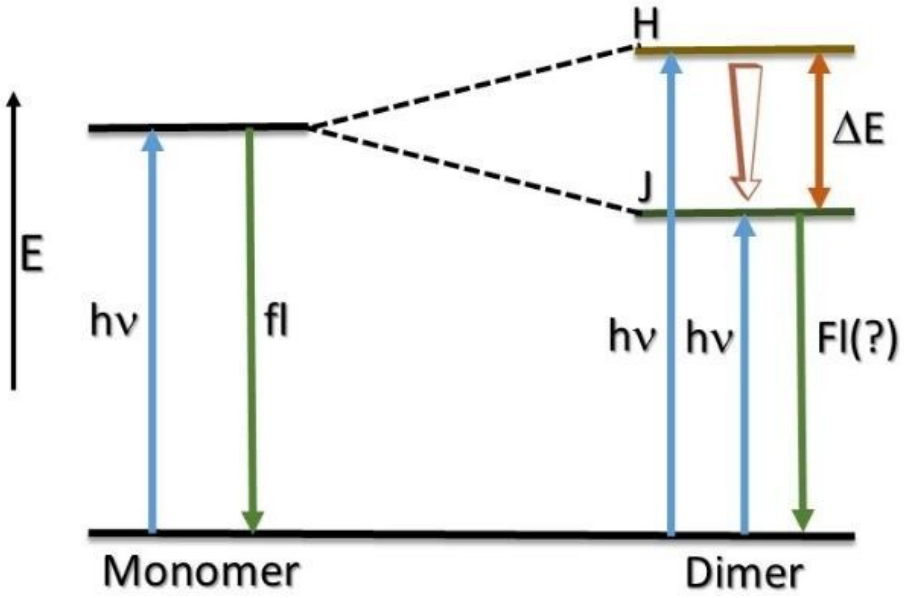

Figure 8. Simple representation of the excitonic splitting induced upon dimerization of the monomer. Fluorescence (Fl) is not detected for the dimer under our conditions.

Similar Gaussian deconstruction was applied to the reduced absorption spectrum for the monomer recorded at very low concentration. Here, the derived Gaussian components refer to the underlying vibronic envelope associated with Franck-Condon excitation (Figure 9).

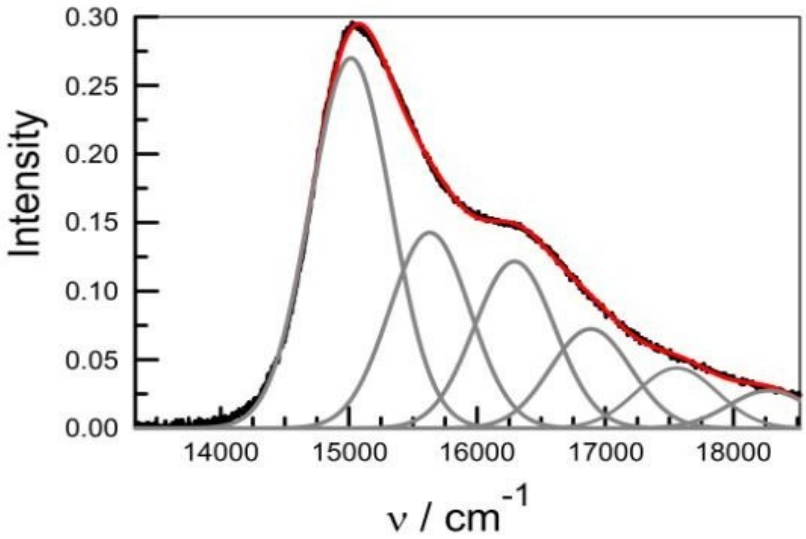

Figure 9. Gaussian analysis applied to the reduced absorption spectrum for the monomer of MB^+ in aqueous solution. The black curve is the experimental spectrum while the red curve red superimposed over the trace refers to the sum of the Gaussian components. The latter are shown as grey curves which displays vibrionic transition, $R^2 = 0.99905125$.

All subsequent photochemical experiments were carried out with an initial MB^+ concentration of <3 μM, where the fraction of dye present as an aggregated species is <3%. The dye is weakly fluorescent under such conditions. More specifically, the fluorescence maximum occurs at 690 nm, while the fluorescence quantum yield (Φ_F) and excited-state lifetime (τ_S) are 0.020 ± 0.005 and 345 ± 15 ps, respectively.[36] The triplet-excited state can be detected by laser flash photolysis following excitation at 610 nm (Figure 10). The triplet-excited state of MB^+ in water at pH 7.4 was monitored using laser flash photolysis with excitation at 610 nm (FWHM = 4 ns). An example of the transient differential absorption spectrum recorded after formation of the meta-stable triplet is provided below as Figure 10. The triplet absorbs primarily in the region around 400-430 nm, in agreement with literature reports.[37] Strong ground-state bleaching accompanies triplet formation and an isosbestic point is preserved around 550 nm. Decay of the triplet state fits reasonably well to first-order kinetics at low triplet concentration. Examples of the decay curves recorded for MB^+ in air-equilibrated water without and with the addition of urea (4M) are given as part of Figure 11. Also shown is the corresponding decay trace recorded for MB^+ after purging the solution with N_2. Kinetic traces were recorded at 410 nm. The derived triplet lifetimes for these three experiments are 3.0 μs, 9.2 μs and 35 μs, respectively.

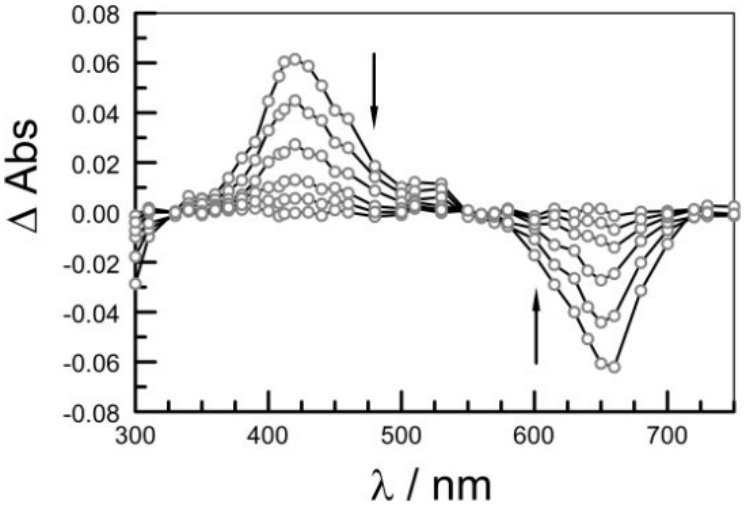

Figure 10. Transient differential absorption spectra recorded following excitation of MB^+ in air-equilibrated aqueous solution at pH 7.4. The excitation wavelength was 610 nm. The arrows indicate the recovery of the ground-state bleaching and decay of triplet absorption. Individual spectra were recorded at delay times of 120 ns, 1.05 μs, 2.65 μs, 4.7 μs, 6.25 μs and 25 μs after the excitation pulse.

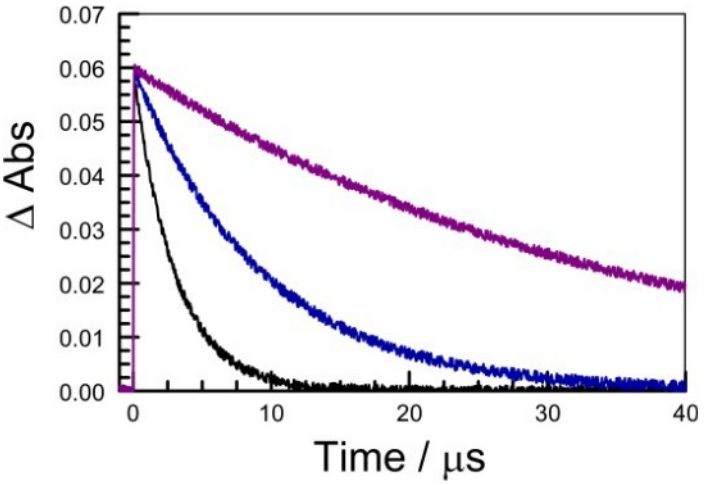

Figure 11. Examples of decay traces recorded for the triplet state of MB^+ in aqueous solution at pH 7.4. Individual traces refer to the triplet state in air-equilibrated solution (black curve), the triplet state in air-equilibrated water containing 4M urea (blue curve), and the triplet state in de-aerated solution (plum curve). The monitoring wavelength was 410 nm and excitation was at 610 nm.

The quantum yield for population of the triplet state is 0.56.[36] The triplet lifetime recorded at low laser intensity in de-aerated solution is 45 ± 7 μs, although decay curves were not strictly mono-exponential. The triplet state is quenched by molecular oxygen with a bimolecular rate constant of

$1.6 \pm 0.5 \times 10^9$ M^{-1} s^{-1}; the triplet lifetime in air-equilibrated water is reduced to 3.0 ± 0.2 μs. Related studies by other researchers have confirmed that such triplet quenching leads to formation of singlet oxygen. [24,38] Broadband (λ> 450 nm) illumination of MB^+ in air-equilibrated aqueous solution at pH 7.4 leads to progressive loss of colour. The course of reaction can be followed conveniently by absorption spectrophotometry and an illustrative example is provided as Figure 12. Under irradiation with white light, the main absorption band bleaches but there is no concomitant accumulation of a permanent product. This situation might be considered consistent with conversion of MB^+ to the corresponding leuco-form. [30] Bleaching is fairly slow and irreversible. The presence of molecular oxygen has no obvious effect on the absorption spectral changes during bleaching but no such fading occurs in the dark. Under otherwise identical conditions in D_2O, the colour loss occurs on a faster timescale but again does not favour build-up of a persistent coloured product. The logic behind this experiment comes from the realisation that the lifetime of singlet oxygen increases from 4 μs to 55 μs on replacing H_2O with D_2O. Under anaerobic conditions in H_2O, bleaching occurs more slowly and follows first-order kinetics.

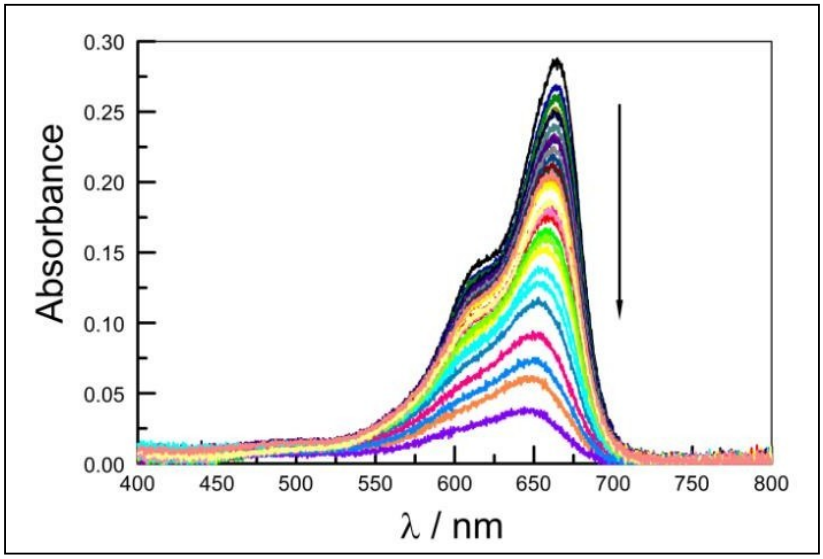

Figure 12. Example of the photobleaching of MB^+ in air-equilibrated aqueous solution at pH 7.4 using a white light source. The arrow shows the course of reaction. Absorption spectra were recorded at regular intervals over a period of 1,000 minutes. Note the 5 nm blue shift accompanying bleaching.

The absorbance change with illumination time, A(t), at any given wavelength gives an approximate fit to first-order kinetics. However, the fit is much improved by using the sum of two

exponentials model exemplified by Equation 4, where A(0) refers to the initial absorbance at that wavelength. The absorbance data extracted from Figure 13, and treated globally[39] across the entire absorption band, has ca. 15% of the initial absorbance (i.e., B = 0.15) decreasing with a first-order rate constant (step is followed by a substantially slower process having a first-order rate constant (k_2) of 0.0019 ± 0.0003 min^{-1} (Figure 3) that accounts for the remainder (C = 0.85) of the chromophore disappearance. Both derived rate constants are dependent on the incident light intensity (adjusted with neutral density filters or by varying the distance between sample and source). The effective rate of bleaching, measured at the beginning of the reaction, increases linearly with light intensity until saturation becomes apparent. A similar effect is observed for increasing MB^+ concentration at intermediate light intensity (Figures 14-15).

$$\frac{A(t)}{A(0)} = B e^{-k_1 t} + C e^{-k_2 t} \quad (4)$$

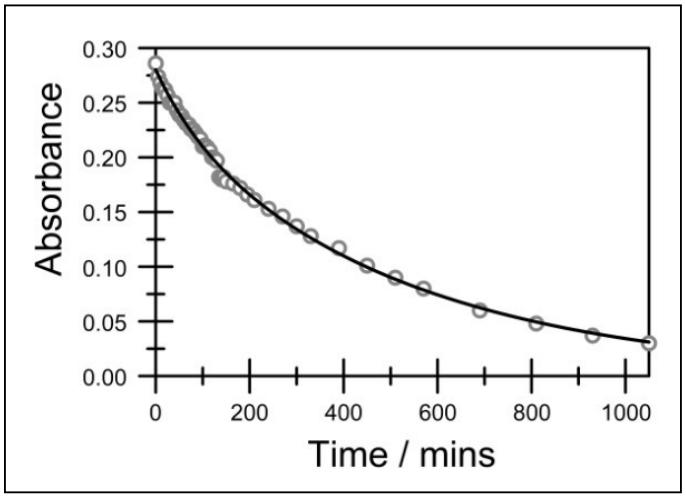

Figure 13. Fit of the experimental data recorded at 664 nm to Equation 4 or Equation 8 for the experiment indicated in Figure 12. The solid line drawn through the data points is a non-linear, least-squares iterative fit with the parameters reported in the text.

4.5 Effect of light intensity on the rate of photobleaching

Bleaching of MB^+ in air-equilibrated aqueous solution at pH 7.4 does not occur in the absence of light. Under illumination with white light (λ>420 nm), bleaching proceeds smoothly and can be followed by absorption spectrophotometry. Experiments were carried out in order to establish the effect of light intensity on the rate of photobleaching. Initial experiments varied the light intensity by changing the distance between the sample cell and the light source. The results are displayed on Figure 14. The light intensity incident on the sample cell was recorded with a power meter. It can be seen that the rate of photobleaching (w) increases with increasing light intensity until reaching a plateau. Separate experiments were made at intermediate light intensity by placing neutral density filters in front of the sample cell. Here, a linear relationship between light intensity and w is observed over the full attenuation region. The results are shown as an inset to Figure 14.

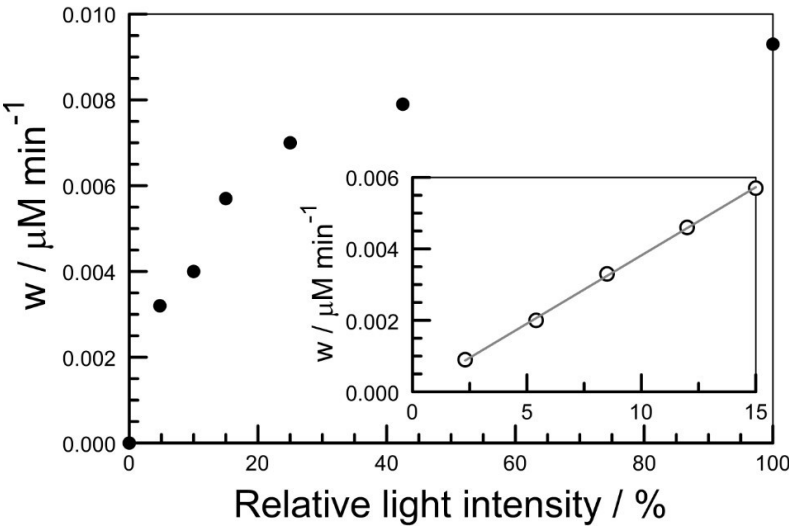

Figure 14. Effect of light intensity on the rate of photobleaching of MB^+ in air-equilibrated aqueous solution at pH 7.4. The filled black circles correspond to measurements made by varying the distance between sample and source. The inset shows the effects of inserting various neutral density filters in front of the sample cell. The composition of the solution was kept constant for all measurements.

Further experiments were made by varying the initial concentration of MB^+. Here, the fraction of the incident light intensity absorbed by MB^+can be determined from the Beer-Lambert law and compared to the rate of photobleaching. This was done by integrating the absorption spectral profile with respect to the spectral output of the lamp. The results are presented in Figure 15 and indicate a linear response between the rate of photobleaching and the photon uptake by the dye.

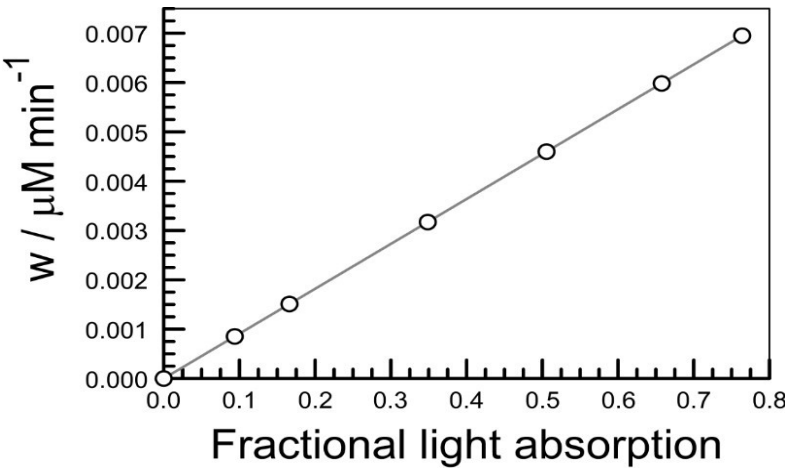

Figure 15. Relationship between the rate of photobleaching of MB^+ in air-equilibrated water at pH 7.4 and the fraction of incident light absorbed by the dye. The latter was varied by changing the concentration.

The problem with this simple model is that it is difficult to assign the two steps to any particular reaction as it is far from obvious why 15% of the initial signal should decay on a fast timescale compared to the residual absorbance.

The bleaching kinetics fit equally well[40] to two consecutive first-order reactions with averaged rate constants of 0.0109 ± 0.0004 min^{-1} and 0.0017 ± 0.0002 min^{-1} at fixed light intensity (Figure 13). The underlying two-step process can be expressed in terms of Equation 8. Equation 8 was derived from standard treatments for successive first-order reactions for a scheme in which the starting compound, A (i.e., MB^+), converts firstly to an intermediate, B, and finally to a transparent product, C (i.e., a form of the leuco-dye). It is assumed that there are no competing side-reactions but, in reality, this is unlikely. The initial absorbance is referred to as A_0. Now, the standard differential equations corresponding to the time-dependence for the absorbances of A and B are considered in Equations 5 and 6. There is no need to consider the concentration of C since this does not affect the absorbance in the visible region. It does not matter if B converts to other products as long as these do not contribute to the absorbance.

$$A(t) = A_0 e^{-k_1 t} \quad (5)$$

$$A_B(t) = \frac{\beta A_0 k_1}{(k_2 - k_1)} \left(e^{-k_1 t} - e^{-k_2 t} \right) \quad (6)$$

Here, k_1 and k_2, respectively, refer to the first-order rate constants for the faster (A → B) and slower (B → C) steps. The overall absorbance change at any wavelength is considered to be the sum of Equations 5 and 6. The coefficient β refers to the ratio of molar absorption coefficients for A and B at that wavelength (Equation 7). Given the limited number of data points, the analysis needs to be performed globally.

$$\beta = \frac{\varepsilon_B}{\varepsilon_A} \quad (7)$$

where it is assumed that Step 1, which is associated with k_1, leads to formation of an adduct that absorbs less strongly than MB^+ but retains a similar absorption profile. The ratio of molar absorption coefficients at that wavelength is incorporated into the parameter in Equation 8. Bleaching is accompanied by a 5nm blue shift that could be indicative of adduct formation (Figure 12). It is further assumed that bleaching of this adduct leads only to transparent products (i.e., the leuco-dye). Photochemical bleaching of the adduct occurs by way of k_2.

+¿
$MB^{¿}$
¿
¿0
¿
¿
$\underline{A(t)}$
¿

This simple model[41] can be refined on the basis of ancillary studies. For example, replacing H_2O with D_2O has an important acceleration on the overall rate of photobleaching of MB^+ in the presence of molecular oxygen. The rate of the first step increases significantly (k_1 = 0.19 ± 0.02 min^{-1}) while the second step becomes slightly faster (k_2 = 0.0052 ± 0.0005 min^{-1}) in D_2O.

The two-step nature[28] of the bleaching process observed under aerobic conditions is considered to be entirely consistent with formation of the leuco-dye as the major product. [30] Given the rather short singlet state lifetime, [36] it seems highly likely that the dominant species responsible for photochemical loss of MB^+ in solution is the triplet-excited state. This meta-stable species is quenched by molecular oxygen and it is reasonable to suppose that part of this quenching process leads to subsequent chemical modification of the chromophore. This step would correspond to k_1

while the observed D_2O effect suggests that singlet oxygen plays some role in this reaction.[43] This cannot involve diffusional attack on a ground-state molecule of MB^+ by singlet oxygen since the concentration of the former is too low and the lifetime of the latter is too short. Geminate addition of molecular oxygen within the precursor complex could explain the observations[44] but this would require regio-specific interactions between singlet oxygen and the aza-N or S atoms. The second step occurs more slowly, by way of k_2, and most likely refers to conversion of the primary adduct to a derivative of the leuco-dye (Scheme 1).

The logic behind this experiment comes from the realisation [42] that the lifetime of singlet oxygen increases from 4 μs to 55 μs on replacing H_2O with D_2O. Under anaerobic conditions in H_2O, bleaching occurs more slowly and follows first-order kinetics. There is no accompanying blue shift. Here, the derived first-order rate constant is 0.0059 ± 0.0005 min^{-1}, as measured under comparable conditions to those used above. Thus, the main effect of removing O_2 from the system is the loss of the initial fast step (i.e., k_1) and an increase in the rate of photochemical bleaching of the dye relative to the second step (i.e., k_2). In de-aerated D_2O, the rate of photochemical bleaching is slightly (i.e., 10%) faster than in de-aerated H_2O.

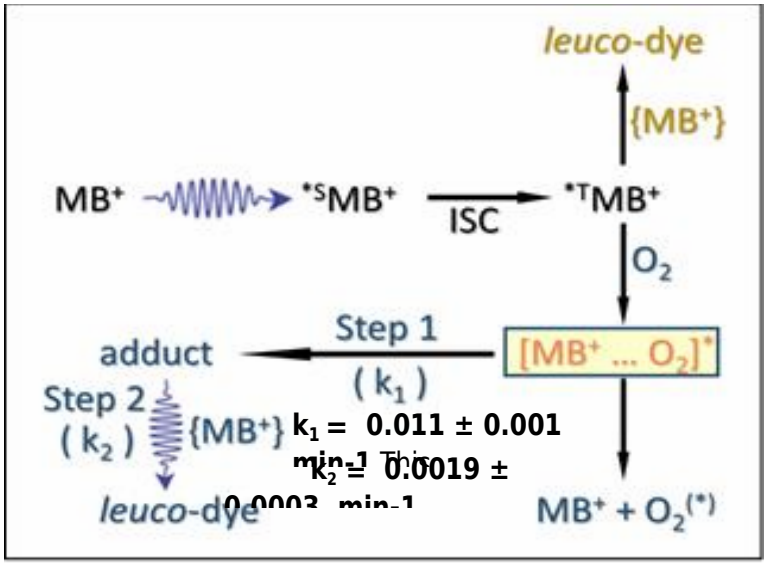

Scheme 1. Illustration of the processes leading to the photochemical bleaching of MB^+ in aqueous solution. Steps given in blue refer to aerobic conditions while anaerobic bleaching is given in brown. The key role assigned to the geminate complex formed between MB^+ and singlet molecular oxygen is highlighted. Both initial population of the excited-triplet state, via intersystem crossing (ISC), and bleaching of the primary adduct require light activation.

A different reaction mechanism must be responsible for anaerobic bleaching of MB^+, but again the reaction is probably promoted by the triplet-excited state. The triplet lifetime is much longer in the absence of oxygen and it is reasonable to suppose that bimolecular reactions, for example light-induced electron transfer between two MB^+ molecules, might initiate loss of the chromophore. Since the overall reaction is best explained in terms of a first-order process under these conditions, it is not possible to make a direct comparison between the rates of bleaching in aerobic and anaerobic conditions. Irreversible formation of the leuco-dye in the absence of oxygen is a possibility (Scheme 1).

It should be stressed[45] that the units used for the various rate constants should include a term for the number of photons absorbed but this has been neglected in order to simplify the text. Experiments have shown that the initial rates of bleaching in both aerobic and anaerobic conditions scale linearly with the number of photons absorbed per unit time. Where comparison is made, it is safe to assume that the initial rate of photon uptake remains the same.

4.6 Empirical expressions for effect of urea on optical properties

The empirical expression used to describe the effect of added urea, introduced as a solid to the solution of MB^+ in aqueous buffer, is presented as Equation 9. Here, λ is the observed wavelength for the absorption peak maximum. The parameters λ_F and λ_C, respectively, refer to the wavelengths for the absorption maxima of free MB^+ and MB^+ complexed with urea. The molar concentration of urea is also required for the calculation. The experimental data were analysed according to Equation 9 using non-linear, least-squares protocols. The equilibrium complex for a 1:1 complex between MB^+ and urea is represented as K (Equation 10). The same treatment was used to derive the molar absorption coefficient for the complex. In the statistical calculation, none of the parameters were constrained.

$$\lambda = (1-\alpha)\,\lambda_F + \alpha\,\lambda_C \quad (9)$$

$$\alpha = \frac{K[urea]}{1+K[urea]} \quad (10)$$

4.7 Effect of added urea

Addition of urea to an aqueous solution of MB^+ at pH 7.4 causes a modest (i.e., 4 nm) red shift for the absorption maximum and a significant increase (i.e., 20%) in the molar absorption coefficient at the peak (Figure 16). Both effects might be explained in terms of urea dissociating a ground-state dimer[46] but this is not the correct explanation. Exactly the same behaviour is observed at very dilute MB^+ concentration, where the fraction of chromophore that might be present as a dimer is below one percent. Likewise, given the very low basicity of urea ($K_B = 1.5 \times 10^{-14}$) [47] these spectral shifts cannot be ascribed to changes in pH. Instead, it appears that urea forms a weak

complex with MB^+ in neutral aqueous solution. Both the absorption shift and the increased absorbance observed on addition of solid urea to the solution can be explained in terms of 1:1 complexation.

The apparent binding constant ($K = 1.2 \pm 0.4\ M^{-1}$) is small, ensuring that high concentrations of urea are required to saturate the complexation event.

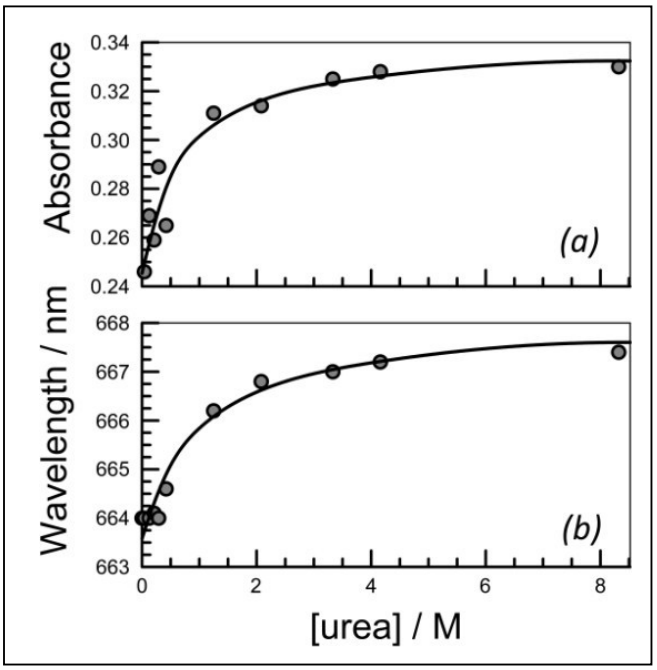

Figure 16. Effect of added urea on (a) absorbance at the maximum wavelength and (b) wavelength of the peak maximum for MB^+ in aqueous solution at pH 7.4. The solid lines drawn through the data points correspond to best fits to empirical expressions.

A series of ^1H NMR spectra were recorded with ratios of MB^+ to urea varying from half a molar equivalent of urea to a 39 times excess. These titration experiments revealed no changes in the ^1H NMR chemical shifts of the aromatic signals of MB^+ that could be regarded as significant. Small shifts of 0.04 to 0.06 ppm were observed, but these are most likely due to the varying concentration of the sample and do not provide conclusive evidence of complexation.

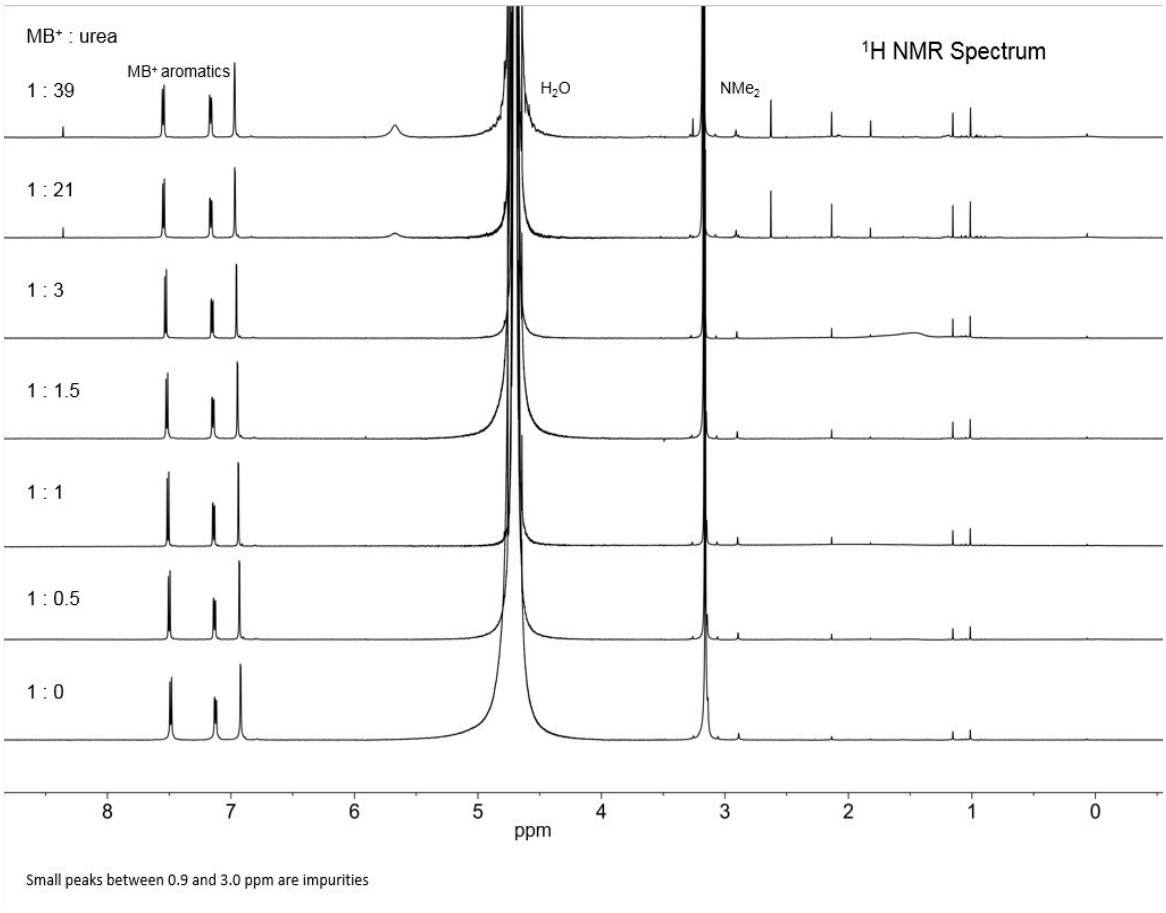

Figure 17. Addition of urea to a solution of MB^+ in D_2O at room temperature. The molar ratio of urea: MB^+ is indicated on each trace.

This finding confirms that complexation is weak and probably transitory. In fact, the only reasonable type of intermolecular interaction is hydrogen bonding between the reagents and, in this aspect, urea has to compete with water.

Complexation between urea and MB^+ can also be followed by way of a fluorescence titration. Addition of urea to an aqueous solution of MB^+ at pH 7.4 causes a small red shift for the emission maximum and an escalation in fluorescence.

4.8 Fluorescence titration with added urea

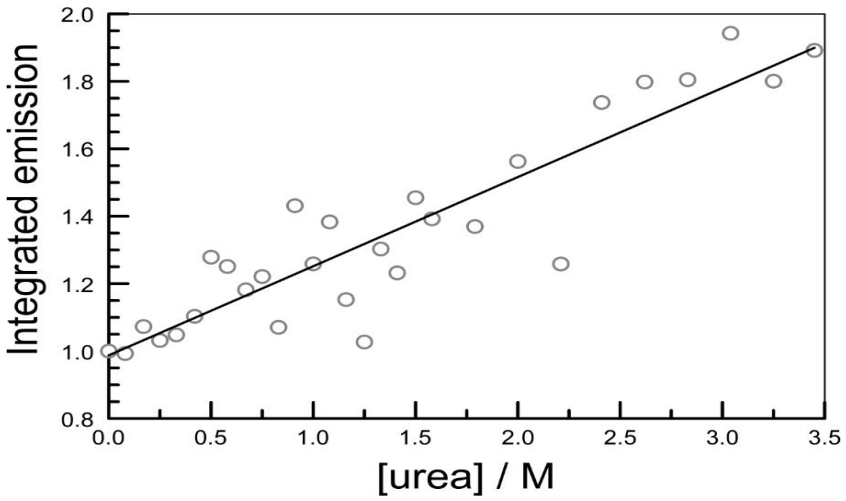

Figure 18. Effect of added urea on the integrated fluorescence yield recorded for MB^+ in water at pH 7.4. The excitation wavelength was 620 nm and the output signal was integrated from 660 to 800 nm. The solid line drawn through the data points corresponds to a fit to a linear increase in fluorescence.

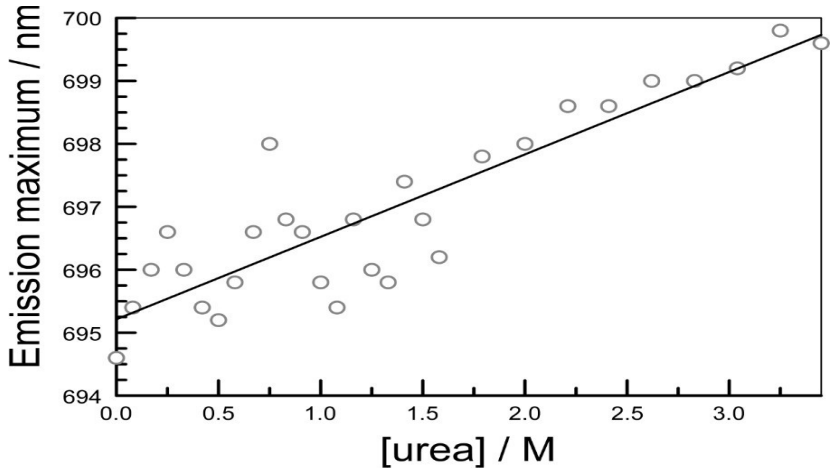

Figure 19. Effect of added urea on the fluorescence maximum recorded for MB^+ in water at pH 7.4. The excitation wavelength was 620 nm. The solid line drawn through the data points corresponds to a fit to 1:1 complexation between MB^+ and urea. The derived binding constant is 1.5 M^{-1}.

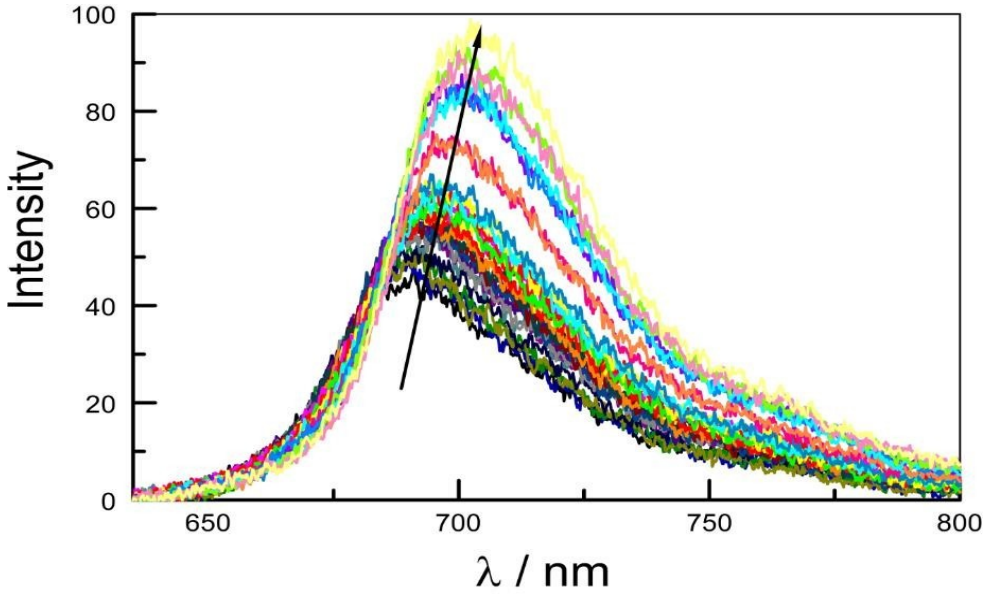

Figure 20. Effect of added urea on the fluorescence spectral profile recorded for MB^+ in water at pH 7.4. The excitation wavelength was 620 nm. The arrow indicates the variation in spectral profile with increasing urea concentration. The experimental data correspond to the information shown on the previous graphs.

These effects are modest, again requiring high concentrations of urea, but fully consistent with the absorption spectral studies; i.e., the increased absorptivity of the complex is matched by its enhanced fluorescence. Again, the fluorescence increase occurs at very low concentration of MB^+ and cannot be attributed to urea dissociating non-emissive dimer molecules into the emissive monomers. The fluorescence data are noisy but consistent with a binding constant of ca. 1 M^{-1}. There is no indication for urea acting as a fluorescence quencher for MB^+ in neutral solution.

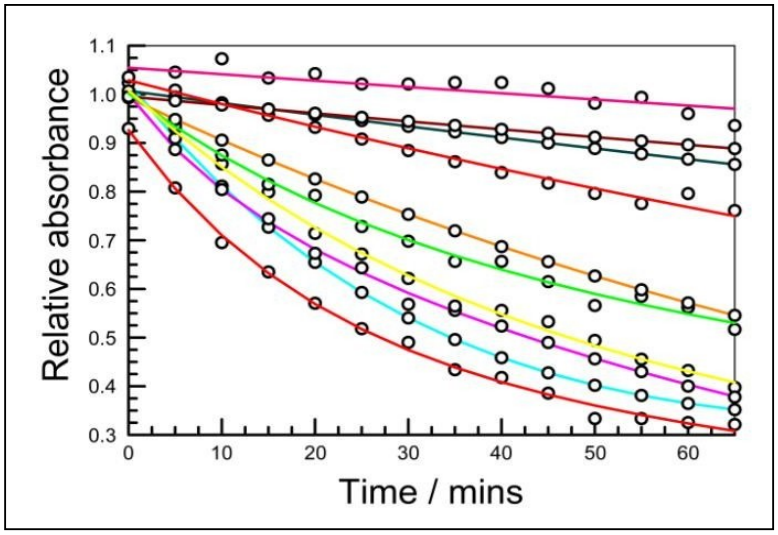

Figure 21. Plots of relative absorbance at the absorption peak for MB^+ (ca. 3 [illegible] solution at pH 7.4 under illumination with visible light. The solutions contained va[illegible] of urea (see Table 1 for composition) and were air-equilibrated before exposure to the light beam. The solid line drawn through each data set corresponds to a non-linear fit to a first-order reaction. The derived rate constants are included in Table 1. NB The reactions conditions, notably the light intensity, differ from those used for Figure 12 and direct comparison should not be attempted.

0.040 M

2.08 M

4.9 Compilation of the rates of photobleaching

Table 1. Collection of the various rate constants for photobleaching of MB^+ in aqueous solution at pH 7.4.

Part A: Effect of added urea at fixed light intensity

[urea] / M	*Oxygen* [a]	k_U / *min-1*	*Kinetics* [b]
0.040	AE	0.0184	1st order
0.125	AE	0.0182	1st order
0.21	AE	0.0151	1st order
0.29	AE	0.0144	1st order
0.42	AE	0.0101	1st order
1.25	AE	0.0092	1st order
2.08	AE	0.0049	1st order
3.33	AE	0.0025	1st order
4.16	AE	0.00175	1st order
8.32	AE	0.00128	1st order
2.08	AE : D_2O	0.0051	1st order
2.08	DA : D_2O	0.0040	1st order
2.08	DA	0.0039	1st order

[a] AE = air-equilibrated solution, DA = de-aerated by N2 bubbling. [b] Kinetics fitted to a simple first-order process.

Part B: Absence of added urea but fixed light intensity

Solvent	*Oxygen*	k_1 / *min-1*	k_2 / *min-1*	*Kinetics*
H_2O	AE	0.0109	0.0017	Consecutive
D_2O	AE	0.190	0.0052	Consecutive
H_2O	DA	0.0059	NA	1st Order
D_2O	DA	0.0068	NA	1st Order

Interaction between urea and MB^+ has an important effect on the kinetics of photochemical bleaching of the dye under visible light illumination (Figure 21). High concentrations (i.e., >0.2 M) of urea at pH 7.4 cause a marked decrease in the rate of loss of the chromophore. The solution pH was kept constant during these studies, as was the incident light intensity and the concentration of dissolved O_2. Under the experimental conditions used, the reaction profile can be analysed satisfactorily in terms of first-order kinetics, at least over early stages (Table 1). That is to say that the two-step mechanism observed for bleaching of MB^+ in air-equilibrated solution is replaced by a single-step (i.e., first-order) reaction in the presence of modest concentrations of urea. This allows facile derivation of the corresponding first-order rate constant (k_U) for photobleaching of MB^+ (Table 1). Interestingly, the rate of bleaching is little affected by the presence of O_2; a typical example has k_U decreasing from 0.0054 ± 0.0005 min^{-1} to 0.0039 ± 0.0004 min^{-1} on removal of the dissolved O_2 (Table 1). Similar behaviour is seen in D_2O, where the corresponding k_U is 0.0033 ± 0.0004 min^{-1} (Table S1). There is no indication for self-catalysis[48] at longer illumination times in the presence of urea. Such events occur if a reactive product accumulates during the bleaching process and promotes further loss of chromophore.[44]

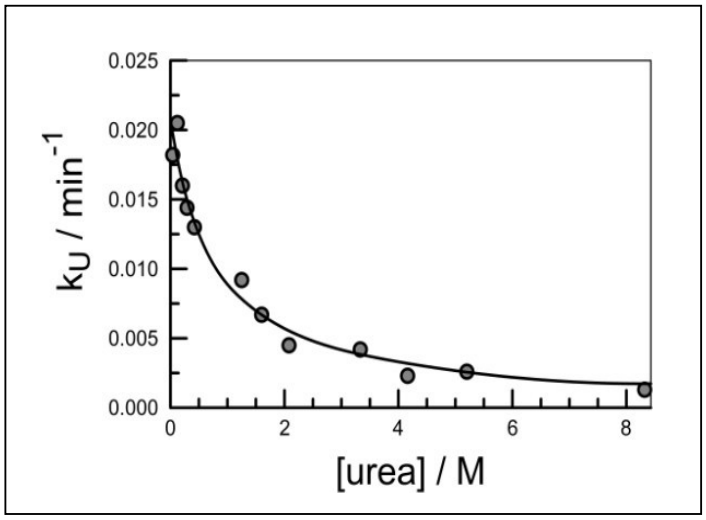

Figure 22. Effect of added urea on the derived first-order rate constant for photochemical bleaching of MB^+ in air-equilibrated water at pH 7.4. The solid line drawn through the data points is a non-linear least-squares fit to Equation 11 with the parameters reported in the text.

Although high solute concentrations are required, it is apparent that urea inhibits photobleaching of MB^+ in neutral aqueous solution. The effect of added urea on the rate constant (k_U) for bleaching of MB^+ can be expressed in terms of Equation 11. This situation is shown pictorially by Scheme 2. Our understanding of this behaviour is that an equilibrium is established between free MB^+ and a complex formed with urea. Analysis of the spectroscopic data is consistent with formation of a 1:1 complex[49] but this might not be an adequate representation of the situation since binding has little effect on the measurable properties. From Equation 11,[50] it appears that the complexed dye does not undergo photo-bleaching on the relevant timescale. The derived rate constant (k_{COMP} = 0.00012 min-1) is essentially zero. In contrast, the free dye bleaches with a global rate constant (k_{FREE}) of 0.021 ± 0.001 min^{-1} under these conditions. From the analysis, the equilibrium constant, K, has a value of 1.5 M^{-1}, in excellent agreement with that derived from the spectroscopic studies.

$$k_U = (1-\sigma)k_{FREE} + \sigma k_{COMP} \quad (11a)$$

$$\sigma = \frac{1}{1+1/(K[urea])} \quad (11b)$$

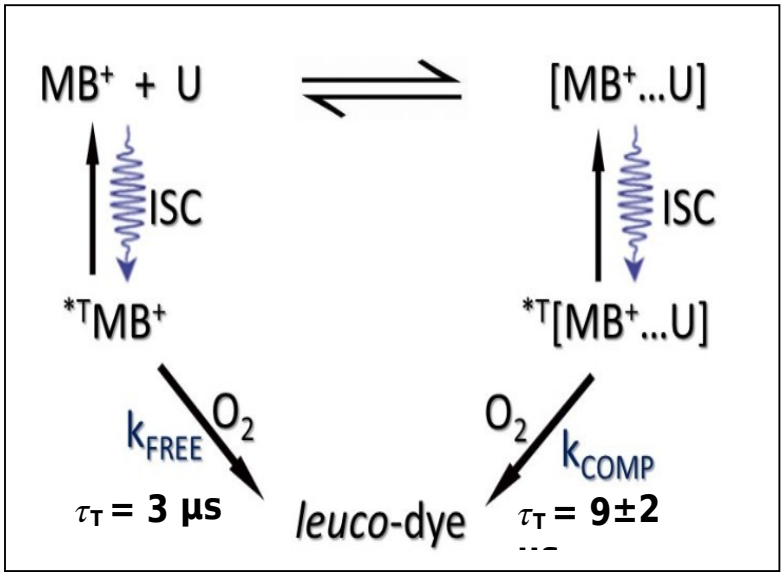

Scheme 2. Outline of reaction sequence proposed to account for the inhibition of MB^+ photobleaching exerted by urea in aqueous solution. The key step is the fast establishment of an equilibrium between free and complexed MB^+.

The presence of urea[51] does not inhibit formation of the MB^+ triplet-excited state but high concentrations lead to an increased triplet lifetime in air-equilibrated solution. For example, laser flash photolysis studies indicate that τ_T increases from 3 μs in the absence of urea to 9 ± 2 μs at a urea concentration of 4 M. In de-aerated solution, urea has no effect on τ_T at pH 7.4, which remains at 45 ± 8 μs. Unlike thiourea,[52] native urea is not a quencher for singlet oxygen and does not compete with molecular O_2 for quenching the triplet-excited state. No information exists about the possible effect of urea on O_2 solubility in water. Since triplet sensitization[53] of singlet oxygen requires orbital contact between the reactants it is plausible to suggest that the urea-MB^+ complex partially restricts close proximity with O_2. This would explain the somewhat extended triplet lifetime. Furthermore, the same argument could be used to suggest that the route to formation of the O_2-adduct is blocked upon complexation. This situation would eliminate the main bleaching processes introduced to explain loss of MB^+ in aerobic conditions. Finally, the complex would also hinder close association of two or more MB^+ molecules and, if so, this would limit the efficacy of any anaerobic bleaching that requires bimolecular electron transfer.[54] Thus, formation of the weak complex at the ground state level appears to be instrumental in protecting the dye against adventitious photobleaching in solution.

4.10 Conclusions

The major finding reported herein concerns the observation that urea protects MB^+ against photochemical bleaching in neutral aqueous solution. Urea is a cheap and abundant reagent, generally regarded as waste material, which dissolves readily in water. It introduces no obvious source of excited-state quenching and, at least in the case of MB^+, increases both the molar absorptivity and the triplet lifetime in air-equilibrated solution. Our NMR spectroscopy studies do not indicate specific interactions between MB^+ and urea, although the optical spectroscopy results could be analyzed in terms of 1:1 complexation. In reality, the effect of urea on the optical spectroscopic properties of MB^+ would pass without notice were it not for the observation that urea inhibits photobleaching of the dye. The effect is profound and, when associated with a urea molecule, MB^+ is effectively protected against photofading in solution. At much higher concentrations of MB^+, where aggregation is an issue,[25] urea is expected[46] to help dissociate any dimers. This effect might be considered an extension of the results described here.

Urea is well known[55] as being a reagent that forms inclusion compounds, or clathrates, with certain substrates. This provides a simple means for separating mixtures or for purifying hydrocarbons. [56] Perhaps the same approach could be developed to construct highly stable artificial light-harvesting antennae by incorporating the chromophore into the porous ordered matrix. In this respect, urea would be a most convenient host. The key rationale for this approach is the acceptance that the multiple electron breakdown of large dye molecules involves some type of bimolecular interactions. Preventing these associations could result in greatly improved photochemical stability.

4.11 References

[1] *Industrial Dyes: Chemistry, Properties and Applications*, 1^{st} *Ed.* (Ed.: K. Hunger) Wiley-VCH, Weinheim, **2003**.

[2] R. E. Blenkinsop in *Molecular Mechanisms of Photosynthesis, 2nd Ed.* John Wiley & Son, Chichester, **2014**.

[3] T. S. Mang, T. J. Dougherty, W. R. Potter, S. Somer, J. Moan, *Photochem. Photobiol*. **1987**, *45*, 501.

[4] a) L. Song, C. A. G. O. Varma, J. W. Verhoeven, H. J. Tanke, *Biophys. J.* **1996**, *70*, 2959. b) J. Widengren, R. Rigler, *Bioimag*. **1996**, *4*, 149. c) J. C. Finlay, S. Mitra, M. S. Patterson, T. H. Foster, *Phys. Med. Biol.* **2004**, *49*, 4837. d) C. Tanielian, R. Mechin, M. Shakirullah, *J. Photochem. Photobiol. A Chem*. **1992**, *64*, 191. e) D. M. Beltukova, I. V. Semenova, A. G. Smolin, O. S. Vasyutinskii, *Chem. Phys. Lett.* **2016**, *662*, 127.

[5] a) K. Li, Y. Xiang, X. Wang, A. Tong, B. Z. Tang, *J. Am. Chem. Soc*. **2014**, *136*, 1643. b) M. A. Van Dijk, L. C. Kapitein, J. Mameren, C. F. Schmidt, E. J. G. Peterman, *J. Phys. Chem. B.* **2004**, *108*, 6479. c) J. R. Saylor, *Exp. Fluids* **1995**, *18*, 445. d) N. A. George, B. Aneeshkumar, P. Radhakrishnan, C. P. G. Vallabhan, J. *Phys. D: Appl. Phys*. **1999**, *32*, 1745.

[6] a) T. Bernas, M. Zarebski, R. R. Cook, J. W. Dobrucki, *J. Microsc*. **2004**, *215*, 281. b) S. Rajagopal, D. Joly, A. Gauthier, M. Beauregard, R. Carpentier, FEBS J. **2005**, 272, 892.

[7] a) A. Harriman, P. Stachelek, A. Sutter, R. Ziessel, *Phys. Chem. Chem. Phys*. **2015**, *17*, 26175. b) M. A. H. Alamiry, A. Harriman, A. Haefele, R. Ziessel, *ChemPhysChem.* **2015**, *16*, 1867.

[8] A. Harriman, P. Stachelek, A. Sutter, R. Ziessel, *Photochem. Photobiol. Sci*. **2015**, *14*, 1100.

[9] a) R. B. Vegh, K. B. Bravaya, D. A. Bloch, A. I. Krylov, K. M. Solntsev, *J. Phys. Chem. B* **2014**, *118*, 4527. b) C. Duan, V. Adam, M. Byrdin, I. Demachy, D. Bourgeois, *J. Am. Chem. Soc*. **2013**, *135*, 15841. c) J. Li, Y. Hao, M. Zhong, J. Nie, X. Zhu, *Dyes Pigm*. **2019**, *165*, 467. d) L. Z. Zhang, G.-Q. Tang, *J. Photochem. Photobiol. B Biol*. **2004**,

74, 119. e) Q. Lin, L. Yang, Z. Wang, X. Gong, L. Zhu, *Angew. Chem. Int. Ed.* **2018**, *57*, 3722. f) V. Octeau, L. Cognet, L. Duchesne, D.
G. Fernig, B. Lounis, *ACS Nano.* **2009**, *3*, 345. g) K. Imura, H. Mizobata, Y. Makita, *Bull. Chem. Soc. Jpn*. **2016**, *89*, 1518.

[10] a) M. P. Gordon, T. Ha, P. R. Selvin, *Proc. Natl. Acad. Sci. USA*. **2004**, *101*, 6462. b) C. Jung, B.
K. Müller, D. C. Lamb, K. Müllen, C. Bräuchle, *J. Am. Chem. Soc.* **2006**, *128*, 5283.

[11] a) C. Wang, M. Taki, Y. Sato, T. Higashiyama, S. Yamaguchi, *J. Am. Chem. Soc*. **2017**, *139*, 10374. b) V. I. Sokolov, A. S. Akhmanov, I. M. Asharchuk, K. V. Khaydukov, M. M. Nazarov, *Opt. Spectro*. **2017**, *122*, 469. c) E. F. F. Da Silva, F. M. Pimenta, B. W. Pedersen, L. G. Arnaut,
P. R. Ogilby, *Integrative Biol.* **2016**, *8*, 177. d) P. A. Dalgarno, C. A. Traina, J. C. Penedo, G. C. Barzan, I. D. W. Samuel, *J. Am. Chem. Soc*. **2013**, *135*, 7187. e) D. Rhinow, M. Imhof, I. Chizhik, R.-P. Bauman, N. Hampp, *J. Phys. Chem. B.* **2012**, *116*, 7455.

[12] a) I. P. Kaminov, L. W. Stulz, E. A. Chandross, C. A. Pry, *Appl. Opt*. **1972**, 11, 1563. b) C. M. Carbonaro, A. Anedda, S. Grandi, A. Magistris, *J. Phys. Chem. B.* **2006**, *110*, 12932. c) A. M. Weiss, E. Yariv, R. Reisfeld, *Opt. Mater*. **2003**, *24*, 31. d) C. Julien, A. Debarre, D. Nutarelli, A. Richard, P. Tchénio, *J. Phys. Chem. B.* **2005**, *109*, 23145.

[13] H. Nakamoto, N. Suzuki, S. K. Roy, *FEBS Lett.* **2000**, *483*, 169.

[14]a) T. Cordes, J. Vogelsang, P. Tinnefeld, *J. Am. Chem. Soc*. **2009**, *131*, 5018. b) L. A. Campos, J. Liu, X. Wang, D. S. English, V. Muñoz, *Nature Methods.* **2011**, *8*, 143. c) J. Widengren, A. Chmyrov, C. Eggeling, P.- Å. Löfdahl, C. A. M. Seidel, *J. Phys. Chem. A.* **2007**, *111*, 429. d) T. J. Pintar, F. Lin, A. W. Girotti, *Free Rad. Biol. Med.* **1994**, *16*, 603.

[15] a) G. T. Dempsey, J. C. Vaughan, K. H. Chen, M. Bates, X. Zhuang, *Nature Methods* **2011**, *8*, 1027. b) T. Ha, P. Tinnefeld, *Ann. Rev. Phys. Chem*. **2012**, *63*, 595.

[16] a) P. P. Lima, M. M. Nolasco, F. A. A. Paz, O. L. Malta, L. D. Carlos, *Chem. Mater*. **2013**, *25*, 586. b) V. Glembockyte, R. Lincoln, G. Cosa, *J. Am. Chem. Soc*. **2015**, *137*, 1116. c) R. B. Altman, Q. Zheng, Z. Zhou, J. D. Watten, S. C. Blanchard, *Nature Methods* **2012**, *9*, 428.

[17] a) M. Ballottari, M. J. P. Alcocer, C. D'Andrea, G. Cerullo, R. Bassi, *Proc. Natl. Acad. Sci. USA* **2014**, *111*, E2431. b) S. Takahashi, M. R. Badger, *Trends Plant Sci*. **2011**, *16*, 53.

[18] A. Nagarayan, R. L. Burnap, *Biochim. Biophys. Acta Bioenergetics*. **2014**, *1837*, 1417.

[19] M. Oz, D. E. Lorke, M. Hasan, G. A. Petroianu, *Med. Res. Rev*. **2011**, *31*, 93.

[20] A. Baeyer, H. Caro, *Engl. Pat*. **1877**, 10, 692.

[21] P. Ehrlich, *Dtsch. Med. Wochenschr*. **1886**, *12*, 49.

[22] a) E. M. Tuite, J. M. Kelly, *J. Photochem. Photobiol. B. Biol*. **1993**, *21*, 103. B) R. Rohs, H. Sklenar, R. Lavery, B. Röder, *J. Am. Chem. Soc*. **2000**, *122*, 2860. c) B. S. Fujimoto, J. B. Clendenning, J. J. Delrow, P. J. Heath, M. Schurr, *J. Phys. Chem*. **1994**, *98*, 6633.

[23] a) M. Wainwright, K. B. Crossley, *J. Chemother*. **2002**, *14*, 431. b) K. Orth, G. Beck, F. Genze, A. Rück, *J. Photochem. Photobiol. B Biol*. **2000**, *57*, 186. c) Y. Lu, R. Jiao, X. Chen, A. Ji, P. Shen, *J. Cell. Biochem*. **2008**, *105*, 1451.

[24] C. A. Parker, *J. Phys. Chem*. **1959**, *63*, 26.

[25] a) Z. Zhao, E. R. Malinowski, *J. Chemometrics* **1999**, *13*, 83. b) J. B. Ghasemi, M. Miladi, *J. Chin. Chem. Soc*. **2009**, *56*, 459. c) J. Vara, C. S. Ortiz, *Spectrochim. Acta Part A Mol. Biomol. Spec*. **2016**, *166*, 112. d) A. Fernández-Pérez, T. Valdés-Solís, G. Marbán, *Dyes Pigm*. **2019**, *161*, 448.

[26] a) P. V. Kamat, N. N. Lichtin, *J. Phys. Chem*. **1981**, *85*, 814. b) R. Bonneau, R. Pottier, O. Bagno, J. Joussot-Dubien, *Photochem. Photobiol.* **1975**, *21*, 159.

[27] a) R. Nilsson, P. B. Merkel, D. R. Kearns, *Photochem. Photobiol*. **1972**, *16*, 109. b) R. H. Kayser,

R. H. Young, *Photochem. Photobiol*. **1976**, *24*, 395. c) R. M. Danziger, *J. Phys. Chem*. **1967**,

71, 2633.

[28] a) S. Kato, M. Morita, M. Koizumi, *Bull. Chem. Soc. Jpn*. **1964**, *37*, 117. b) R. D. Lowe, R. D. Snook, *Analyst*. **1993**, *118*, 613. c) C. Eggeling, J. Widengren, R. Rigler, C. A. M. Seidel, *Anal. Chem*. **1998**, *70*, 2651.

[29] a) A. Mills, J. Wang, *J. Photochem. Photobiol. A Chem*. **1999**, *127*, 123. b) Y.-H. Xu, D.-H. Liang, M.-I. Liu, D.-Z. Liu, *Mater. Res. Bull*. **2008**, *43*, 3474. c) E. L. Quitevis, J. Martorell, Y. Chang,

T. W. Scott, *Chem. Phys. Lett*. **2000**, *319*, 138. d) J. W. Lekse, B. J. Haycock, J. P. Lewis, D. R. Kaufman, C. Matranga, *J. Mater. Chem. A.* **2014**, *2*, 9331. e) F. Fu, Y. Zhang, L. Yan, X. Gao, D. Wang, *J. Mater. Sci. Mater. Electronics.* **2017**, *28*, 691.

[30] a) G. N. Lewis, O. Goldschmid, T. T. Magel, J. Bigeleisen, *J. Am. Chem. Soc.* **1943**, *65*, 1150. b)

G. N. Lewis, J. Bigeleisen, *J. Am. Chem. Soc*. **1943**, *65*, 2419. c) G. Oster, N. Wotherspoon, *J. Am. Chem. Soc*. **1957**, *79*, 4836.

[31]K. Bergmann, C. T. O'Konski, *J. Phys. Chem*. **1963**, *67*, 21.

[32] a) K. Patil, R. Pawar, P. Talap, *Phys. Chem. Chem. Phys*. **2000**, *2*, 4313. b) P. Mukerjee, A. K. Ghosh, *J. Am. Chem. Soc*. **1970**, *92*, 6403. c) W. Spencer, J. R. Sutter, *J. Phys. Chem*. **1979**, *83*, 1573. d) A. Ghanadzadeh, A. Zeini, A. Kashet, M. Moghadam, *J. Mol. Liquids.* **2008**, *138*,

100. e) G. N. Lewis, O. Goldschmid, T. T. Magel, J. Bigeleisen, *J. Am. Chem. Soc*. **1943**, *65*, 1150. f) K. Fujita, K. Taniguchi, H. Ohno, *Talanta*, **2005**, *65*, 1066. g) A. Fernandez-Perez, T. Valdes-Solis, G. Marban, *Dyes Pigm*. **2019**, *161*, 448. h) N. Florence, H. Naorem, *J. Mol. Liquids* **2014**, *198*, 255. i) D. R. Lemin, T. Vickerstaff, *Trans. Faraday Soc*. **1947**, *43*, 491.

[33] a) V. S. Shelkovsky, M. V. Kosevich, O. A. Boryak, I. V. Shmigol, V. A. Pokrovskiy, *RSC Advances*

2014, *4*, 60260. b) S. K. Mehta, S. Chaudhary, K. K. Bhasin, *J. Colloid. Interfac. Sci.* **2008**, *321*, 426. c) S. Yamamoto, S. Kobashi, K.-i. Tsutsui, Y. Sueishi, *Spectrochim. Acta Part A Mol. Biomol. Spectr*. **2007**, *66*, 302.

[34] a) O. Yazdani, M. Irandoust, J. B. Ghasemi, Sh. Hooshmand, *Dyes Pigm*. **2012**, *92*, 1031. b) J. C. Dean, D. G. Oblinsky, S. Ratiq, G. D. Scholes, *J. Phys. Chem. B* **2016**, *120*, 440. c) K. Bergmann, C. T. O'Konski, *J. Phys. Chem*. **1967**, *67*, 2169. d) E. Rabinowitch, C. F. Epstein, *J. Am. Chem. Soc*. **1941**, *63*, 69. e) P. Mukerjee, A. K. Ghosh, *J. Am. Chem. Soc*. **1970**, *92*, 6419.

[35] P. Stachelek, A. Harriman, *J. Phys. Chem.* **2016**, *120*, 8104.

[36] S. J. Atherton, A. Harriman, *J. Am. Chem. Soc*. **1993**, *115*, 1816.

[37] a) M. Gonzalez-Bejar, P. Montes-Navajas, H. Garcia, J. C. Scaiano, *Langmuir*. **2009**, *25*, 10490. b) R. Bonneau, P. F. Violet, J. Joussot-Dubien, *Photochem. Photobiol.* **1974**, *19*, 129. c) A. Knowles, S. Gurnani, *Photochem. Photobiol*. **1972**, *16*, 95. d) C. A. Parker, *J. Phys. Chem*. **1959**, *63*, 26. e) P. V. Kamat, N. N. Lichtin, *J. Phys. Chem.* **1981**, *85*, 3864. f) R. M. Danziger, *J. Phys. Chem*. **1967**, *71*, 2633.

[38] S. J. Wagner, A. Skripchenko, D. Robinette, J. W. Foley, L. Cincotta, *Photochem. Photobiol*. **1998**, *67*, 343.

[39] A. de Juan, R. Tauter, R. Dyson, C. Marcolli, M. Rault, M. Maeder, *Trends Anal. Chem*. **2004**, *23*, 70.

[40] J. H. Espenson, "in Chemical Kinetics and Reaction Mechanisms", 2nd Edition, Chap. 4, McGraw-Hill, New York, **2002**.

[41] a) D. Ball, *J. Chem. Educ*. **1998**, *75*, 917. b) T. A. Bak, P. Salaman, B. Andresen, *J. Phys. Chem. A* **2002**, *106*, 10961.

[42] M. A. J. Rodgers, P. T. Snowden, *J. Am. Chem. Soc*. **1982**, *104*, 5541.

[43] R. A. Floyd, M. S. West, K. L. Eneff, J. E. Schneider, *Arch, Biochem. Biophys.* **1989**, *273*, 106.

[44]J. K. G. Karlsson, O. J. Woodford, R. Al-Aqar, A. Harriman, *J. Phys. Chem. A* **2017**, *121*, 8569.

[45] a) G. Terrones, A. J. Pearlstein, *Macromol*. **2001**, *34*, 8894. b) A. Rück, C. Hildebrandt, T. Köllner, H. Schneckenburger, R. Steiner, *J. Photochem. Photobiol. B Biol.* **1990**, *5*, 311.

[46] a) K. Patil, R. Pawar, P. Talup, *Phys. Chem. Chem. Phys*. **2000**, *2*, 4313. b) S. C. Nunez, T. M. Yoshimura, M. S. Ribeiro, H. C. Junqueira, C. Maciel, M. D. Coutinho-Neto, M. S. Baptista, *J. Photochem. Photobiol. B Biol*. **2015**, *150*, 31.

[47]M. Levy, *Comptes Rendus des Travaux du Laboratoire Carlsberg, Ser. Chim*. **1958**, *30*, 291.

[48] S. Sirbu, O. J. Woodford, A. C. Benniston, A. Harriman, *Photochem. Photobiol. Sci.* **2018**, *17*, 750.

[49]T. L. Nemzek, W. R. Ware, *J. Chem. Phys*. **1975**, *62*, 477.

[50]A. Harriman, M. Hissler, A. Khatyr, R. Ziessel, *Chem. Commun*. **1999**, 5, 735.

[51]S. C. Nunez, T. M. Yoshimura, M. S. Ribeiro, H. C. Jungueira, C. Maciel, M. D. Neto, M. S. Baptista, *J. Photochem. Photobiol. B: Biol.* **2015**, 150, 31.

[52]G. Crank, A. Mursyidi, *J. Photochem. Photobiol. A Chem*. **1992**, *64*, 263.

[53]O. L. J. Gijzeman, F. Kaufman, G. Porter, *J. Chem. Soc., Faraday Trans.* **1973**, *69*, 727.

[54] A. Rosspeinter, D. R. Kattnig, G. Angulo, S. Landgruf, A. Grampp, *Chem. Eur. J.* **2008**, *14*, 6213.

[55]J. Le Brumant, M. Jaffrain, G. Lacrampe, *J. Phys. Chem*. **1984**, *88*, 1548.

[56]a) A. E. Tonelli, *Macromol*. **1991**, *24*, 275. b) A. E. Tonelli, *Macromol*. **1990**, *23*, 3134.

[57]N. Wen, M. H. Brooker, *Can. J. Chem*. **1994**, *72*, 1099.

[58]R. R. W. Ellerton, E. W. Mayne, *Anal. Chem*. **1980**, *52*, 773.

[59] D. R. Kearns, *Chem. Rev*. **1971**, 71, 395.

[60] J. P.Tardivo, A. D. Giglio, C. S. Oliveira, D. S. Gabrielli, H. C. Junquueira, D. B. Tada, D. Severino,

R. Turchiello, M. S. Baptista, *Photodiagn. Photodyn. Ther.* **2005**, 2, 175.

[61] G. Lepore, C. H. Miranda, C. H. Yokomizo, L. Cassiavilani, I. L. Nantes, N. A. Daghastanli, "VI Latin American Congress on Biomedical Engineering CLAIB", Argentina, Springer, Cham. **2014**.

[62] S. L. Logunov, T. S. Ahmadi, M. A. El-Sayed, *J. Phys. Chem. B.* **1997**, 101, 3713.

[63] J. Chen, C. Thomas, Cesario, P. M. Rentzepis, *J. Phys. Chem. A*. **2011,** 115, 2702.

[64] C. Foote, R. Denny, *J. Am. Chem*. **1968**, 90, 6232.

[65] S. Afonso, E. D. Salamanca, D. C. Batlle, *J. Dairy Sci*. **1999,** 58, 1609.

[66] D. B. Min, J. M. Boff, *Food Science &Technology*. **2002**, 1, 58.

[67] A. A. Osunlaja, S. O. Idris, J. F. Iyun, Int. *J. ChemTech Res.* **2012**, 2, 609.

[68] J. Campell, *J. Chem. Education*. **1948**, 9, 498.

[69] E. S. Abechi, C. E. Gimba, A. Uzairu, J. A. Kagbu, *Arch. Apple. Sci. Res*. **2011**, 3, 154.

Chapter 5.

Photobleaching of an N,N,O,O-Boron-Chelated Dipyrromethene Dye in Solution

Getting ready for winter…

5.1 Summary

This chapter describes the results obtained with a doubly-strapped BODIPY derivative bearing an unconstrained *meso*-phenyl ring. Rotation of the *meso*-ring around the connecting C-C bond should cause significant loss of fluorescence by way of the molecular rotor effect, as concluded by comparison to derivatives lacking the straps. This is not the case, however, and the derived excited-singlet state lifetime is the longest yet reported for a conventional BODIPY fluorophore. The molecule is subject to considerable steric strain and it was anticipated that this excess energy could be released by breaking one or both of the C-O bonds. This would create an oxy-radical that might be a useful bleaching agent. We test this hypothesis by studying the photobleaching of the compound in the absence and presence of a sacrificial redox agent. The compound is also used as a photocatalyst for oxidative degradation of indigo in solution.

5.2 Introduction

The term "molecular rotor" refers to that class of molecules where a small unit can rotate around a larger structure in such a way that the molecular properties are perturbed.[1] Often, the ease of rotation is reflected by the fluorescence yield or lifetime.[2] A key requisite for an effective molecular rotor is that the rotational behavior can be controlled via frictional forces exerted by the

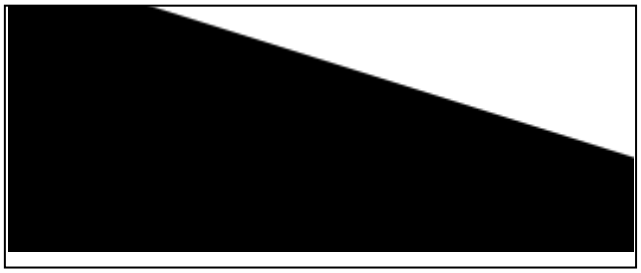

surrounding environment.[3-6] Thus, the rotor functions as a sensitive probe for changes in local conditions, including temperature, pressure, rheology, polarity, micro-structure or composition. [7,8] It follows that the rotary action must perturb the geometry of the stationary unit in order to modulate its photophysical properties. Simple rotation of an ancillary aryl group around a fluorophore will not be sufficient to import sensory behavior. Although several classes of fluorophores have been proposed as putative molecular rotors, the industry standard being cyanovinyl-julolidine derivatives, unconstrained boron dipyrromethene (BODIPY) dyes have

become dominant of late.[9] These BODIPY dyes, being reported first by Holten et al.[10-13] feature a small aryl group at the pseudo-*meso* position and control the ease of rotation by steric effects between substituents on the aryl ring and/or dipyrrin backbone. Scheme 1 illustrates the basic principles of BODIPY-based molecular rotors. Substituents at the aryl ring are known to affect the fluorescence quantum yield by restricting rotation around the dipyrrin unit. Likewise, bulky substituents positioned on the upper rim of the dipyrrin unit tend to further maximize emission by way of minimizing rotation of the aryl group. Full rotation buckles the dipyrrin nucleus and it is this latter effect that serves to reduce the fluorescence quantum yield and lifetime. Quite remarkably, it was shown very recently that aryl groups appended at the 3,5-positions (i.e., the lower rim of the dipyrrin unit) perturbed the photophysical properties of the BODIPY dye.[14 -16] One aryl ring at the 3-position improved the sensing performance but rings at both 3- and 5- positions hindered rotation. We now extend this observation by reporting the photochemical properties of a symmetrically strapped analogue. This target compound shows no aptitude for environmental sensing despite the ready availability of an unconstrained *meso*-aryl substituent.

Scheme 1. Prototypic BODIPY-based molecular rotor capable of full rotation and its structurally constrained analogue restricted to small-scale gyration.

The main target, ST1, comprises a BODIPY dye with an unconstrained upper dipyyrin backbone and a *meso*-aryl substituent. A key feature of the compound is that aryl substituents at the 3,5-positions are locked in place via a C-O-B linkage involving the ortho-carbon atom on the substituent and the boron atom. This linkage is fairly rigid and, according to X-ray crystallography, imposes dihedral angles of ca. 20^0 and 17^0 on the aryl rings. The compound was prepared in the laboratory of Dr. JG Knight (SNES, Newcastle University) and full synthetic details have been published, together with full structural characterization.[17] The molecular formula for ST1 is shown in Figure 1. This compound, which displays circularly polarized fluorescence.

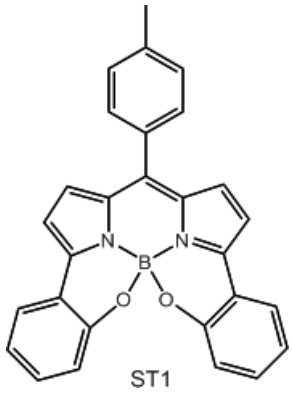

Figure 1. Molecular formula and 3D cartoon representation of the target compound used in this chapter.

Our interest in this compound is to examine its photochemical stability in solution. The molecular structure differs from that of conventional boron dipyrromethene (BODIPY) dyes because of the strap at the lower rim. A further difference concerns the replacement of the B-F bonds with B-O bonds. In general, BODIPY dyes are reported in the literature as being extremely stable towards both heat and light.[18-24] In this chapter, we consider the photostability of the dye under some different conditions. It might be mentioned that there is not much information in the literature for these strapped BODIPY derivatives although the literature for conventional BODIPY dyes is vast.

5.3 Photophysical properties

In 2-methyltetrahydrofuran (MTHF) solution, ST1 exhibits well-defined absorption and fluorescence transitions in the red region that are in good accord with expectations based on many other BODIPY-based chromophores. The lowest-energy absorption transition has a clear maximum (λ_{MAX}) located at 621 nm and displays a series of vibrational satellites. In fact, the absorption maximum is considerably red shifted compared to BODIPY lacking the 3,5-phenylene rings.[25] This latter effect is attributed to partial π-conjugation between the subunits that serves to extend the delocalisation pathway. The measured molar absorption coefficient at the band maximum (λ_{MAX} = 48,730 M-1 cm-1) is rather low compared to conventional BODIPY dyes but this might be a consequence of the buckled dipyrrin nucleus. At much higher energies, the onset of transitions to

upper-lying excited-singlet levels begins at about 480 nm. The corresponding emission transition has a maximum at 646 nm, giving rise to a modest Stokes' shift of 625 cm^{-1}.

The fluorescence quantum yield (λ_F) measured in MTHF at room temperature is 0.64, which is in line with values reported for conventional BODIPY dyes. Good agreement exists between the excitation and absorption spectra and the Φ_F remains independent of excitation wavelength. The excited-singlet state lifetime (λ_S) is approximately 10.0 ns, which provides an estimate for the radiative rate constant ($k_{RAD} = \Phi_F / \tau_S$) of 6.4 x 10^8 s^{-1}. This seems quite reasonable for a highly fluorescent dye but exceeds the range of values reported for other members of the BODIPY family. It should be mentioned here that the Φ_F and τ_S values found for ST1 are significantly greater than values found for BODIPY dyes possessing a *meso*-phenylene ring but lacking the 3,5-aryl units. Such dyes are known to operate as fluorescent rotors whereby gyration of the *meso*-phenylene ring causes minor distortion of the upper rim of the dipyrrin framework and this situation promotes nonradiative decay of the excited state. In fact, Φ_F and τ_S reported for this non-strapped derivative are 0.023 and 150 ps, respectively.

Table 1. Compilation of the photophysical properties recorded for the target compound in fluid solution.

λ_{ABS} / nm	621
λ_{FLU} / nm	646
ε_{MAX} / $M^{-1}cm^{-1}$	48,730
Φ_F	0.64
τ_S / ns	10.0
E_S / eV	1.96
Δ_{SS} / cm^{-1}	625
k_{RAD} / 10^8 s^{-1}	0.64
k_{NR} / 10^8 s^{-1}	0.36
meso-aryl / °	54 (58)
3-aryl / °	14 (11)
5-aryl / °	15 (11)

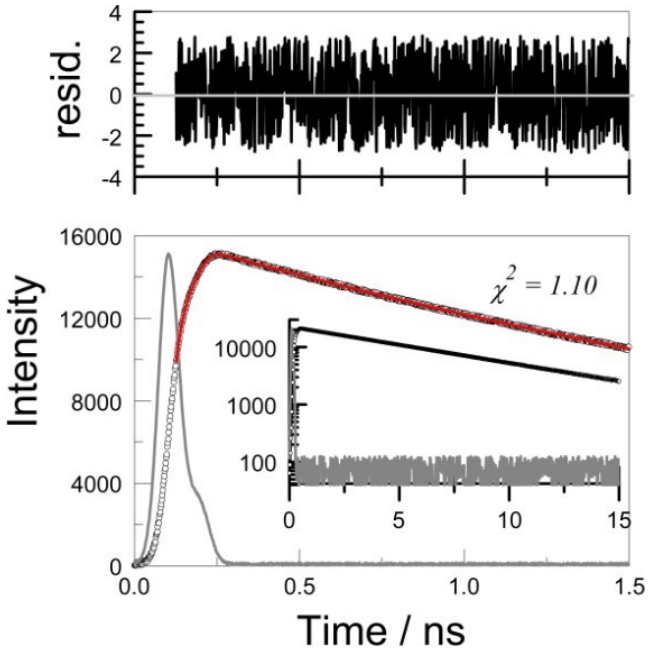

Figure 2. Example of a time-resolved fluorescence decay trace recorded for ST1 in MTHF solution at room temperature. The instrument response function is shown as a grey curve while the red curve drawn through the data points is a nonlinear least-squares fit to a partial growth and subsequent decay of 10 ns. This experiment was performed in collaboration with Dr. Patrycja Stachelek.

On closer examination, the time-resolved fluorescence decay profile recorded for ST1 in MTHF solution shows that part of the signal grows in on a timescale longer than the instrumental response function. This situation is shown in Figure 2. The photophysical properties were determined in collaboration with Dr. Patrycja Stachelek and are not the main subject of this work.

The X-ray structure for ST1 was determined by the synthetic chemists and has been published.[17] Our computed structure (DFT/PBE0/B3LYP/6-311G,d) is remarkably similar to the experimental solid-state structure (Figure 3). The meso-phenylene ring adopts an angle of ca. 45-60°, according to the method employed, and there is a slight barrier to attaining an orthogonal geometry. Probably, this situation reflects a compromise between steric relief and loss of resonance energy. More importantly, the calculations show that the *meso*-phenylene ring can gyrate over a wide range before encountering a substantial barrier for full rotation. This barrier is caused by steric clashes between the relevant hydrogen atoms and is slightly reduced for the excited state. In

order to accommodate full rotation it is necessary for the dipyrrin backbone to buckle slightly and this gives rise to the so-called fluorescent rotor effect.

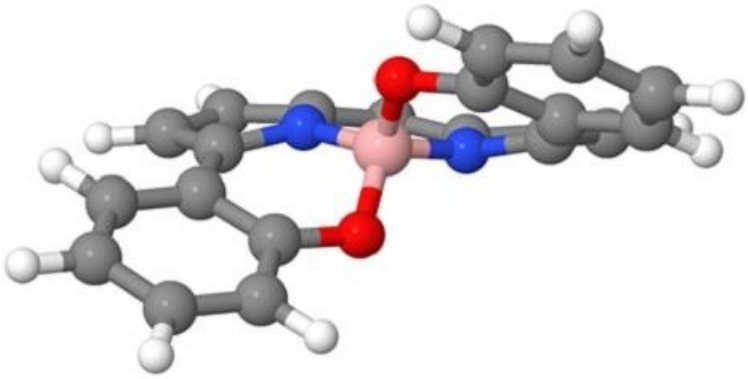

Figure 3. Partial structure computed for ST1 showing the structural distortion imposed by the straps. The dipyrrin unit bends to accommodate these straps and this will most likely introduce considerable angle steric strain. Breaking one or both B-O or O-C bonds will likely relieve this strain.

The cyclic voltammogram for ST1 in dichloromethane solution was recorded by Dr. Patrycja Stachelek as part of her PhD studies and shows a quasi-reversible reduction wave with a half-wave potential of -1.15 V vs SCE. The corresponding oxidation wave is electrochemically irreversible. The oxidation peak lies at +0.9 V vs SCE. Even at fast scan rates (i.e., 1 V s^{-1}), the oxidation wave remained irreversible. This indicates that the radical cation formed on oxidation undergoes a fast chemical reaction. Our computer models indicate that the HOMO is localised on the dipyrromethene unit but spreads onto the appended phenoxyl rings (Figure 4). This might indicate that oxidation could lead to breakage of one of the C-O bonds, followed by fast rotation of the free aryl ring. Computer simulation shows a possible structure for such a process (Figure 5).

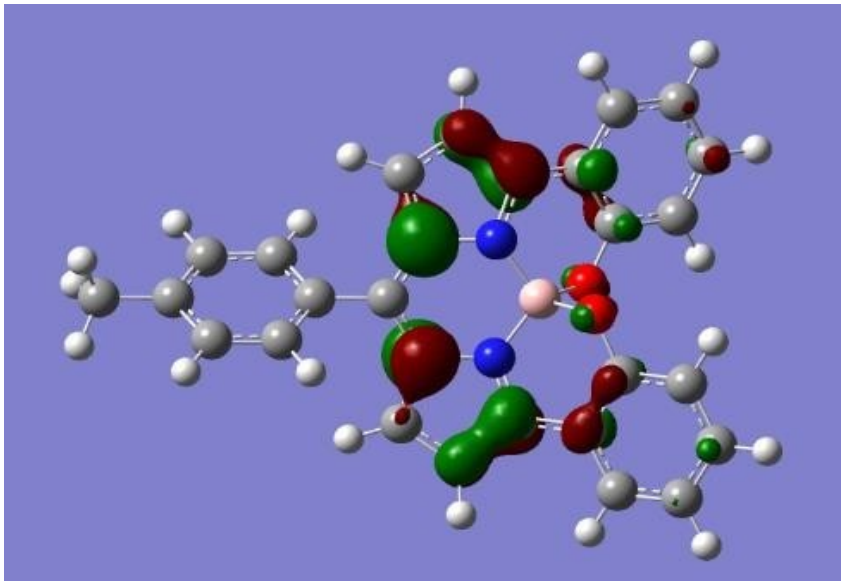

Figure 4. Kohn-Sham representation of the HOMO computed for ST1 by DFT methods with the molecule embedded in a reservoir of $CHCl_3$ molecules.

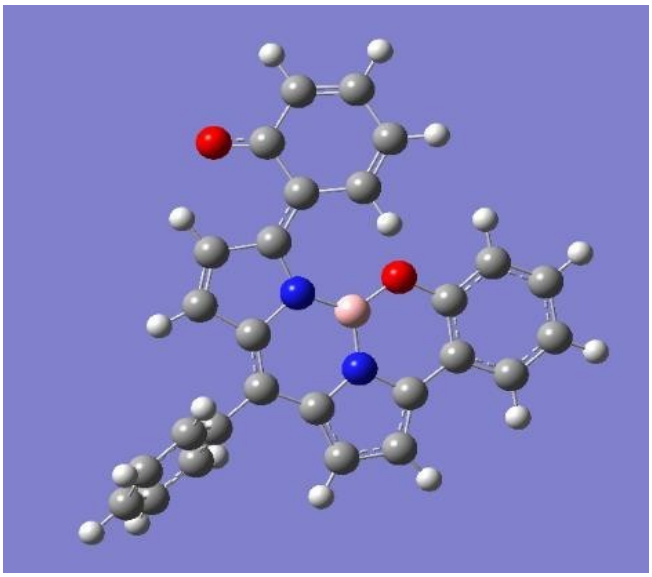

Figure 5. Computed structure having one of the phenoxyl rings dissociated from the boron centre. This is the result of a 2e oxidation of the target compound.

Electrochemical studies made with many conventional BODIPY derivatives show that both oxidation and reduction processes are electrochemically reversible. Oxidation or reduction steps lead to formation of stable radical cations or anions that are localized on the dipyrrin unit. This

suggests that the irreversible oxidation of ST1 is in some way connected with the steric strain imposed by the phenoxyl rings. In turn, this raises the possibility that photochemical oxidation could also lead to rapid loss of the compound. The rest of this chapter considers the photobleaching of ST1 in solution.

5.4 Photobleaching studies

Initial studies were made with the objective of making a cursory examination of the photostability of ST1 in dimethylsulfoxide solution under visible light illumination. Aliquots of the air- equilibrated solution were exposed to the white light source for periods of one hour. The solution bleached fairly quickly whereas solution protected from light retained its colour. Removing molecular oxygen from the solution by purging with a stream of N_2 had little effect on the loss of colour. Under more controlled conditions, with illumination at 620 nm being provided by a high power LED, photobleaching of ST1 occurred as above. That is to say, excitation into the lowest- energy absorption transition around 620 nm is responsible for the bleaching process. Figure 6 shows absorption spectral profiles recorded each 30 minutes during the illumination.

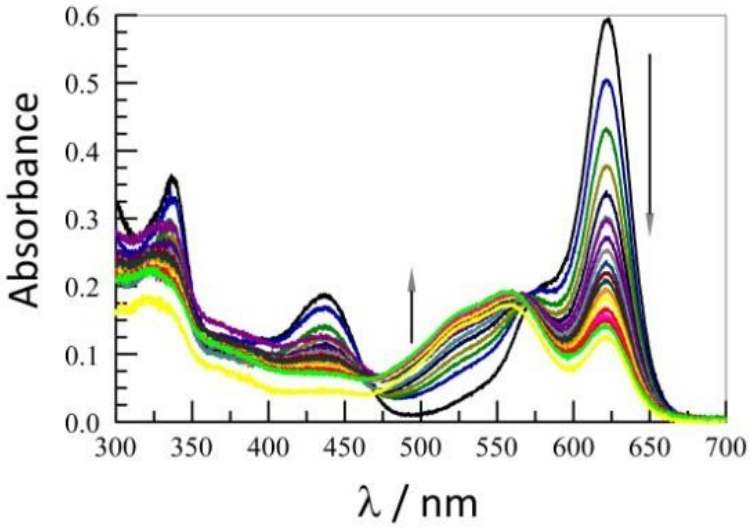

Figure 6. Series of absorption spectra recorded during the photobleaching of ST1 in air-equilibrated DMSO at room temperature. Spectra were recorded each 30 minutes.

The reaction profile shows two important features: Firstly, loss of absorbance at 620 nm is matched by the appearance of absorption in the region around 525 nm. Secondly, loss of absorbance at 620 nm is incomplete, even at long illumination periods. Kinetic measurements made at 620 nm show that photobleaching does not follow a first-order rate law at fixed light intensity. This behavior can be seen from Figure 7a which shows a plot of absorbance at 620 nm versus illumination time. The corresponding semi-logarithmic plot is shown as Figure 7b and is clearly non-linear. In fact, as can be seen from Figure 8, the kinetic data fit well to a dual-

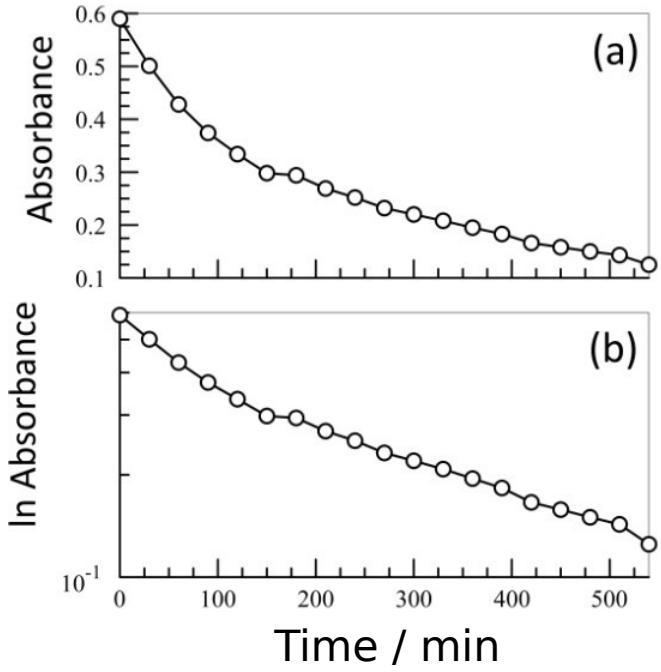

exponential fit with apparent rate constants [illegible] min^{-1}. Separate studies found that the rate of bleaching increased with increasing light intensity so that the derived rate constants are applicable only to a particular set of experimental conditions.

Figure 7. Examples of kinetic measurements made for photobleaching of ST1 in air-equilibrated DMSO solution. Data refer to 620 nm. Plots are for (a) absorbance vs time and (b) ln (absorbance) vs time. The solid lines connect the data points and are not statistical fits.

Figure 8. Fit to the data displayed in Figure 7 to the sum of two-exponential components. The solid line drawn through the data points corresponds to a non-linear, least-squares fit to a dual-exponential fit with the rate constants mentioned in the text.

Time / min

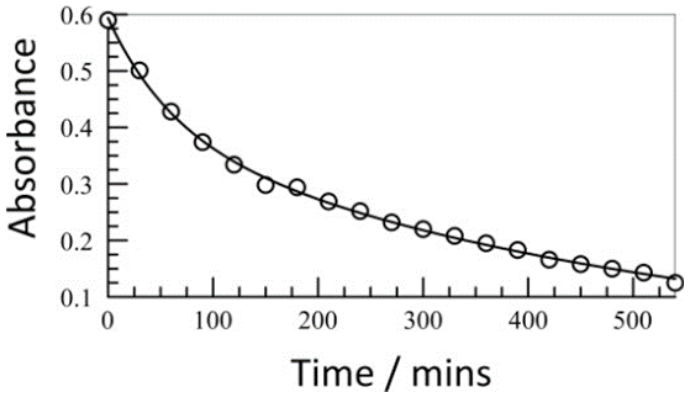

In order to allow for the light-intensity effect, the data displayed in Figure 8 were corrected for changes in absorbance at 620 nm. This was done by firstly converting from absorbance to concentration (in units of μM) using the known molar absorption coefficient (Table 5.1). Secondly, the fraction of incident light intensity absorbed by the dye was calculated from the Beer-Lambert law. Dividing micromolar concentration by this fraction (I_{ABS} = 1 – 10-A) gives the "corrected" concentration at each time interval. These corrected values give a good fit to a dual-exponential bleaching reaction for the data measured at 620 nm. This situation is shown by Figure 9, where the two derived rate constants are k_1 = 0.014 min-1 and k_2 = 0.0004 min-1. These are the preferred rate constants for this reaction. Confirmation of the derived parameters was obtained using a global analysis for data collected between 600 and 630 nm.

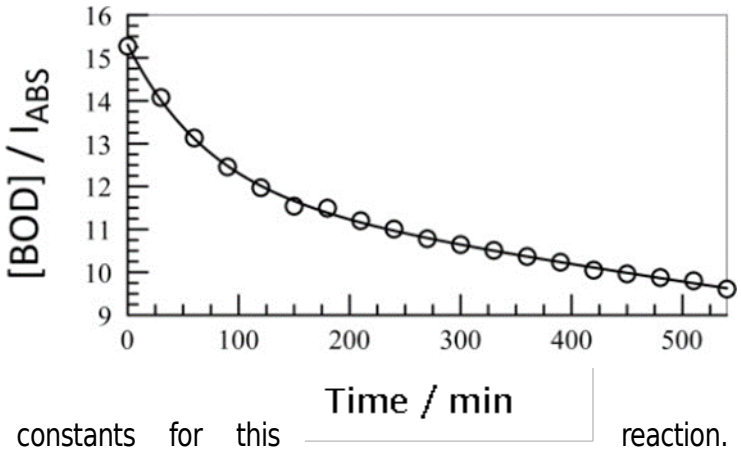

Figure 9. Replot of the kinetic data provided as Figure 7 but allowing for the light-intensity effect. The solid line drawn through the data points corresponds to a non-linear, least-squares fit to Equation 5.1 with the rate constants given in the text.

$$I_0 \times I_{|\zeta|} = A_1 e^{-k_1 t} + A_2 e^{-k_2 t} \quad (Equation\ 5.1)$$

$$\frac{[ST1]}{\zeta}$$

According to Figure 6, and confirmed by kinetic measurements, there is an approximate isosbestic point at around 570 nm. Roughly 75% of the initial absorbance at 620 nm bleaches quickly with the rate constant k_1 while the remaining 25% hardly decays under continued illumination. The ratio k_1/k_2 is about 35. The absorption spectrum recorded across the red region shows that bleaching causes the formation of a new product absorbing in the region around 625 nm; that is to say that the 25% of the initial absorbance at 620 that is resistant to photobleaching is due to a new compound rather a fraction of ST1 that does not bleach. We refer to this new product as being P_{625}. Since the appended phenoxyl rings contribute significantly to the red-shifted absorption[26] profile (relative to conventional BODIPY dyes) it might be argued that the B-O linkages remain intact during this reaction. At shorter wavelengths, a second product accumulates. This latter species has an absorption maximum centred at around 525 nm. Kinetics measurements made at this wavelength indicate that formation of the product occurs via first-order kinetics with a light-intensity corrected rate constant of 0.0030 min^{-1} (Figure 10). The blue shifted absorption maximum might be indicative of the breakage of one or both of the B-O linkages. We refer to this product as P_{525}. Like P_{625}, it is quite stable towards further exposure to light as confirmed by broadband illumination studies. The rate of formation of this product is somewhat slower than the rate of loss of ST1, thereby indication partitioning of the reaction at early stages.

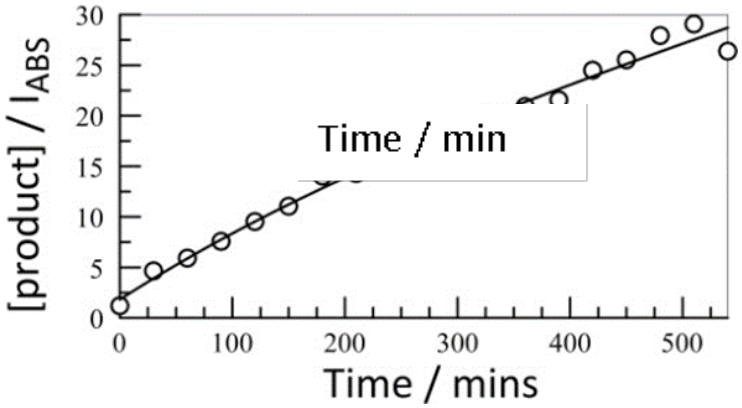

Figure 10. Kinetic plot for the formation of P_{525} at 525 nm following photobleaching of ST1 in air-equilibrated DMSO. The y-axis corresponds to concentration of P_{525} divided by the fraction of incident light absorbed by ST1 at 620 nm. This implies that P_{525} evolves from loss of ST1.

The overall photobleaching behavior deduced for ST1 in air-equilibrated DMSO can be expressed by way of Scheme 1. It is not straightforward to remove all the dissolved O_2 from the viscous solvent so it is not possible to claim that oxygen is not required for the bleaching reaction. It is possible, however, to confirm that the reaction occurs only on exposure to visible light. According to the scheme, illumination of ST1 leads to formation of two products, designated according to their crude absorption maxima as being P_{625} and P_{525}. Both products are relatively photostable. The individual rate constants for formation of each product can be estimated from the kinetic measurements made in the red and green regions and these are indicated on the scheme.

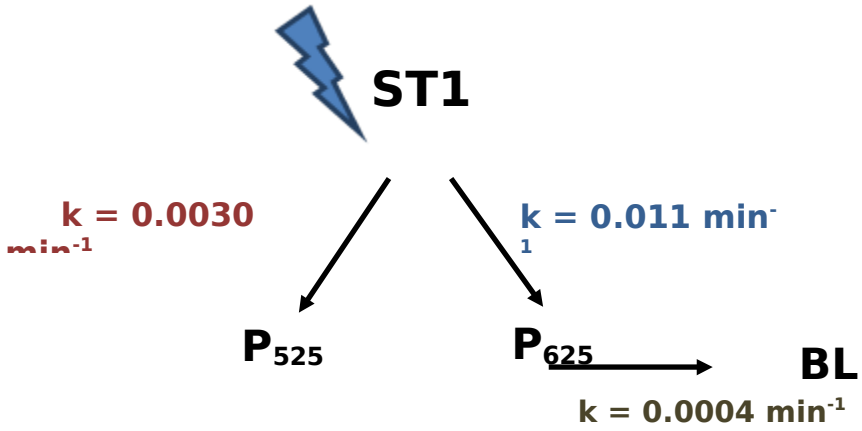

Scheme 1. Generic outline of the partitioning of the photobleaching process that leads to loss of ST1 under illumination. The major process leads to formation of P625 but there is a competing reaction that forms P525. On the timescale of the experiment, P525 is considered to be photostable but P625 bleaches to form a transparent product designated as BL.

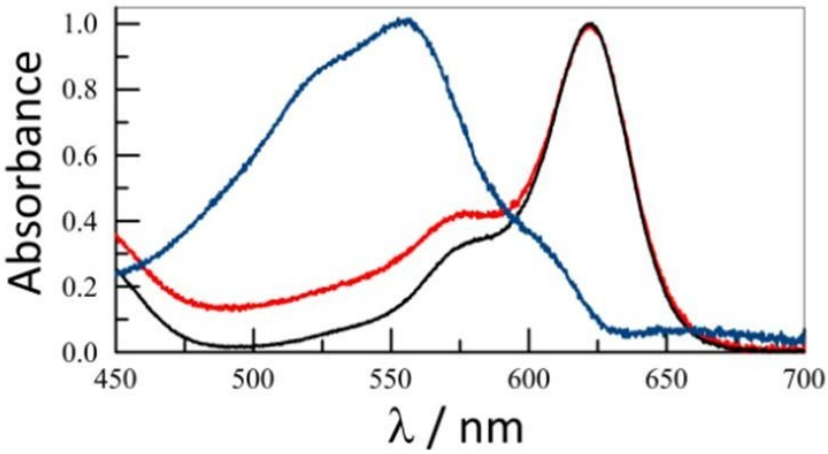

Figure 11. An attempt to extract absorption spectra for the two products by iterative procedures. The initial spectrum for ST1 is shown as a black curve. Part of the signal does not bleach, even on long times, and the resultant spectrum is shown in red. This latter spectrum was obtained by illumination in the presence of TEOA (1M) where build-up of P525 is less apparent.
Removing the spectrum for P625 from the spectrum observed towards the end of a long illumination gives the spectrum shown in blue. This latter spectrum is attributed to P525 (note the peak lies at 555 nm). It can be considered that the absorption spectral features for P625 are basically the same as those of the starting compound, ST1.

5.5 Attempted inhibition of photobleaching

The next phase of the project involved an attempt to hinder the photobleaching of ST1 by the addition of triethanolamine (TEOA). The rationale behind this experiment has its origin in the fact that TEOA fulfils the role of a sacrificial redox agent to reduce oxidized species and return them to their original state.[27-31] For many decades, this basic strategy acts as a convenient means to circumvent charge recombination in photochemical systems aimed at H_2 or O_2 production from water.[32-36] Here, we consider if the photobleaching process leads to transient formation of an oxidized state that might be pushed back to ST1 by way of electron addition from TEOA. In the first experiment, we found that TEOA quenches fluorescence from ST1 in DMSO solution. A reasonably linear Stern-Volmer plot[37] arises from successive addition of TEOA to the solution (Figure 12). The Stern-Volmer constant (K_{SV}) was derived as 0.53 M-1 from Equation 2, which used together with the excited-singlet state lifetime of 10 ns, gives a bimolecular quenching rate constant (k_Q) of 5.3 x 107 M-1 s-1. Note that we consider this quenching step as involving electron donation to the singlet-excited state rather than trapping of an oxidized intermediate.

$$\frac{I_0}{I} - 1 = K_{SV}[TEOA] = k_Q \tau_S [TEOA] \quad (Equation\ 2)$$

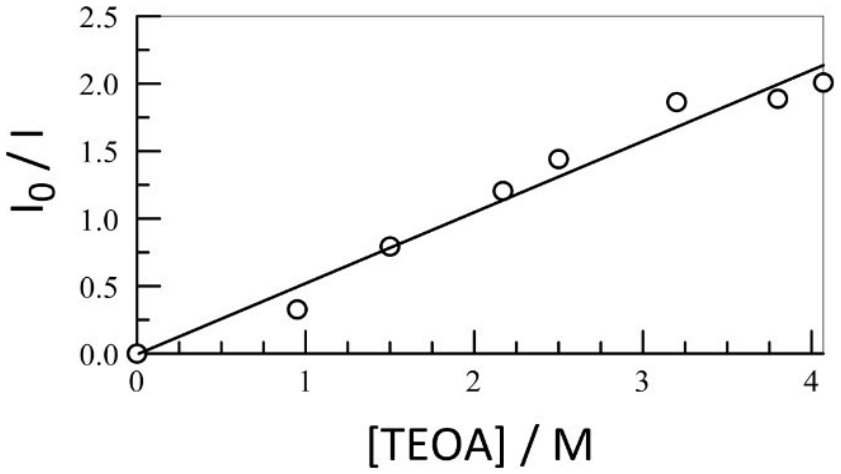

Figure 12. Stern-Volmer plot constructed for the addition of TEOA to a solution of ST1 in DMSO. The solid line drawn through the data points is a fit to Equation 2 with the parameters given in the text.

Subsequent experiments involved adding a small volume of pure TEOA to the solution of ST1 in DMSO prior to illumination. The course of reaction could be followed conveniently by absorption spectroscopy as before and a typical profile is provided as Figure 13. Now, it can be seen that bleaching of ST1 occurs as before, with a relatively fast disappearance of absorbance in the red region. Again, loss of absorbance occurs until reaching about 80% of the initial signal after which bleaching is very slow. As found in the absence of TEOA, a satisfactory fit to the experimental data was attained with a dual exponential model. This leads to derivation of the two accompanying rate constants for the fast (i.e., k_1) and slow (i.e., k_2) bleaching events. It is seen that whereas k_2 remains much the same as observed in the absence of TEOA, k_1 is greatly enhanced. Table 2 provides a compilation of the rate constants obtained as a function of added TEOA concentration.

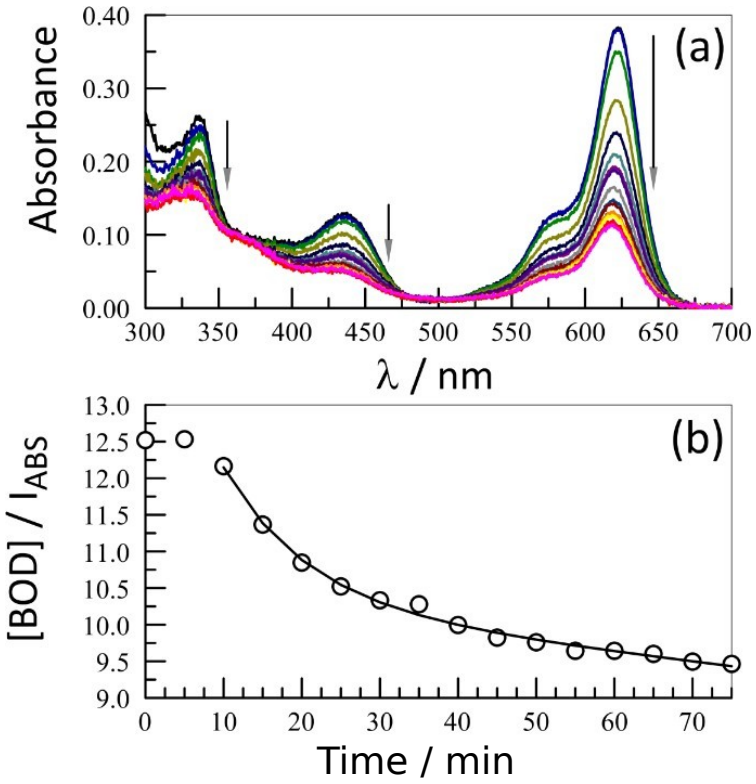

Figure 13. (a) Series of absorption spectral profiles recorded during the photobleaching of ST1 in air-equilibrated DMSO containing a low concentration of TEOA. (b) Kinetic plot recorded for absorbance changes at 620 nm. The solid line drawn through the data points corresponds to a non-linear, least-squares fit to a first-order process. Note the appearance of an induction period at the onset of reaction.

Two interesting features emerge from examination of Figure 13. It is clear that, at least at low concentrations of TEOA, there is a short inhibition period before bleaching takes place. At an initial concentration of TEOA of 0.64 M, the inhibition period is about 10 minutes. This shortens at higher concentration of TEOA but does not disappear altogether, as shown by the kinetic plot given as Figure 14. A further point of interest is that the presence of TEOA prevents build-up of the product absorbing around 525 nm. Indeed, in the presence of TEOA there is no sign of this product, although the second product designated as P_{625} still evolves. We might speculate, therefore, that TEOA intercepts the intermediate species responsible for formation of P_{525}. The introduction of the inhibition period, which is highly reproducible and therefore considered to be of significance in terms of the reaction mechanism, adds an interesting level of complexity.

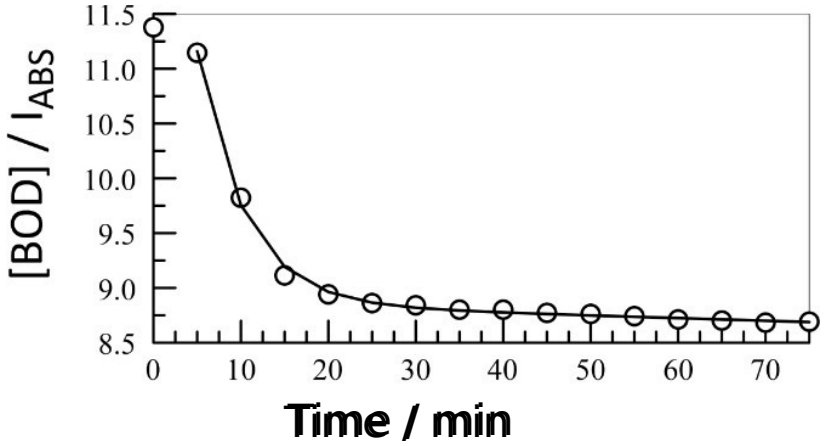

Figure 14. Kinetic plot recorded for absorbance changes at 620 nm during the photobleaching of ST1 in air-equilibrated DMAO containing a high concentration of TEOA. The solid line drawn through the data points corresponds to a non-linear, least-squares fit to a first-order process. Note the reduction but not elimination of the induction period at the onset of reaction.

Table 2. Effect of concentration of triethanolamine on the rate constants for photobleaching of ST1 in air-equilibrated DMSO. The experimental data were analysed in terms of a dual- exponential fit.

[TEOA] / M	k_1 / min-1	k_2 / min-1
0	0.0035	0.0003
0.01	0.058	0.0003
0.07	0.093	0.0013
0.26	0.111	0.0005
0.64	0.127	0.0004
3.42	0.119	0.0002
4.00	0.132	0.0005
5.30	0.156	0.0003

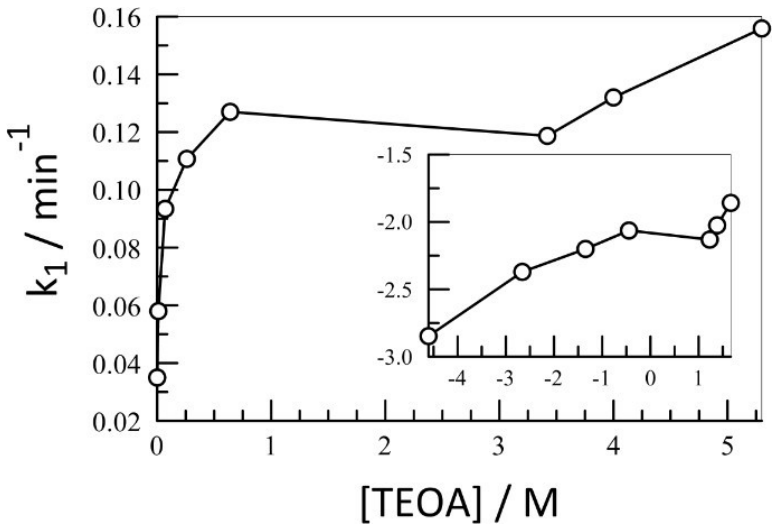

Figure 15. Effect of added TEOA concentration on the dominant rate constant derived for the photobleaching of ST1 in air-equilibrated DMSO. The insert shows the data presented as a log- log plot.

The shape of Figure 15 is consistent with a situation in which TEOA traps an intermediate species. This would account for the near saturation seen at high concentrations. On the other hand, Figure 13a appears to indicate that TEOA curtails formation of P_{525} but does not prevent build-up of P_{625}.

Other factors for us to consider include (i) the inhibition period and (ii) the fact that TEOA quenches fluorescence from the chromophore by way of Stern-Volmer kinetics. There is no inhibition period in the absence of TEOA but it becomes less pronounced with increasing concentration of TEOA. This overall behavior is rather unusual. Before attempting to explain the reaction sequence, attention turns to the use of a more selective substrate – namely indigo.

5.6 Attempted catalysis of secondary bleaching

We have successfully demonstrated photobleaching of the strapped BODIPY chromophore in DMSO solution using visible light illumination. Compared to many other dyes, bleaching of ST1 is relatively fast. For example, under comparable experimental conditions, illumination of the commercial dye indigo has almost no effect on the absorption spectrum. Thus, indigo and ST1 possess comparable absorption spectral profiles as can be seen from Figure 16. Both compounds absorb in the red region, with a maximum located at around 620 nm. Illumination of indigo in air-equilibrated DMSO solution for 250 minutes results in loss of only a small fraction of the initial concentration (Figure 17). Under the same conditions, more than 75% of the initial concentration of ST1 is lost by way of photobleaching.

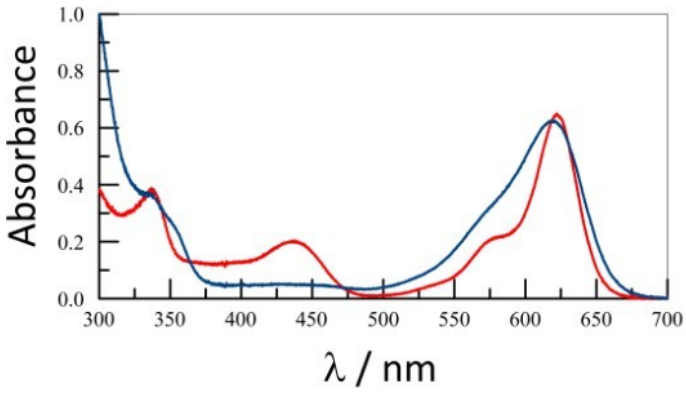

Figure 16. Absorption spectra recorded for ST1 (red curve) and indigo (blue curve) in DMSO. At the absorption maxima in the red region, the molar absorption coefficients are 48,730 M^{-1} cm^{-1} and 20,500 M^{-1} cm^{-1} for ST1 and indigo, respectively.

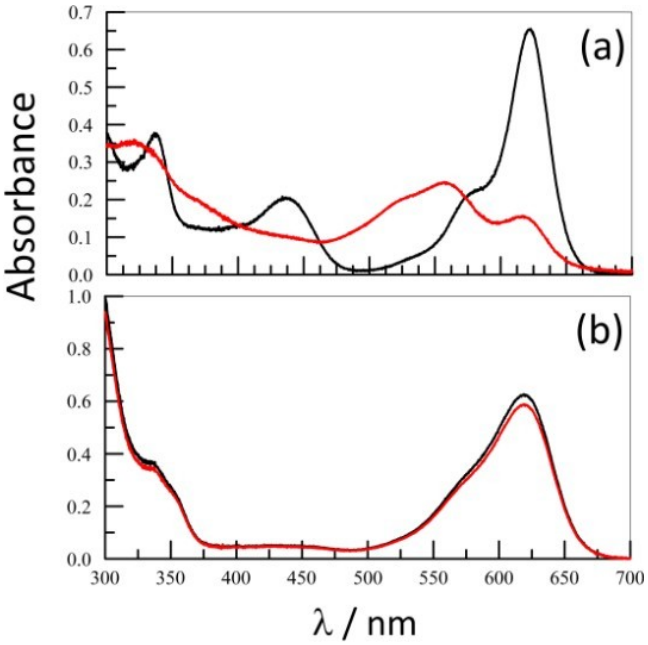

Figure 17. Absorption spectra recorded before (black curve) and after 250 minutes exposure to the broadband illuminator (red curve). Records refer to (a) ST1 and (b) indigo.

Figure 18 shows the results of illumination of a mixture of ST1 (6 μM) and indigo (15 μM) in air-equilibrated DMSO at room temperature. From the spectral records it is possible to see that iso-indigo accumulates as a breakdown product. This species absorbs in the near-UV region, with significant absorption around 380 nm. Since bleaching of indigo is extremely slow in the absence of ST1, it follows that formation of iso-indigo is a consequence of reaction with one or more decomposition products arising from ST1. Bleaching of ST1 is also evident from the figure and, at long exposure times, the characteristic spectral features of P_{625} are noticeable among the spectral records. Although P_{525} evolves during bleaching of ST1, it appears that the yield is significantly lower than obtained in the absence of indigo. Furthermore, accumulation of P_{525} begins only after much of the indigo has been lost. This situation is reasonable if indigo intercepts one of the key intermediates involved in conversion of ST1 to P_{525}. This behaviour is comparable to that found for addition of TEOA, except for the fact that the concentration of indigo is very much lower. It is known that indigo is susceptible to attack by oxy-radicals

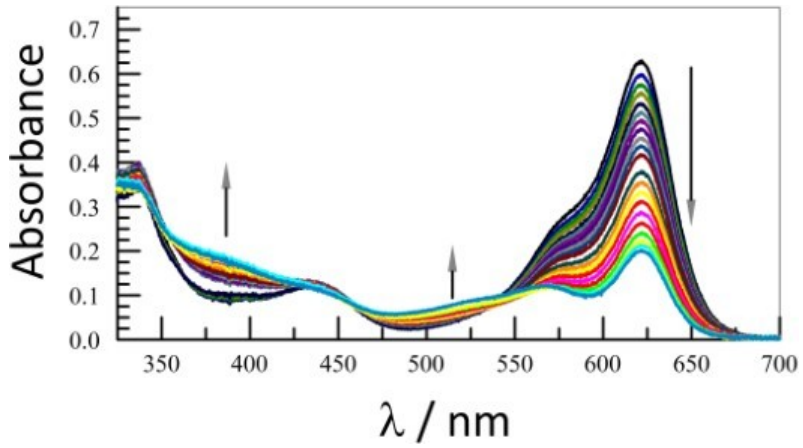

Figure 18. Photobleaching of a mixture of ST1 and indigo in air-equilibrated DMSO at room temperature. Individual absorption spectral profiles were recorded at various times throughout the reaction. The arrows indicate the course of increased exposure time.

The build-up of iso-indigo, monitored at 380 nm, begins as soon as illumination starts but the rate of formation essentially stops after about 150 minutes (Figure 19). Presumably, this reflects quantitative consumption of indigo. In contrast, formation of P525 is initially slow but increases markedly with decreasing concentration of indigo (Figure 19). Therefore, the two reactions are in direct competition but bleaching of indigo must be far more efficient than is formation of P_{525}, under these conditions. The bleaching of indigo might involve sensitized formation of singlet molecular oxygen, which has a lifetime of only 5.5 μs in DMSO, or more likely attack by an oxy-radical associated with ST1. At the low concentration of indigo used for these experiments, it seems unrealistic for this substrate to intercept singlet oxygen before is decays nonradiatively. Any oxy-radical derived from the bleaching of ST1, however, is likely to be longer-lived and therefore more likely to react with indigo. It follows that this same oxy-radical must be implicit in the conversion of ST1 to P_{525}.

Monitoring at 620 nm, we see that the loss of absorbance gives a reasonable fit to first-order kinetics with a rate constant of 0.040 min^{-1} for the initial 100 minutes or so (Figure 19). After this period, the rate of loss of absorbance begins to increase.

This situation can be explained in terms of ST1 catalyzing the conversion of indigo to iso-indigo with a rate constant of 0.040 min^{-1}. This situation requires that no appreciable amount of ST1 is lost during this period. As the concentration of indigo falls below some critical level, bleaching of

ST1 begins and P_{525} starts to accumulate with a first-order rate constant of 0.020 min^{-1}. This leads us to the modified reaction sequence shown as Scheme 3. It might be emphasized that the concentration of indigo is too low for this species to be a direct quencher of the excited state and that there is no spectroscopic evidence for complexation between ST1 and indigo.

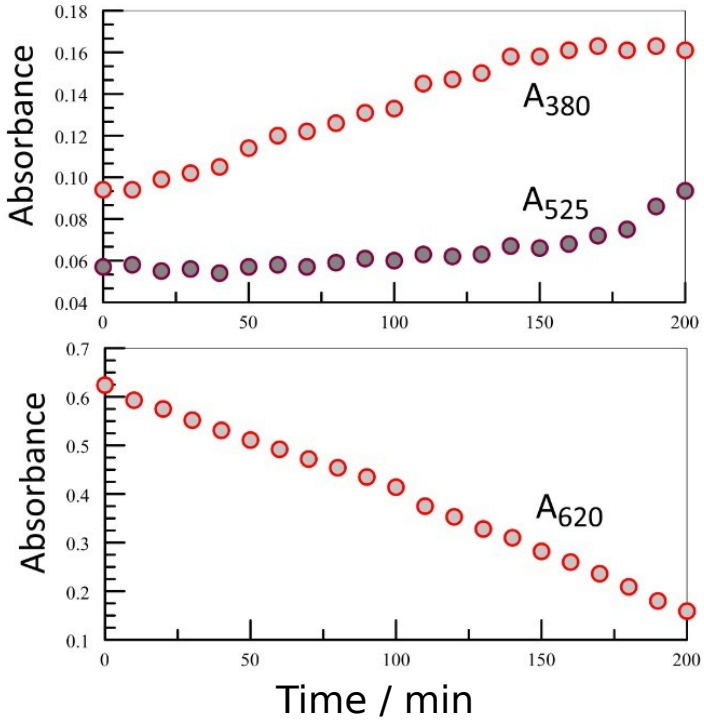

Figure 19. Absorbance changes recorded at different monitoring wavelengths following illumination of ST1 (6 µM) in air-equilibrated DMSO containing indigo (15 µM). The upper panel shows the accumulation of iso0indigo at 380 nm and of P525 at 525 nm. The lower panel shows the loss of ST1 as monitored at 620 nm.

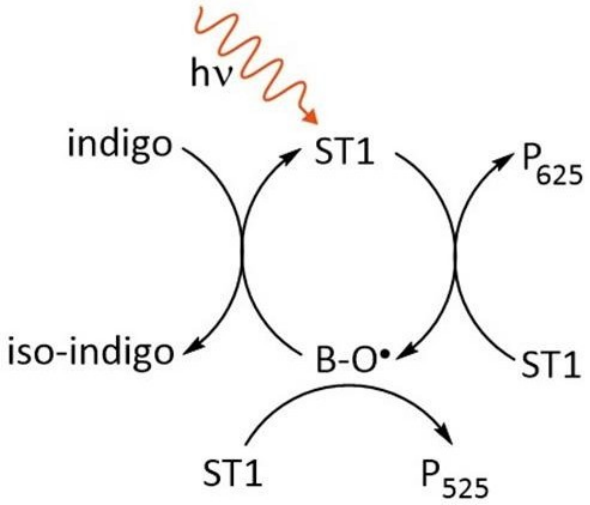

Scheme 3. Representation of the reactions involved in the photobleaching of ST1 in the presence of indigo. We consider that illumination of ST1 forms, presumably in low yield, an oxy-radical of the type B-O. This latter species reacts catalytically with indigo to form iso-indigo. The radical also reacts with a further molecule of ST1 to form either P625 or P525. These latter products begin to accumulate only when the rate of formation of iso-indigo slows down.

We now return to the photobleaching of ST1 in the presence of TEOA. The approximate quantum yield for bleaching of ST1 in air-equilibrated DMSO containing TEOA (1M) was determined to be 2 ± 1 x 10^{-5}. Compared to many fluorescent dyes, such as Rhodamine 6G, this is relatively high. Under the same conditions, TEOA quenches ca. 30% of the fluorescence from ST1. Given the great disparity in these two values, we might argue that bleaching is not associated with electron donation to the excited-singlet state by TEOA. We can explain the observed Stern-Volmer quenching in terms of light-induced charge transfer from TEOA to the excited state of ST1. Any π-radical anion that dissociates from the geminate pair will be immediately-re-oxidized by molecular oxygen. It was reported many years ago that the one-electron oxidized form of TEOA undergoes deprotonation to form a reducing, neutral radical, at least in aqueous solution. The net result is consumption of TEOA but no change in terms of ST1. The triplet-excited state of ST1, which forms in low yield, is also likely to react with added TEOA by way of bimolecular electron transfer with the same general effect.

Figure 15 is suggestive of TEOA trapping a critical intermediate species, possibly the oxy-radical referred to above. To be correct, this finding would require that the trapped species leads to an increase in the rate of overall bleaching of the chromophore but by-passes conversion to P_{525}. Of course, TEOA is well set up to deliver a hydrogen atom (i.e., a proton and an electron) to the oxy-radical to produce a neutral species B-OH. This latter reaction might require the presence of water

but NMR spectroscopy confirmed contamination of our sample of DMSO with trace amounts of water. The actual identity of B-OH is outside the scope of this work but, since colour is lost during photobleaching, it might involve serious perturbation of the dipyrrin backbone. The cause of the inhibition period is equally difficult to define.

5.7 Conclusion

In this chapter, we have considered the photobleaching of a doubly-strapped BODIPY derivative. The rationale for examining this compound is based on the fact that the X-ray crystal structure shows the dipyrrin unit to be distorted from planarity due to internal strain. It might be considered that this stress could be removed by breaking one of the B-O (or C-O) bonds. The second argument for studying this compound comes from the realization that electrochemical oxidation is irreversible and leads to chemical transformation. Most conventional BODIPY compounds exhibit fully reversible electrochemistry so the situation found for ST1 must be due to the straps. Separate to our investigations, Dr. Patrycja Stachelek is looking in great detail at the photophysics of ST1 and related compounds. She has confirmed that the triplet-excited state is formed in low yield, specifically in acetonitrile solution. We have found that ST1 is susceptible to photobleaching in solution. The quantum yield is around 1×10^{-5}, which taken with the fluorescence lifetime of 10 ns leads to a first-order rate constant for excited-state bleaching of ca. 10^3 s^{-1}. The fact that the apparent rate constant for the photobleaching event is ca. 0.01 min^{-1} reflects the relative probability for excitation of any particular solute molecule. This is the limiting step in our work but might not be under different experimental conditions. For example, very high photon densities are used for single molecule spectroscopy and for super-resolution microscopy. We might anticipate that ST1 would bleach very quickly under such circumstances.

We are not able to identify the breakdown products. Although relatively fast, the rate of photobleaching is too slow for the reaction to be followed by NMR spectroscopy. Instead, we have used trapping studies to help resolve the steps involved in the bleaching chemistry. There are indications that ST1 functions as a photocatalyst for conversion of indigo to the colourless iso-indigo. If this is indeed correct, compounds similar to ST1 might be useful as photobleaches. This

would require preparation of a water-soluble derivative. The photocatalysed bleaching of indigo is considered in more detail in Chapter 3.

5.8 References

[1] M. A. Haidekker, E. A. Theodorakis, *J. Bio. Eng.* **2010**, 4, 11.

[2] A. V. Niauskas, I. Lopez-Duarte, N. Duchemin, T.-T. Vu, Y. W. Wu, E. M. Budynina, Y. A. Volkova, E. P. Cabrera, D. E. R. Ramı´rez-Ornelasc, M. K. Kuimova, *Phys.Chem.Chem.Phys*. **2017**, 19, 25252.

[3] M. A. Haidekker, M. Nipper, A. Mustafic, D. Lichlyter, M. Dakanali, E. A. Theodorakis, "Dyes with Segmental Mobility: Molecular Rotors", Springer Berlin Heidelberg, Berlin, Heidelberg, 2010.

[4] M. K. Kuimova, *Phys. Chem. Chem. Phys.* **2012**, 14, 12671.

[5] M. K. Kuimova, S. W. Botchway, A. W. Parker, M. Balaz, H. A. Collins, H. L. Anderson, K. Suhling, P. R. Ogilby, *Nat. Chem.* **2009**, 1, 69.

[6] M. A. Haidekker, E. A. Theodorakis, *Org. Biomol. Chem*. **2007**, 5, 1669.

[7] M. A. H. Alamiry, A. C. Benniston, A. Harriman, *J. Phys. Chem*. A. **2011**, 44, 12111.

[8] M. A. H. Alamiry, A. C. Benniston, G. Copley, K. J. Elliott, A. Harriman, B. Stewart, Y. GangZhi, *Chem. Mater*. **2008**, 20, 4024.

[9] G. R. Ziessel, A. Harriman, *Angew. Chem., Int. Ed.* **2008**, 47, 1184.

[10] H. L. Kee , C. Kirmaier , L. Yu , P. Thamyongkit , W. J. Youngblood , M. E. Calder , L. Ramos , B. C. Noll , D. F. Bocian , W. R. Scheidt , R. R. Birge , J. S. Lindsey, D. Holten, *J. Phys. Chem. B.* **2005**, 109 , 20433.

[11] E. Bahaidarah, A. Harriman, P. Stachelek, S. Rihn, E. Heyerb, R. Ziessel, *Photochem. Photobiol. Sci.* **2014**, 13, 1397.

[12] E. Bodio, C. Goze, Dyes and Pigments, **2019**, 160, 700.

[13] H. Kee, C. Kirmaier, L. Yu, P. T, W. J. Youngblood, M. E. Calder, L. Ramos, B. C. Noll, D. F. Bocian, W. R. Schiedt, R. R. Birge, J. S. Lindsey, D. Holten, J. Phys. Chem. B. **2005**, 09, 20433.

[14] R. Ziessel, G. Ulrich, A. Harriman, *New J. Chem*. **2007**, 31, 496.

[15] G. Ulrich, R. Ziessel, A. Harriman, *Angew. Chem. Int. Ed. Engl*. **2008**, 47, 1184.

[16] A. Loudet, K. Burgess, *Chem. Rev*. **2007**, 107, 4891.

[17] R. B. Alnoman, S. Rihn, D. C. O'Connor, F. A. Black, B. Costello, P. G. Waddell, W. Clegg, R. D. Peacock, W. Herrebout, J. G. Knight, M. J. Hall, *Chem. Eur. J.* **2016**, 22, 93.

[18] G. Ulrich, R. Ziessel, A. Harriman, *Angew. Chem. Int. Ed*. **2008**, 47, 1184.

[19] T. Nabeshima, M. Yamamura, G. J. Richards, T. Nakamura, *J. Synth. Org. Chem. Jpn.* **2015,** 11, 1111.

[20] M. Wang, M. Grace, H. Vicente, D. Mason, P. B. Parvanova, *ACS Omega.* **2018**, 3, 5502.

[21] K. Trofymchuk, J. Valanciunaite, B. Andreiuk, A. Reisch, M. Collot, A. S. Klymchenko, *J. Mater. Chem. B* **2019**, 7, 5199.

[22] M. Hecht, T. Fischer, P. Dietrich, W. Kraus, A. B. Descalzo, W. E. S. Unger, K. Rurack, *ChemistryOpen*. **2013**, 2, 25.

[23] N. Boens, V. Leen, W. Dehaen, *Chem. Soc. Rev*. **2012**, 41, 1130.

[24] J. Rumin, H. Bonnefond, B. Saint-Jean, C. Rouxel, A. Sciandra, O. Bernard, J.-P. Cadoret, G. Bougaran, *Biotechnology for Biofuels.* **2015**, 8, 42.

[25] X.-D. Jiang, R. Gao, Y. Yue, G.-T. Sun, W. Zhao, *Org. Biomol. Chem*. **2012**, 10, 6861.

[26] T. Aotake, M. Suzuki, N. Aratani, J. Yuasa, D. Kuzuhara, H. Hayashi, H. Nakano, T. Kawai, J. Wuc, H. Yamada, *Chem. Commun*. **2015**, 51, 6734.

[27] Y. Pellegrin, F. Odobel, *C. R. Chimie*, **2017**, 20, 238.

[28] E.D. Cline, S.E. Adamson, S. Bernhard, *Inorg. Chem.* **2008**, 47, 10378.

[29] K. Kalyanasundaram, J. Kiwi, M. Gratzel, *Helv. Chim. Acta*. **1978**, 61, 2720.

[30] J. Hawecker, J.M. Lehn, R. Ziessel, *J. Chem. Soc. eChem. Commun*. **1983**, 5, 36.

[31] Y.L. Chow, W.C. Danen, S.F. Nelsen, D.H. Rosenblatt, *Chem. Rev*. **1978**, 78, 243.

[32] T. Jafari, E. Moharreri, A. S. Amin, R. Miao, W. Song, S. L. Suib, *Molecules,* **2016**, 21, 900.

[33] A. A. Ismail, D.W. Bahnemann, *Solar Energy Materials & Solar Cells.* **2014**, 128, 85.

[34] A. J. Bard, M. A. Bard, *Acc. Chem. Res*. **1995**, 8, 141.

[35] W. Lubitz, E. J. Reijerse, J. Messinger, *Energy Environ. Sci*. **2008**, 1, 15.

[36] K. Han, M. Wang, S. Zhang, S. Wu, Y. Yanga, L. Sun, *Chem. Commun.* **2015**, 51, 7008.

[37] G. K. Rollefson, H. Boaz, *J. Phys. Colloid Chem*, **1948**, 52, 518.

Chapter 6.

The *in-situ* production of chlorine dioxide

Drinking water on tap…

6.1 Summary

In this chapter we examine the possibility of forming chlorine dioxide by the one-electron oxidation of the chlorite ion in neutral aqueous solution. This is intended to be a relatively stable oxidant that might be used as a bleaching agent in secondary chemical processes. Together with the chemical oxidation, a simple means for quantitative analysis of chlorine dioxide has been developed based on the oxidation of Chlorophenol Red in alkaline solution. The chemical oxidation of chlorite proceeded in fairly low yield. An improved protocol was established using photochemical methods. The first such approach is based on the sacrificial oxidation of tris(2,2-bipyridyl)ruthenium(II) using persulfate. The second approach dispenses with the sensitizer and makes use of a photovoltaic cell. This latter method works very well and it is possible to produce high concentrations of chlorine dioxide using visible light illumination. The final section describes briefly the photobleaching of the BOPHY chromophore in the presence of molecular oxygen and (high concentrations of) chlorite.

6.2 Introduction

The main difficulty associated with using photochemistry to effect bleaching of substrates in solution concerns the short lifetime of the intermediates species. Excited singlet and triplet states possess typical lifetimes of a few nanoseconds and a few microseconds, respectively, in air-equilibrated water. Such lifetimes are far too short for viable bleaching chemistry unless the substrate is present at very high concentration. For example, incorporating a benzophenone residue into the backbone of a polymer before fabricating a plastic bottle will result in a photodegradable material. Dissolving the benzophenone in water and filling the bottle with solution is not going to have any effect on the structure of the bottle, regardless of how long it is left in strong sunlight. Singlet molecular oxygen is a highly reactive species but its lifetime in water is only 5 τ_s or so and does not overcome the kinetic problems mentioned here. Organic hydroperoxides and peroxides offer more promise in as much as their lifetimes can be minutes or even many hours but, at least in most cases, organic solvents are needed. The approach based on in-situ preparation of an organic hydroperoxide is interesting, and perhaps practical, but we need also to develop something that works in water. In considering alternative bleaching agents we turn our attention to chlorine dioxide. This free radical species has received almost no attention as a

photochemical bleaching agent but it has several useful properties that make it an attractive reagent. Chlorine dioxide is soluble in water and is known to be a powerful antiseptic agent with demonstrated capability to sterilise surfaces.[1] It is safe for human use[2] and has been proposed as a replacement for chlorine in sterilising drinking water.[3] Chlorine dioxide, being a volatile gas, escapes from warm aqueous solution such that the solution needs to be prepared in situ. It is a modest oxidising agent.[4] Under near-UV light, chlorine dioxide is converted to the chlorine peroxyl radical, which is a much more powerful oxidant.[5,6]

The usual way to prepare chlorine dioxide is by oxidation of sodium chlorite in water at pH 7. A convenient oxidant is acetic anhydride,[7] which has been shown to give overall yields of chlorine dioxide in solution in the region of 45-50%. This, of course, is a thermal reaction that does not require light. It is also possible to prepare chlorine dioxide using a simple electrochemical method based on the electrolysis of sodium chlorite in water.[8] This latter method appears to be effective and can be used to produce solutions of chlorine dioxide in the region of 15% within relative short electrolysis periods.[9] The absorption spectrum of chlorine dioxide in water is not particularly useful as an analytical tool since it falls in the near-UV region. Indeed, it is more convenient to use the bleaching of a dye for analytical purposes and it has been proposed that chlorophenol red, a well-known pH indicator for neutral solution, is a good reagent for the quantitative analysis of chlorine dioxide in water. This provides a simple but reliable test[10] that can be carried out in the presence of other oxidizing agents.[11-14] Chlorine dioxide possesses useful properties as an aqueous bleach and, being a free radical with a delocalised structure, reacts quickly with many substrates. Sodium chlorite is a readily available reagent used as a mild antiseptic agent in toothpaste and related products. It is stable, both as a solid and in aqueous solution, and inexpensive. It is sometimes used to clean bottles for subsequent filling with wine or water but it is not safe to drink. Our interest is to identify a convenient photochemical protocol that might be used to produce large quantities of chlorine dioxide that could be used as a strong bleaching agent in remote locations. Ideally, this process would consist of dissolving sodium chlorite in “dirty” water and exposing to sunlight after setting up the photochemical component. Illumination would be used either to generate water for drinking or washing purposes or to remove toxins. Because

chlorine dioxide easily escapes from water at ambient temperature, analysis needs to be performed in real time. It is not practical to employ absorption spectroscopy for the routine analysis of ClO_2 because the absorption profile lies at 380 nm[15] and the molar absorption coefficient is only 1,100 M^{-1} cm^{-1}. Furthermore, it is highly unlikely that an absorption spectrophotometer would be readily available in the same remote site where clean water is scarce. As such, part of our work involves setting up a reliable test for estimating the concentration of chlorine dioxide in water.

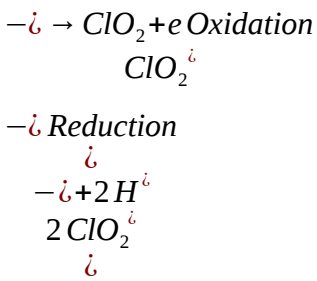

6.3 Oxidation of chlorite

Chlorine dioxide has to be freshly prepared but there are no universally recognised preparative procedures. Cyclic voltammetry studies made with sodium chlorite in water showed the one-electron oxidation potential to be 0.66 V vs NHE at pH 7 but 0.79 V vs NHE at pH 4 communication with Dr. Patrycja Stachelek. As such, it should be relatively straightforward to bring about the one-electron oxidation of chlorite in neutral aqueous solution. One of the most common chemical procedures involves oxidation of sodium chlorite with chlorine gas. This reaction forms hypochlorous acid as an intermediate but was considered too dangerous for us to use. Instead, our initial studies focused on the oxidation of sodium chlorite by acetic anhydride,[16] with the concentration of ClO_2 being detected by iodometric titration.[17,18] The maximum yield that could be obtained by this route was limited to about 45%, even after careful optimisation of the reaction conditions. In particular, the initial pH was found to be important, as was the relative concentration of oxidant. After initial trials, the pH was fixed at 7.0 with phosphate buffer while the molar ratio of oxidant to chlorite was maintained at 1.2. It was necessary to firstly dissolve the sodium chlorite in buffer and to vigorously stir the solution before addition of the acetic anhydride. Even after varying

all the possible reaction conditions, it was not possible to obtain chlorine dioxide at a conversion yield in excess of 45%. However, adding one equivalent of the strong oxidant sodium hypochlorite before adding the acetic anhydride resulted in quantitative formation of chlorine dioxide. The impression is formed that acetic anhydride hydrolyses in a competing reaction. Even so, it was possible to produce chlorine dioxide in acceptable quantities on a routine manner. The next phase of the work involved setting up a standard procedure for routine analysis of chlorine dioxide using Chlorophenol Red as indicator (Figure 1).

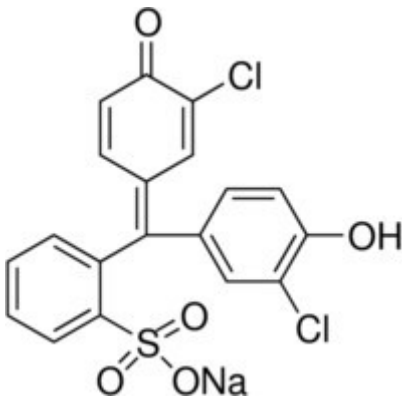

Figure 1. Molecular formula for Chlorophenol Red used as chemical indicator for detecting chlorine dioxide. Samples were purchased from Sigma-Aldrich and used as received.

The absorption spectrum recorded for Chlorophenol Red (CPR) in alkaline aqueous solution shows a pronounced absorption maximum centred at 573 nm (ε_{MAX} = 1.51×104 M-1 cm-1). The absorption spectrum is sensitive to changes in pH and a new absorption maximum appears at 434 nm in acidic solution. This is due to a Pk_A transition associated with the two phenolic residues,[19,20] which can be followed by a spectrophotometric titration (Figure 2). Only a single step is observed, indicating that each phenol acts independently (Figure 3). From the pH effect on the ratio of the absorbance values at the respective maxima, the pK_A is calculated to be 7.3. Since the anionic form of CPR is more coloured, it follows that the negative charge is delocalized around the aromatic structure. On treating an aqueous solution of CPR with ClO_2, the dye is irreversibly bleached in what appears to be a 1:2 stoichiometry. This process was studied by first standardizing the oxidant solution with starch-iodine and adding small volumes of the standard solution to a stirred solution of CPR buffered at pH8. The reaction is attributed to oxidation of the dye by ClO_2. A convenient way to carry out this analysis involved removal of ClO_2 from the solution using in a stream of N_2 and subsequent trapping with CPR (Figure 4).

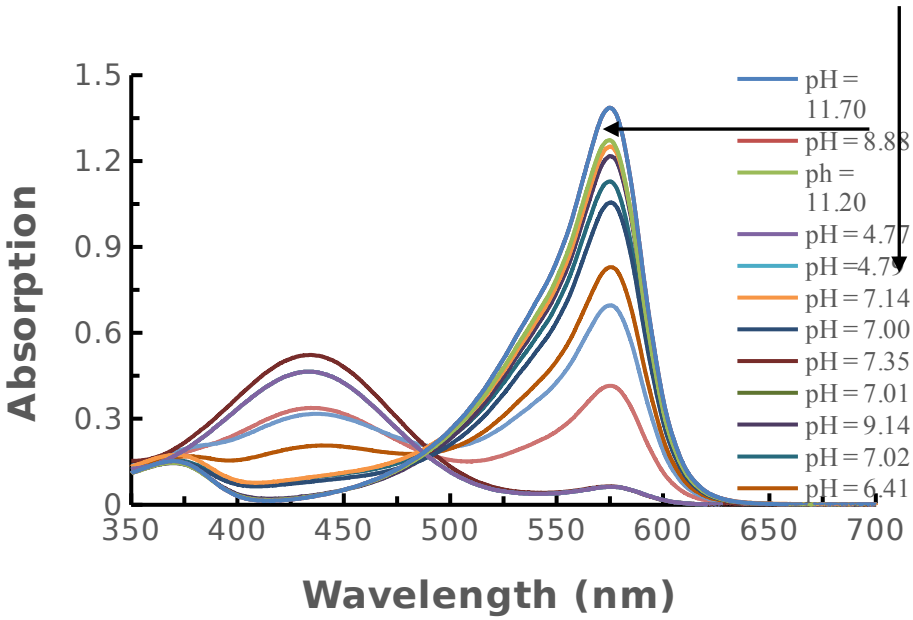

Figure 2. Absorption spectra recorded for Chlorophenol Red (CPR) in water at different pH values.

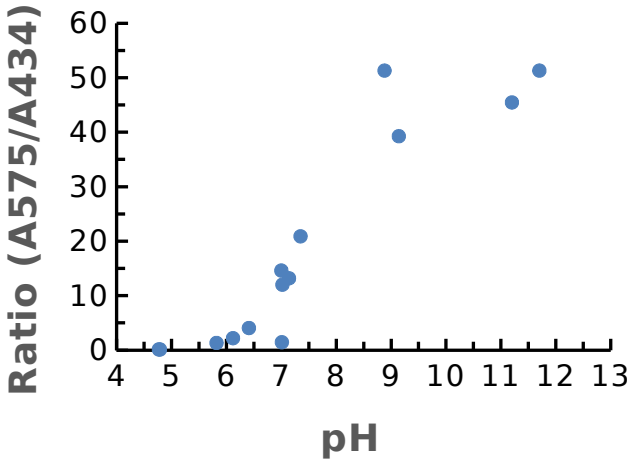

Figure 3. Effect of pH on the absorbance ratio Ratio (A_{575}/A_{434}) at different pH values.

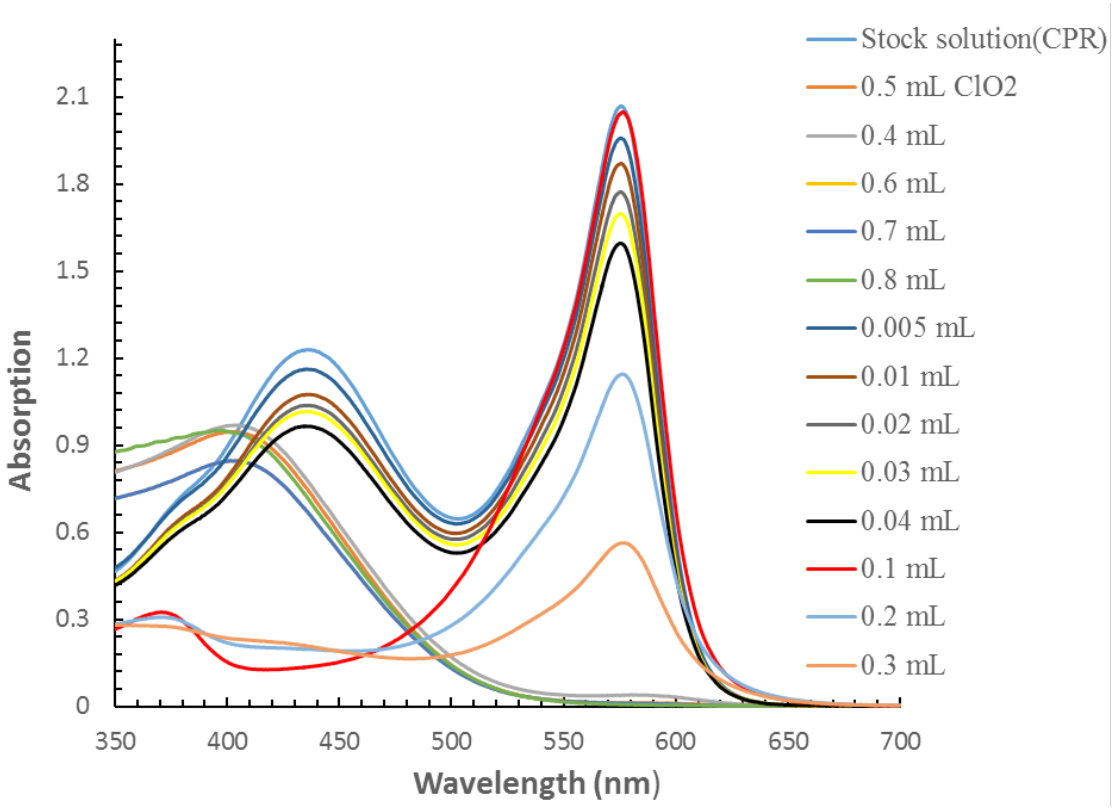

Figure 4. Absorption spectra recorded following addition of different amounts of chlorine dioxide solution to Chlorophenol Red (CPR) solution.

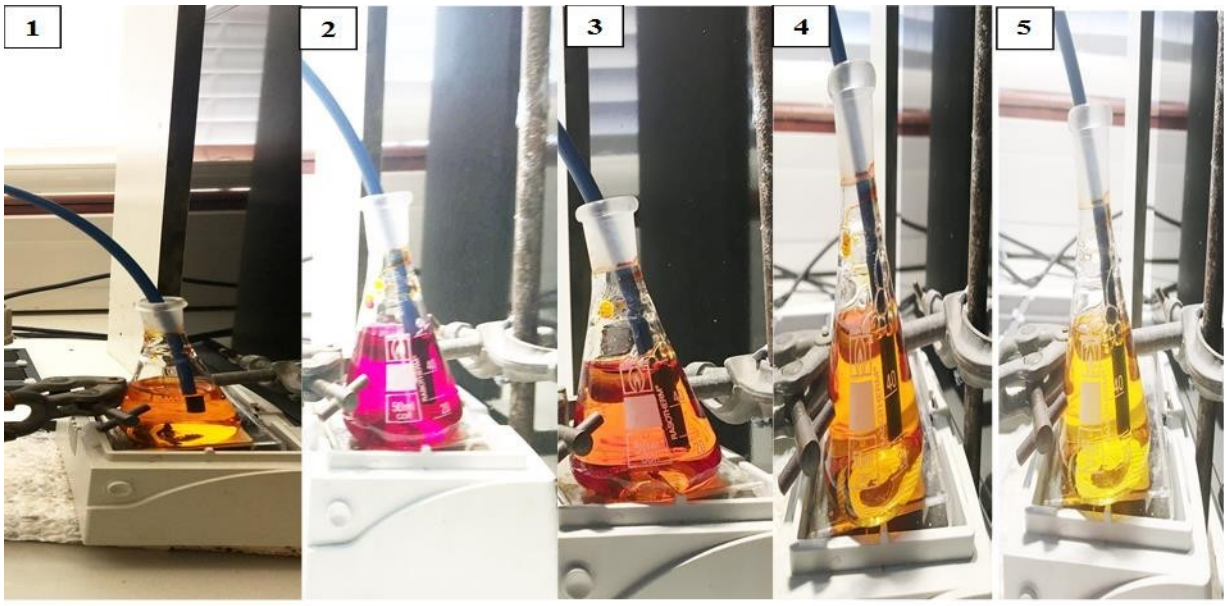

Figure 5. The photographs illustrate stages of discoloration of CPR that confirm formation of chlorine dioxide.

An obvious problem inherent to the use of acetic anhydride as chemical oxidant is that the solution contains acetic acid which will affect the pH. The reaction leading to formation of chlorine dioxide is also quite complex and far from stoichiometric. Therefore, addition was turned towards seeking a simpler alternative, preferably a reaction that could be initiated by light. One such chemical oxidant is the tris(2,2'-bipyridyl)ruthenium(III) cation which is a powerful one- electron oxidant. This species is easily formed from the corresponding dication in water, which absorbs strongly (ε_{453} = 14,500 M-1 cm-1) at 453 nm (Figure 6).21 For several decades, the dication has been used to test potential catalysts for oxidation of water to molecular oxygen.

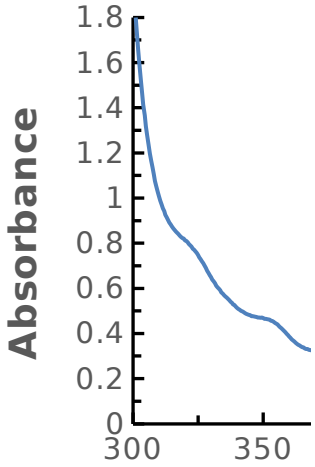

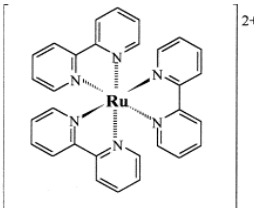

Figure 6. Absorption spectrum recorded for the tris(2,2'-bipyridyl)ruthenium(II) dication in water at pH 7.

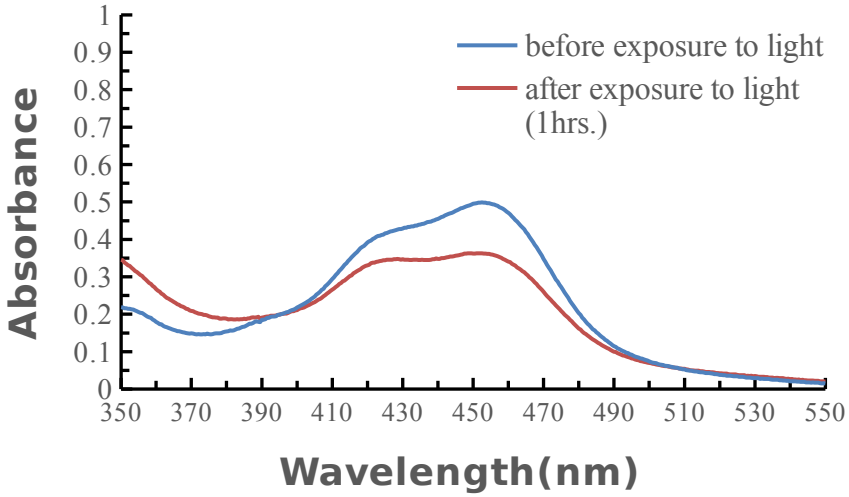

Illumination of a solution of tris(2,2'-bipyridyl)ruthenium(II) dication in water at pH 7 containing $Na_2S_2O_8$ (0.05 M) causes one-electron oxidation of the sensitizer. This is a well-known reaction using what is often termed a sacrificial redox agent – namely, sodium persulfate. After removing molecular oxygen with a steady stream of N_2, the reaction was found to proceed much faster (Figure 7).

Figure 7. Absorption spectra recorded before and after illumination of a mixture of tris(2,2'-bipyridyl)ruthenium(II)
dication in de-aerated water containing $Na_2S_2O_8$ (0.05 M).

This experiment was repeated but with two significant changes. Firstly, sodium chlorite (0.1 M) was added to the solution and secondly a slow stream of N_2 was passed through the solution during the illumination period. The exit stream was bubbled through a solution of CPR in water at pH 8. The course of reaction was monitored by changes in colour of the CPR solution. It was noted that the characteristic red colour of the solution faded quickly and the solution turned a faint orange colour, which is characteristic of the oxidized form of CPR. Figure 8 shows the effect of a 3-hour illumination period.

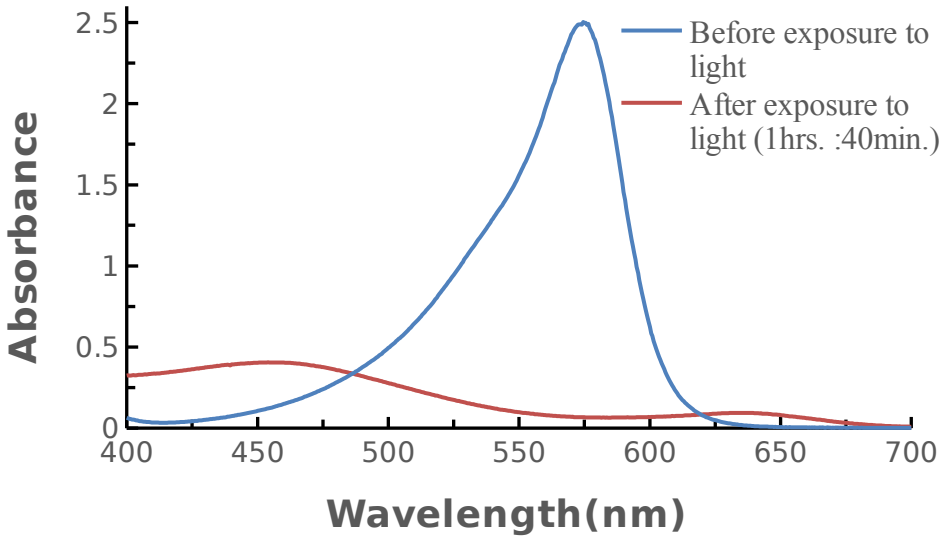

Figure 8. Absorption spectra recorded for a solution of CPR in water at pH 8 before and after illumination of the sensitizer solution containing both persulfate and chlorite. A slow stream of N_2 was used to transfer any chlorine dioxide from the sensitizer solution to the CPR solution.

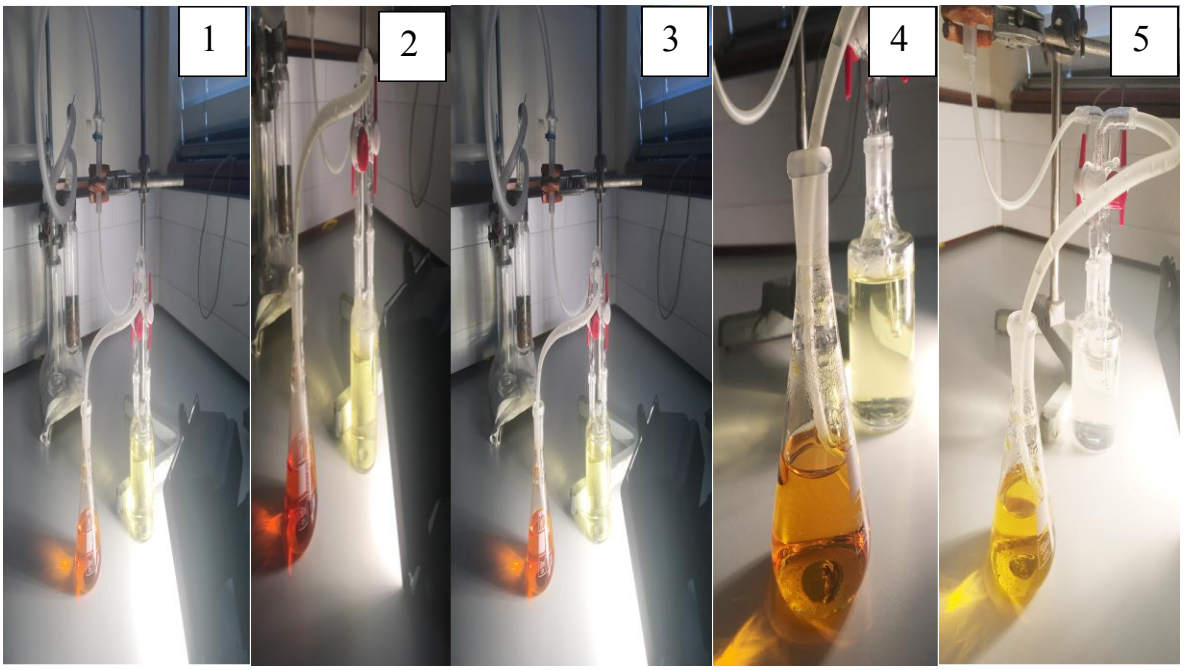

Figure 9. The photograph illustrates stages of discoloration of CPR that confirm formation of chlorine dioxide under illumination.

The reaction can be considered to take place as follows: Illumination of the sensitizer in de-aerated solution causes electron transfer from the excited-triplet state to the ground state of the persulfate ion. This results in formation of tris(2,2'-bipyridyl)ruthenium(III). The reduced form of persulfate quickly dissociates to sulfate and the sulfate radical cation. The latter is a powerful oxidant and, under the conditions of the experiment, will oxidize a molecule of chlorite to chlorine dioxide. The tris(2,2'-bipyridyl)ruthenium(III) cation is also sufficiently strong to oxidise chlorite to chlorine dioxide and itself is restored to the original sensitizer. The reaction, therefore, is catalytic with respect to formation of chlorine dioxide. The latter is removed from solution by the stream of N_2 and used to oxidize CPR in a separate solution (Figure 9). It was observed that the oxidation potential for ruthenium (III) occurs at 1.53 V vs NHE and for SO_4^{-2} radicals is ranging from 2.5 to 3.1 V.[22]

This reaction sequence works reproducibly and was able to generate substantial amounts of chlorite to chlorine dioxide. There was no accompanying change in pH but over prolonged illumination the sensitizer was destroyed. Adding more sensitizer restored the capacity to generate chlorine dioxide. No chlorine dioxide was formed in the dark, thereby indicating that persulfate reacts too slowly with chlorite to be a viable chemical oxidant for this reaction. Although

the reactions works well and can be driven by sunlight, it is expensive to operate. Other sensitizers are possible but the conditions are somewhat hazardous for organic reagents and the chromophore is destroyed on long illuminations. A more stable solution was sought.

6.4 Photovoltaic synthesis

The above studies indicate that the chemical and photochemical oxidation of chlorite to chlorine dioxide is a viable route to a bleaching agent. Chlorine dioxide is not a particularly powerful oxidant but is has excellent antiseptic properties. Furthermore, CPR is a useful indicator for quantitative detection of chlorine dioxide in water.[23] In seeking for an improved method for production of chlorine dioxide it was decided to use a simple photovoltaic approach. Silicon- based photovoltaic cells have become ever cheaper to produce and install and it is now possible to obtain reliable photovoltaic panels for a reasonable price. These panel have an operating lifetime in excess of ten years and can be set up so as to produce a steady potential in excess of 2 V. [24,25] This should be sufficient to oxidize chlorite to chlorine dioxide and to complete the circuit by the reduction of some complementary system. Our earlier cyclic voltammetry studies showed oxidation of chlorite to be electrochemically reversible so it is important to restrict access to the photocathode by chlorine dioxide.

Our experimental set up used three silicon photocells arranged in series so as to generate 1.5 V of output potential. The cell was wired to two large graphite electrodes. The panel was positioned beneath a 250 W quartz iodide lamp fitted with a heat filter. The distance between lamp and solar cell could be varied up to 2 meters. The cell did not oxidize water to H_2 and O_2 and, in fact, no gas was evolved at the electrodes when the solution was aqueous KCl (0.5 M). The over- potentials for water cleavage are too high with graphite to make this process viable. However, an electrochemical reaction occurred when the electrolyte solution contained sodium chlorite (0.5 M) at pH 7. Here, chlorite is oxidized to chlorine dioxide at the anode while chlorite is reduced to chlorine at the cathode. The latter reaction causes a change in pH, which can be followed during the reaction. Chlorine gas is a powerful oxidant and oxidizes chlorite to chlorine dioxide. Apart from the change in pH, this is a highly promising reaction. As before, purging the anode compartment with a slow stream of N_2 transfers the chlorine dioxide to a vessel containing a standard solution of CPR (Figure 10).

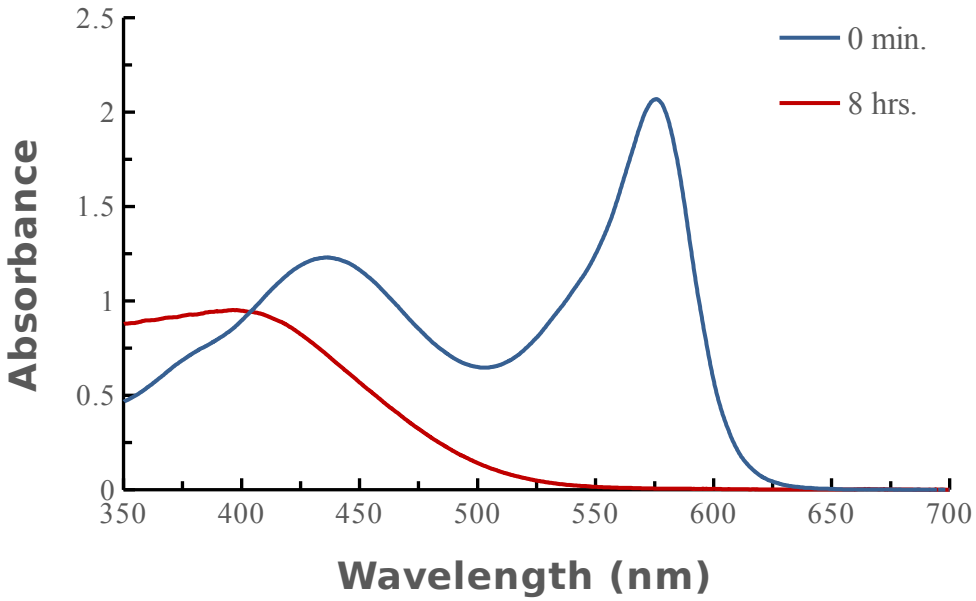

Figure 10. Absorption spectra recorded before and after photoelectrolysis of chlorite with the photovoltaic cell. The spectra refer to the CPR solution being constantly bubbled with a slow stream of N_2 gas to remove chlorine dioxide.

The above experiment was repeated but with reaction pH being monitored at different stages of reaction (Figure 11). Illumination causes the pH to increase quite substantially if no buffer is present.

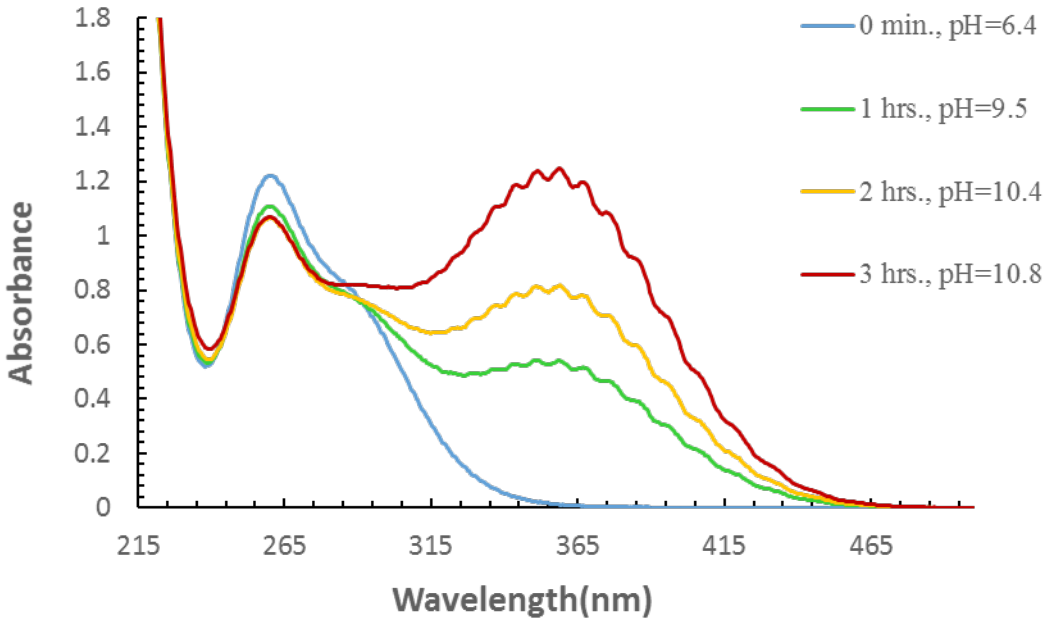

Figure 11. Following the reaction where chlorite is oxidized to chlorine dioxide at the anode while chlorite is reduced to chlorine at the cathode by recording the pH at different illumination times. The solution was not purged with N_2 so chlorine dioxide accumulates during photoelectrolysis.

The overall reaction proposed for this system is shown below:

$$ClO_2^- \longrightarrow ClO_2 + e$$

$$2ClO_2^- + 2H^+ + 2e \longrightarrow Cl_2 + 2OH^-$$

$$Cl_2 + 2ClO_2^- \longrightarrow ClO_2 + 2Cl^-$$

As mentioned earlier, the only issue with this reaction concerns the increase in pH that occurs under illumination. For this reason, attention was turned to alternative schemes for the anode compartment. As a simple replacement, it was noted that with silver nitrate solution (0.1 M) in the cathode compartment, illumination of the silicon solar panel resulted in generation of chlorine dioxide in the anode compartment and reduction of silver(I) to colloidal silver(0) in the cathode (Figure 12). The latter was evident as a grey suspension.

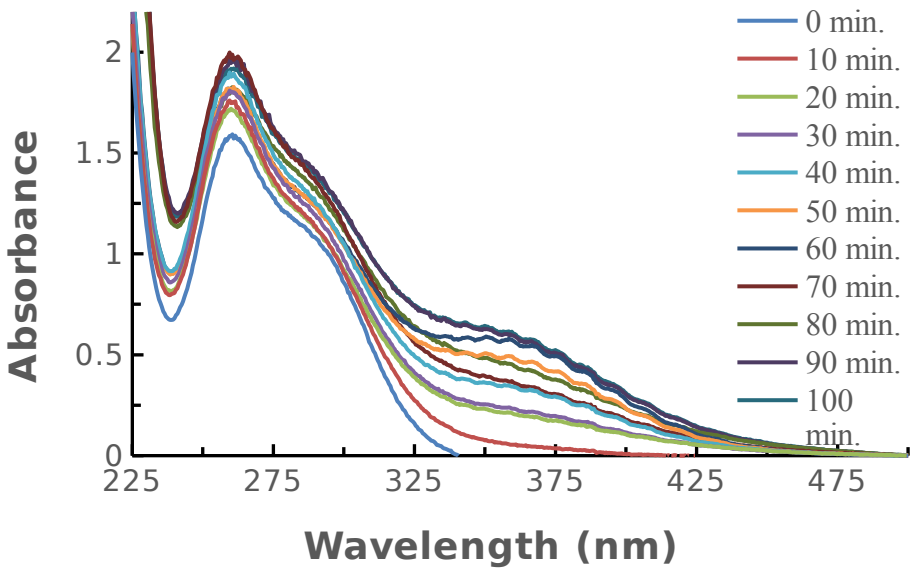

Figure 12. Absorption spectral changes occurring during photovoltaic electrolysis of sodium chlorite with silver nitrate in the cathode compartment. The spectra show accumulation of chlorine dioxide under illumination.

Of course, the photochemical reduction of silver(I) is not intended as anything other than a simple demonstration model. Replacing silver nitrate with ammonium ferric sulphate (0.1 M) in acetate buffer gave a much cheaper option. After illumination of the silicon solar cell, small aliquots of 1,10-phenanthroline[26] were added to the cathode compartment in order to detect formation of iron(II) cations. This is done through formation of the red coloured iron tris(1,10-phenathroline) ion which absorbs strongly at 508 nm.[27-29] In fact, the red coloration builds up smoothly during the illumination period but not in the dark (Figure 13). The rate of accumulation of iron(II) depends on the initial concentration of iron(III), indicating that the reaction conditions are not optimal.

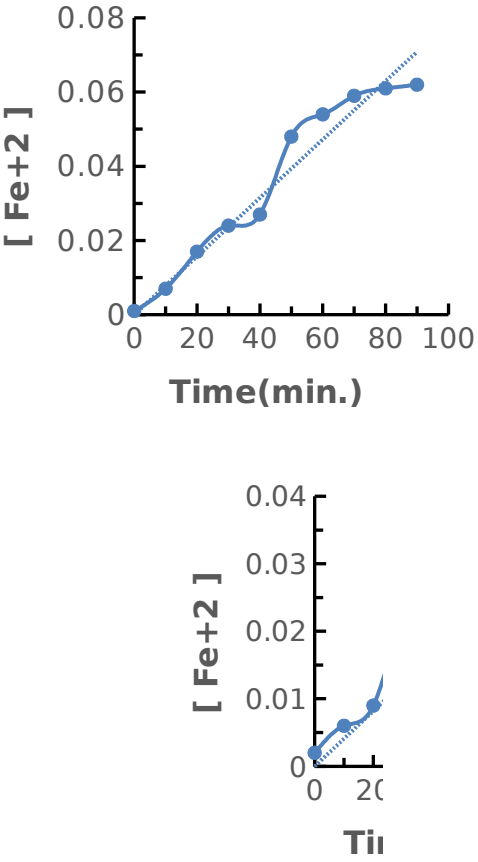

Figure 13. Increased absorbance observed at 508 nm corresponding to accumulation of iron(II) in the cathode compartment during illumination of the solar cell.

At the same time, chlorine dioxide accumulates in a linear manner with increasing illumination time. (Figure 14). Under controlled conditions, the reaction stoichiometry is 1:1 and reaction continues until one of the reactants is consumed. Note it is very important to ensure that iron(III) does not come into contact with sodium chlorite solution.

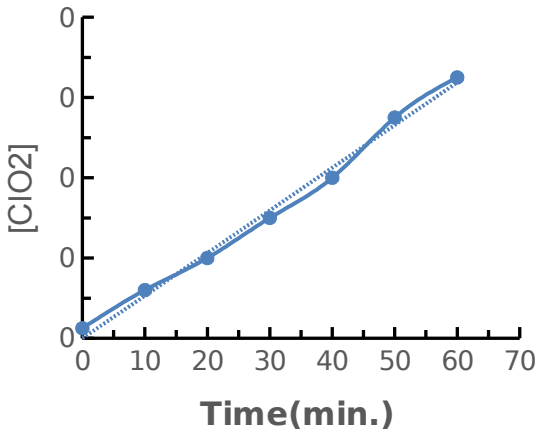

Figure 14. Accumulation of chlorine dioxide during illumination of the silicon solar cell. The product was quantified using the CPR indicator after removing small aliquots of solution.

The overall cell design is shown in Figure 15.

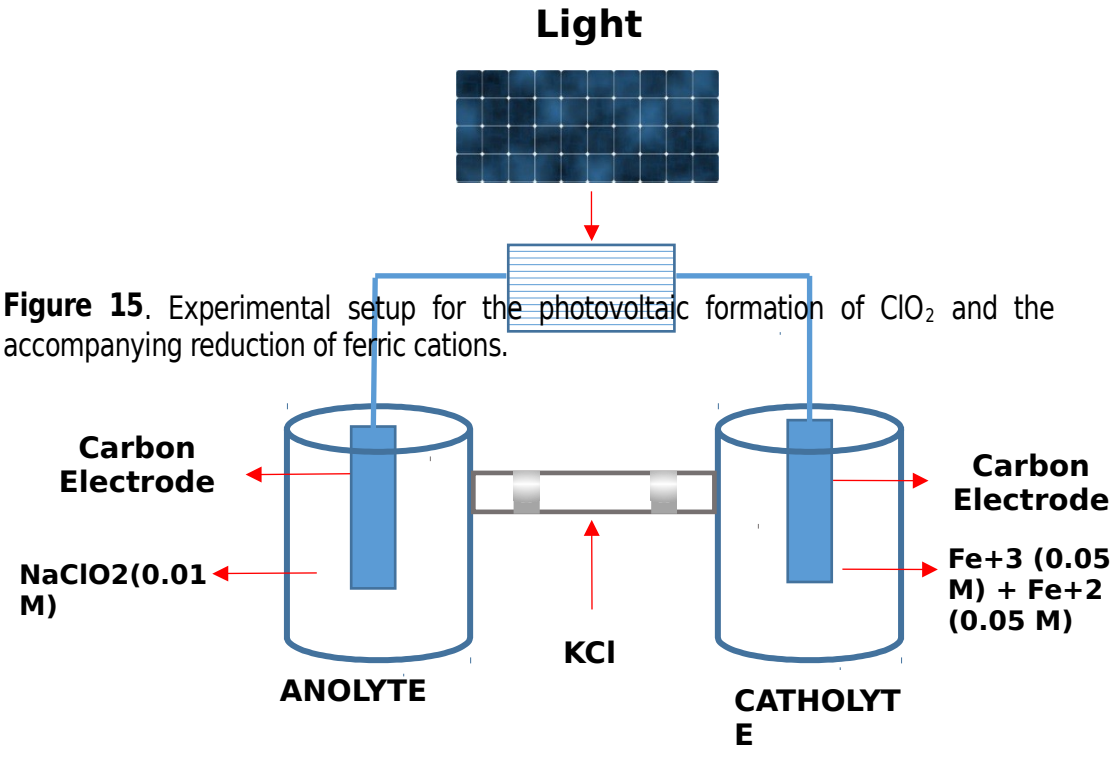

Figure 15. Experimental setup for the photovoltaic formation of ClO_2 and the accompanying reduction of ferric cations.

6.5 Photochemical bleaching of the BOPHY

As a final test of the possible value of using chlorine dioxide as a photochemical bleach, a limited number of experiments was conducted with sodium chlorite as an electron donor in solution. The chromophore was the parent BOPHY introduced earlier. This compound is insoluble in water and so a mixture of tetrahydrofuran (THF) and water was used as solvent. The BOPHY dye was dissolved in THF while sodium chlorite was dissolved in water prior to preparing the mixture. The intention was to determine if chlorite could promote the photobleaching of the chromophore.[30-32] It is recognized that BOPHY exhibits a high level of photostability[33] while it has been reported that these compounds might have important applications in OLEDs.[34-36] It was observed that BOPHY undergoes slow degradation under illumination in the THF-water mixture in the presence of sodium chlorite (0.10 M). This effect is illustrated by way of Figure 16.

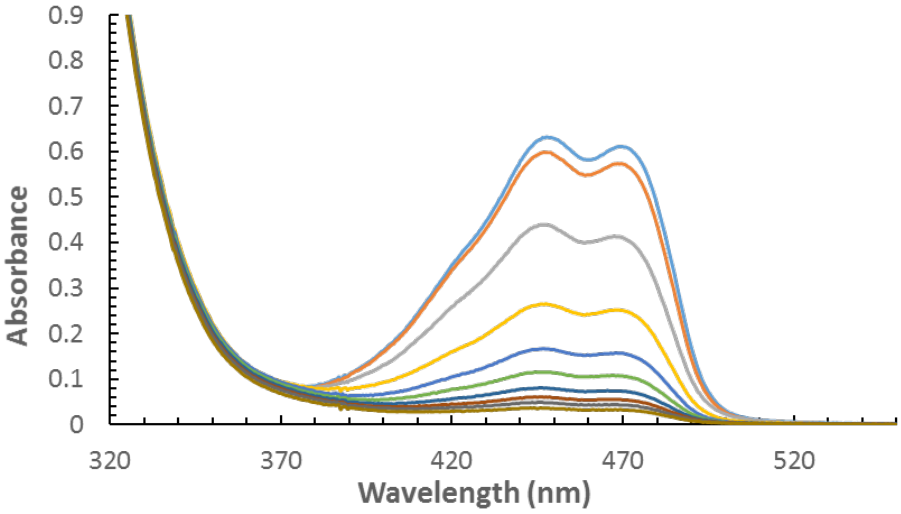

Figure 16. Photobleaching of BOPHY in the THF-water mixture under exposure to visible light. The solution contains sodium chlorite (0.1 M) and dissolved oxygen.

Similar experiments were made in the presence of CPR in an effort to better understand the reaction mechanism. However, it was found that the absorption spectral profile of CPR did not change under these conditions while that of BOPHY decreased in intensity (Figure 17). This confirms that BOPHY is susceptible to photobleaching under these conditions but the fact that CPR is not bleached is puzzling. There is no obvious reason why chlorine dioxide, if formed, should react preferentially with BOPHY. However, increasing the concentration of BOPHY increased the rate of photobleaching of this chromophore without effecting loss of CPR. One possibility is that

chlorine dioxide attacks the BOPHY π-radical anion formed by light-induced electron transfer before separation of the species. In other words, free chlorine dioxide is not formed. Shortage of time prevented further examination of this system.

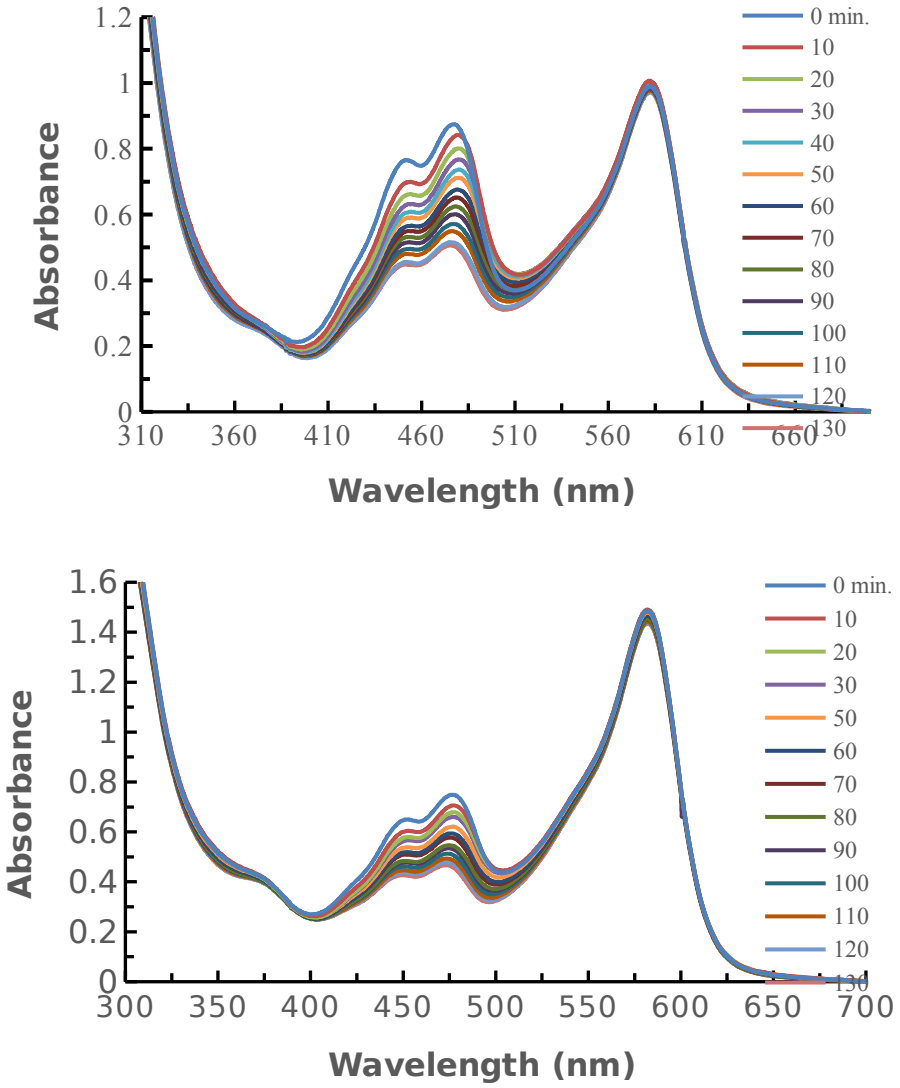

Figure 17. Two examples of absorption spectral changes recorded during the illumination of a mixture of BOPHY and CPR in mixed THE/water. The solution contained sodium chlorite (0.05 M) and molecular oxygen. Absorbance spectra were recorded at different exposure times.

6.6 Conclusion

This chapter has considered an alternative photochemical oxidative system based on the oxidation of sodium chlorite. The latter is a cheap and readily available compound that is currently used in

certain health products. It is a known anti-septic agent that has applications for water treatment. We have demonstrated that chlorite can be oxidized to chlorine dioxide via a photovoltaic cell. Chlorine dioxide is a better bleach than is chlorite and works by mild oxidation.

It has genuine possibilities as a largescale water-treatment reagent. Our set-up has been kept simple and inexpensive. It requires only a few silicon solar cells wired so as to produce around 1.5 V. Graphite rods are used as electrodes. These are non-selective but cheap and easily fabricated. The most successful system uses only sodium chlorite in water. It generates chlorine dioxide under illumination of the solar cell but suffers from an increase in pH due to the production of hydroxide ions as a side-reaction. For many purposes, this is not seen as a problem. The next phase of the project involves setting up a largescale demonstration model but this will happen outside of the current PhD programme.

6.7 References

[1] C. Lodge, K. Allen, A. Lowe, Dha. *Int. J. Environ. Res. Public Health.* **2013**, 10, 2597.

[2] B. R. Deshwal, S. H. Lee, *J. Hazardous. Mat.* **2004**, 108, 173.

[3] H-S. Shin, D-G. Jung, *J. Chromatogr. A.* **2006**, 1123, 92.

[4] B. R. Deshwal, D. S. Jin, S. H. Lee, S. H. Moon, J. H. Jung, H. K. Lee, *J. Hazardous. Mat.* **2008**, 150, 649.

[5] C. J. Pursell, J. Conyers, P. Alapat, R. Parveen, *J. Phys. Chem.* **1995**, 10433, 99.

[6] R. C. Dunn, B. N. Flanders, J. D. Simon, *J. Phys. Chem.* **1995**, 7360, 99.

[7] W. Masschelein, *Ind. Eng. Chem. Prod. Res. Dev.* **1967**, 6, 137.

[8] H. Bergmann, S. Koparal, *Electrochimica Acta.* **2005**, 50, 5218.

[9] J. J. Kaczur, D. W. Cawlfield, "Electrochemical process for producing chlorine dioxide solutions from chlorites". U. S. Patent 5092970, Mar. 3, **1992.**

[10] I. Fletcher, P. Hemmings, *Analyst*. **1985**, 110, 695.

[11] J. Tkacova, J. Bozikova, *Journal of Civil Engineering*. **2014**, 22, 21.

[12] M. P. Xavier, B. Vallejo, M. D. Marazuela, M. C. Moreno-Bondi, B. A. Falai, *Biosensors & Bioelectronics.* **2000**, 14, 895.

[13] I. J. Fletcher, P. Hemmings, *J. Anal.* **1985**, 110, 695.

[14] D. L. Sweetin, E. Sullivan, G. J. Gordon, *Talanta.* **1996**, 43, 103.

[15] Q. Wang, K. Chen, J. Li, J. Xu, S. Liu, *Bioresource. com.* **2011**, 6, 1868.

[16] W. Masschelein, *Ind. Eng. Chem. Res. W.* **1967**, 2, 137.

[17] T-F. Tang, G. Gordon, *Environ. Sci. Technol*. **1984**, 18, 212.

[18] F. Quental, C. Elleouet, C. Madec, *Analytica Chimica Acta.* **1994**, 295, 85.

[19] D. Sirbu, O. Woodford, A. Benniston, A. Harriman, *Photochem Photobiol Sci.* **2018**, 17, 750.

[20] R. D. Gerardi, N. W. Barnett, S. W. Lewis, *Analytica Chimica Acta*. **1999**, 378, 1.

[21] H. Rensmo, S. Lunell, H. Siegbhn, *Journal of Photochemistry and Photobiology A: Chemistry*.

1998, 114, 117.

[22] A. B. Lever, *Inorganic Chemistry.* **1990**, 6, 1272

[23] I. A. Capuano, D. L. Defelice, "Electrochemical Chlorine Dioxide Process". U. S. Patent 4542008, Sep. 17, **1985.**

[24] J. G. Ibanez, A. G. Gonzalez, R. C. Vasquez-Medrano, U. Paramo-Garcia, D. Zavala-Araiza, *Int. J. Electrochem. Sci*. **2013**, 8, 12097.

[25] C. A. Paddon, M. Atobe, T. Fuchigami, P. He, P. Watts, S. J. Haswell, G. J. Pritchard, S. D. Bull, F. J. Marken, *Apple. Electrochem*. **2006**, 36, 617.

[26] R. C. Atkins, *J. Chem. Educ*. **1975**, 52, 550.

[27] W. B. Fortune, M. G. Mellon, *Ind. Eng. Chem. Annual. Ed.* **1938**, 10, 60.

[28] D. A. Skoog, D. M. West, F. J. Holler, S. R. Crouch, Analytical Chemistry: An Introduction, 7th ed., Chapters 21 and 22, pp. 547.

[29] I. Fabian, G. Gordon, *Inorg. Chem*. **1991**, 30, 3999.

[30] I. Fabian, G. Gordon, *Inorg. Chem*. **1992**, 31, 2144.

[31] K. W. Wilson, T. Park, "Iron-Catalyzed Decomposition of Sodium Chlorite". U. S. Patent 2739032, Mar. 30, **1953**.

[32] K. Henbest, P. Douglas, M. S. Garley, A. Mills, *J. Photochem. Photobiol. A; Chem*. **1994**, 80, 299.

[33] J. Glembockyte, A. Cosa. *J. Am. Chem. Soc.* **2017**, 139, 13227.

[34] R. G. Kieffer, G. Gordon, *Inorg. Chem*. **1968,** 7, 235.

[35] R. G. Kieffer, G. Gordon, *Inorg. Chem*. **1968,** 7, 239.

[36] L. Xiaokang, L. Tingtin, W. Qinghua, Y. Changjiang, J. Lijuan, H. Erhong, *J. Org. Chem*. **2018**, 83, 1134.

ChemPubSoc Europe
DOI: 10.1002/cptc.201900141
CHEMPHOTOCHEM Articles

Inhibition of the Photobleaching of Methylene Blue by Association with Urea

Sulafa Jamal M. Nassar,[a] Corinne Wills,[b] and Anthony Harriman*[a]

This contribution is dedicated to the memory of Prof. Roger J. Griffin.

Methylene Blue has a long history as a photochemical reagent and is known to undergo photofading on exposure to visible light in aqueous solution. Under aerobic conditions, photobleaching occurs by way of a two-step process involving intermediary formation of singlet oxygen. The first step is ascribed to regio-selective addition of singlet oxygen within the precursor complex. This geminate reaction ultimately leads to formation of the leuco-dye via a slower second step. Urea forms a weak ground-state complex with Methylene Blue which affects the optical properties of the dye but is not evident by NMR spectroscopy. This complex is weakly fluorescent and undergoes intersystem crossing to the triplet manifold. The presence of urea decreases the rate of photobleaching of the dye and, at high concentrations of urea, the bleaching kinetics are consistent with an equilibrium mixture of complexed and free dye. The complexed dye does not bleach on the timescale of the experiment. Such protection might arise from urea blocking access to the site where geminate addition of O_2 takes place.

1. Introduction

Most organic substances are susceptible to light-induced degradation in both solution and solid phases.[1] Such photochemical bleaching, which is also a feature of natural photosynthesis,[2] can restrict the usefulness of certain classes of dye as components in optical devices. However, controlled photofading can be a valuable tool in terms of removing the chromophore after completion of desired tasks, for example following photodynamic therapy.[3] Numerous disparate mechanisms have been proposed to account for dye photobleaching in particular cases, the most common being the triplet sensitization[4] of singlet molecular oxygen. Dyes that do not populate the triplet state with reasonable efficacy are not immune to photobleaching[5] and removal of molecular oxygen is not guaranteed to prevent colour loss.[6] More often than not, unique products do not evolve during the bleaching chemistry, especially under white light illumination, and instead a distribution of breakdown products arises. In certain cases,[7] a cascade of well-defined intermediate species develops during the reaction so that the bleaching kinetics can be considered in some detail. In general, quantum yields for photofading tend to be very low but recent observations[7,8] of autocatalysis mean that such measurements could be misleading. The most common method by which to follow chromophore photobleaching is via absorption spectrophotometry[9] and numerous sophisticated protocols have been reported.[10,11] This prior work, in particular, has indicated the significance of light intensity and the role of molecular oxygen.

Well accepted practices for minimizing the effects of photofading include immobilisation of the dye in solid media,[12] incorporation of UV screens[13] and removal of heat from the system. Other simple approaches to increasing the duty cycle for the dye include incorporation of anti-oxidants.[14] The emergence of super-resolution microscopy and single-molecule spectroscopy has emphasized the need for photochemically stable dyes[15] and new strategies for protecting the chromophores have been introduced over the past decade or so.[16] Unlike in natural photosynthesis,[17] however, these protective methods do not include *in-situ* repair processes and more-often-than-not involve encasing the dye in an expensive package. As more-and-more dyes enter the marketplace, new and innovative protocols are needed to circumvent the destructive bleaching events. One way to achieve this ideal, taken from natural systems,[18] is to identify and block a key intermediate or reaction cycle. This type of smart technology, which must be closely associated with the underlying mechanism responsible for light-induced damage, has rarely been applied in artificial systems.

In developing a prototypic defensive strategy against photobleaching in fluid solution, we have turned our attention to Methylene Blue. This is a very well-known photosensitizer,[19] that exhibits photo-bactericidal activity in water. In fact, Methylene Blue was first synthesized in 1876 by Caro[20] and its capability to stain biological media was recognized[21] almost immediately. The dye associates strongly with DNA[22] and has found key applications in certain types of photodynamic

[a] S. J. M. Nassar, Prof. A. Harriman
Molecular Photonics Laboratory, SNES- Chemistry
Newcastle University
Newcastle upon Tyne, NE1 7RU (UK)
E-mail: anthony.harriman@ncl.ac.uk
[b] Dr. C. Wills
NMR Laboratory
School of Natural and Environmental Science
Newcastle University
Newcastle upon Tyne, NE1 7RU (UK)

Supporting information for this article is available on the WWW under https://doi.org/10.1002/cptc.201900141

therapy.[23] Under illumination in aqueous solution, Methylene Blue can be used to sensitize formation of singlet molecular oxygen and/or superoxide ions.[24] Although water soluble, the dye is prone to aggregation in aqueous solution[25] and its properties are pH sensitive.[26] Photobleaching of Methylene Blue has been studied in some detail and the role of the triplet-excited state has been recognised.[27] The dye fades relatively quickly on exposure to sunlight, even in the absence of added electron donors, and has been reported to follow two-step kinetics.[28] By way of separate studies, considerable effort has been expended on following the destruction of Methylene Blue under illumination of certain semiconductors, such as TiO_2, which function as electron donors.[29] The *leuco*-form of the dye, generated by addition of a hydride anion, is often cited as being the most likely candidate for any transparent product (See Scheme 1 for molecular formulae).[30]

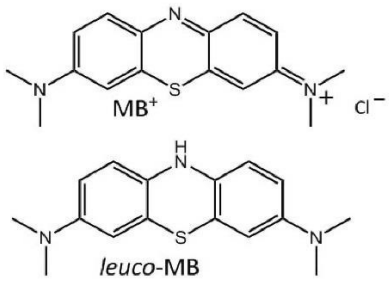

Scheme 1. Molecular formulae for methylene blue and its *leuco*-form.

The present work seeks to develop a simple and inexpensive strategy that inhibits photochemical bleaching of Methylene Blue in aqueous solution. The intention is to extinguish the bleaching reaction by blocking access to a crucial intermediate species. To simply the reaction, air-equilibrated solutions are used. This ensures that the triplet-excited state of the dye reacts almost exclusively with molecular oxygen. It is also appropriate to avoid high (i.e., >10 μM) concentrations of dye where aggregation[25] should be anticipated. As an inhibitor, we have selected urea because of its molecular dimensions and ready availability.

2. Results and Discussion

2.1. Properties of Methylene Blue

Methylene Blue (hereafter abbreviated as MB^+) in water at pH 7.4 exhibits a strong absorption maximum centred at 665 nm for which the molar absorption coefficient at the peak (ε_{MAX}) was determined to be $84{,}285 \pm 5{,}000\ M^{-1}cm^{-1}$ at low concentration. At higher concentrations, the absorption transition broadens and a new absorption band can be discerned with a maximum at ca. 610 nm (Figure 1). The ratio of

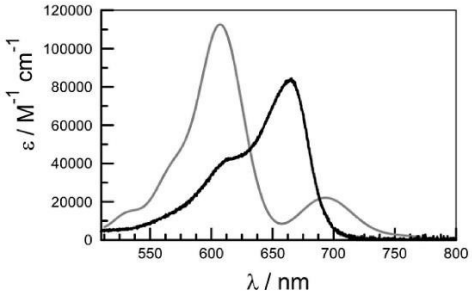

Figure 1. Absorption spectrum recorded for MB^+ in aqueous solution at pH 7.4 for a 0.4 μM concentration of the dye (black curve). The grey curve shows the corresponding absorption spectrum derived for the dimer as obtained by spectral deconstruction of spectra recorded at much higher concentration. See Supporting Information for further details.

absorbance values recorded at 665 and 610 nm can be used as a rough indication of the state of aggregation of the dye[31] (Figures S1–S3). All subsequent photochemical experiments were carried out with an initial MB^+ concentration of <4 μM, where the fraction of dye present as an aggregated species is $<2\%$. The dye is weakly fluorescent under these conditions. More specifically, the fluorescence maximum occurs at 690 nm, while the fluorescence quantum yield (Φ_F) and excited-state lifetime (τ_S) are 0.020 ± 0.005 and 345 ± 15 ps, respectively.[32] The triplet-excited state can be detected by laser flash photolysis following excitation at 610 nm (Figure S14), where the quantum yield for population of the triplet state is 0.56.[32] The triplet lifetime recorded at low laser intensity in de-aerated solution is 45 ± 7 μs, although decay curves were not strictly mono-exponential. The triplet state is quenched by molecular oxygen with a bimolecular rate constant of $1.6 \pm 0.5 \times 10^9\ M^{-1}s^{-1}$; the triplet lifetime in air-equilibrated water is reduced to 3.0 ± 0.2 μs (Figure S15). Related studies by other researchers have confirmed that such triplet quenching leads to formation of singlet oxygen.[24,33]

Broadband ($\lambda > 450$ nm) illumination of MB^+ in air-equilibrated aqueous solution at pH 7.4 leads to progressive loss of colour. The course of reaction can be followed conveniently by absorption spectrophotometry and an illustrative example is provided as Figure 2. Under irradiation with white light, the main absorption band bleaches but there is no concomitant accumulation of a permanent product. This situation might be considered consistent with conversion of MB^+ to the corresponding *leuco*-form.[30] Bleaching is fairly slow and irreversible. The presence of molecular oxygen has no obvious effect on the absorption spectral changes during bleaching but no such fading occurs in the dark. Under otherwise identical conditions in D_2O, the colour loss occurs on a faster timescale but again does not favour build-up of a persistent coloured product.

The absorbance change with illumination time, A(t), at any given wavelength gives an approximate fit to first-order kinetics. However, the fit is much improved by using the sum of two exponentials model exemplified by Equation (1), where

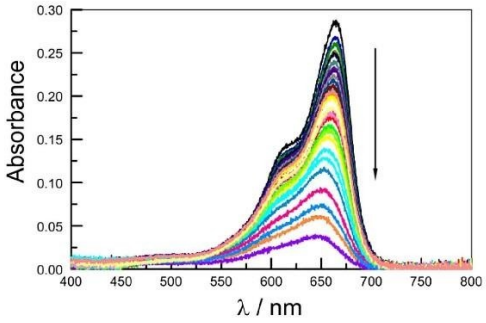

Figure 2. Example of the photobleaching of MB^- in air-equilibrated aqueous solution at pH 7.4 using a white light source ($\lambda > 420$ nm). The arrow shows the course of the reaction. Absorption spectra were recorded at regular intervals over a period of 1000 min. Note the 5 nm blue shift accompanying bleaching.

A(0) refers to the initial absorbance at that wavelength. The absorbance data extracted from Figure 2, and treated globally[34] across the entire absorption band, has ca. 15% of the initial absorbance (i.e., B = 0.15) decreasing with a first-order rate constant (k_1) of 0.011 ± 0.001 min^{-1}. This step is followed by a substantially slower process having a first-order rate constant (k_2) of 0.0019 ± 0.0003 min^{-1} (Figure 3) that

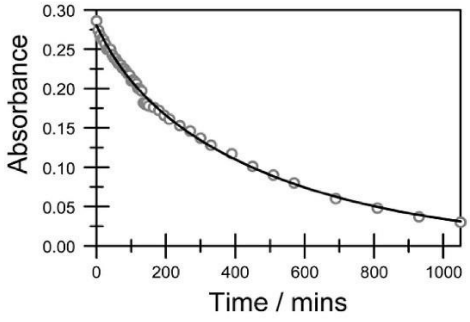

Figure 3. Fit to Equation (1) or Equation (2) of the experimental data recorded at 665 nm for the experiment indicated in Figure 2. The solid line drawn through the data points is a non-linear, least-squares iterative fit with the parameters reported in the text.

accounts for the remainder (C = 0.85) of chromophore disappearance. Both derived rate constants are dependent on the incident light intensity (adjusted with neutral density filters or by varying the distance between sample and source). The effective rate of bleaching, measured at the beginning of the reaction, increases linearly with light intensity until saturation becomes apparent. A similar effect is observed for increasing MB^+ concentration at intermediate light intensity (Figures S8–S9). The problem with this simple model is that it is difficult to assign the two steps to any particular reaction as it is far from obvious why 15% of the initial signal should decay on a fast timescale compared to the residual absorbance.

$$\frac{A(t)}{A(0)} = Be^{-k_1 t} + Ce^{-k_2 t} \quad (1)$$

The bleaching kinetics fit equally well[35] to two consecutive first-order reactions with averaged rate constants of 0.0109 ± 0.0004 min^{-1} and 0.0017 ± 0.0002 min^{-1} at fixed light intensity (Figure 3). The underlying two-step process can be expressed in terms of Equation 2 (see Supporting Information) where it is assumed that Step 1, which is associated with k_1, leads to formation of an adduct that absorbs less strongly than MB^+ but retains a similar absorption profile. The ratio of molar absorption coefficients at that wavelength is incorporated into the parameter β in Equation (2). Bleaching is accompanied by a 5-nm blue shift that could be indicative of adduct formation (Figure 2). It is further assumed that bleaching of this adduct leads only to transparent products (i.e., the *leuco*-dye). Photochemical bleaching of the adduct occurs by way of k_2.

$$\frac{A(t)}{[MB^+]_0} = e^{-k_1 t} + \beta\left(e^{-k_1 t} - e^{-k_2 t}\right) \quad (2)$$

This simple model[36] can be refined on the basis of ancillary studies. For example, replacing H_2O with D_2O has an important acceleration on the overall rate of photobleaching of MB^+ in the presence of molecular oxygen. The rate of the first step increases significantly ($k_1 = 0.19 \pm 0.02$ min^{-1}) while the second step becomes slightly faster ($k_2 = 0.0052 \pm 0.0005$ min^{-1}) in D_2O. The logic behind this experiment comes from the realisation[37] that the lifetime of singlet oxygen increases from 4 μs to 55 μs on replacing H_2O with D_2O. Under anaerobic conditions in H_2O, bleaching occurs more slowly and follows first-order kinetics. There is no accompanying blue shift. Here, the derived first-order rate constant is 0.0059 ± 0.0005 min^{-1}, as measured under comparable conditions to those used above. Thus, the main effect of removing O_2 from the system is the loss of the initial fast step (i.e., k_1) and an increase in the rate of photochemical bleaching of the dye relative to the second step (i.e., k_2). In de-aerated D_2O, the rate of photochemical bleaching is slightly (i.e., 10%) faster than in de-aerated H_2O.

The two-step nature[28] of the bleaching process observed under aerobic conditions is considered to be entirely consistent with formation of the *leuco*-dye as the major product.[30] Given the rather short singlet state lifetime,[32] it seems highly likely that the dominant species responsible for photochemical loss of MB in solution is the triplet-excited state. This meta-stable species is quenched by molecular oxygen and it is reasonable to suppose that part of this quenching process leads to subsequent chemical modification of the chromophore. This step would correspond to k_1 while the observed D_2O effect suggests that singlet oxygen plays some role in this reaction.[38] This cannot involve diffusional attack on a ground-state molecule of MB^- by singlet oxygen since the concentration of the former is too low and the lifetime of the latter is too short. Geminate addition of molecular oxygen within the precursor

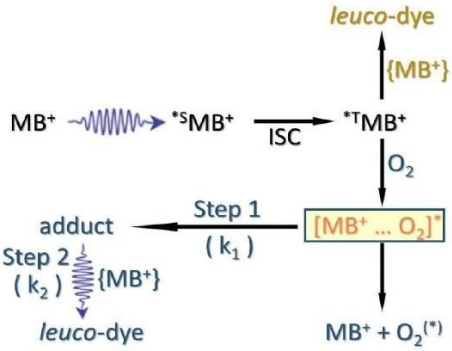

Scheme 2. Illustration of the processes proposed for the photochemical bleaching of MB^+ in aqueous solution. Steps given in blue refer to aerobic conditions while anaerobic bleaching appears in brown. The key role assigned to the geminate complex formed between MB^+ and singlet molecular oxygen is highlighted. Both initial population of the excited-triplet state, via intersystem crossing (ISC), and bleaching of the primary adduct require light activation.

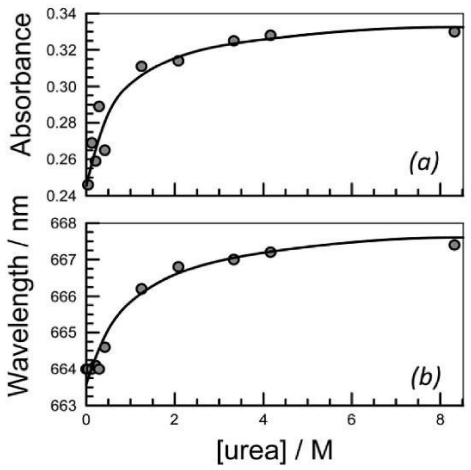

Figure 4. Effect of added urea on (a) absorbance at the maximum wavelength and (b) wavelength of the peak maximum for MB^+ in aqueous solution at pH 7.4. The solid lines drawn through the data points correspond to best fits to empirical expressions (see Supporting Information).

complex could explain the observations[39] but this would require regio-specific interactions between singlet oxygen and the aza-N or S atoms. The second step occurs more slowly, by way of k_2, and most likely refers to conversion of the primary adduct to a derivative of the *leuco*-dye (Scheme 2).

A different reaction mechanism must be responsible for anaerobic bleaching of MB^-, but again the reaction is probably promoted by the triplet-excited state. The triplet lifetime is much longer in the absence of oxygen and it is reasonable to suppose that bimolecular reactions, for example light-induced electron transfer between two MB^- molecules, might initiate loss of the chromophore. Since the overall reaction is best explained in terms of a first-order process under these conditions, it is not possible to make a direct comparison between the rates of bleaching in aerobic and anaerobic conditions. Irreversible formation of the *leuco*-dye in the absence of oxygen is a possibility (Scheme 2).

It should be stressed[40] that the units used for the various rate constants should include a term for the number of photons absorbed but this has been neglected in order to simply the text. Experiments have shown that the initial rates of bleaching in both aerobic and anaerobic conditions scale linearly with the number of photons absorbed per unit time (Figures S8-S9). Where comparison is made, it is safe to assume that the initial rate of photon uptake remains the same.

2.2. Effect of Added Urea

Addition of urea to an aqueous solution of MB^+ at pH 7.4 causes a modest (i.e., 4 nm) red shift for the absorption maximum and a significant increase (i.e., >20%) in the molar absorption coefficient at the peak (Figure 4). Both effects might be explained in terms of urea dissociating a ground-state dimer[41] but this is not the correct explanation. Exactly the same behaviour is observed at very dilute MB^+ concentration, where the fraction of chromophore that might be present as a dimer is below one percent. Likewise, given the very low basicity of urea ($K_B = 1.5\times10^{-14}$)[42] these spectral shifts cannot be ascribed to changes in pH. Instead, it appears that urea forms a weak complex with MB^+ in neutral aqueous solution. Both the absorption shift and the increased absorbance observed on addition of solid urea to the solution can be explained in terms of 1:1 complexation (see Supporting Information). The apparent binding constant ($K = 1.2 \pm 0.4\ M^{-1}$) is small, ensuring that high concentrations of urea are required to saturate the complexation event.

A series of ^1H NMR spectra were recorded with ratios of MB^+ to urea varying from half a molar equivalent of urea to a 39 times excess. These titration experiments revealed no changes in the ^1H NMR chemical shifts of the aromatic signals of MB^+ that could be regarded as significant. Small shifts of 0.04 to 0.06 ppm were observed, but these are most likely due to the varying concentration of the sample and do not provide conclusive evidence of complexation (Figures S11, S12). This finding indicates that any complexation is weak and probably transitory. In fact, the only reasonable type of intermolecular interaction is hydrogen bonding between the reagents and, in this aspect, urea has to compete with water.

Complexation between urea and MB^- can also be followed by way of a fluorescence titration. Addition of urea to an aqueous solution of MB^+ at pH 7.4 causes a small red shift for the emission maximum and an escalation in fluorescence (Figures S11–S13). These effects are modest, again requiring high concentrations of urea, but fully consistent with the absorption spectral studies; i.e., the increased absorptivity of

the complex is matched by its enhanced fluorescence. Again, the fluorescence changes occur at very low concentration of MB^+ and cannot be attributed to urea dissociating non-emissive dimer molecules into the emissive monomers. The fluorescence data are noisy but consistent with a binding constant of ca. 1 M^{-1}. There is no indication for urea acting as a fluorescence quencher for MB^+ in neutral solution.

Interaction between urea and MB^+ has an important effect on the kinetics of photochemical bleaching of the dye under visible light illumination (Figure 5). High concentrations (i.e., >0.2 M) of urea at pH 7.4 cause a marked decrease in the rate of loss of the chromophore (Table S1). The solution pH was kept constant during these studies, as was the incident light intensity and the concentration of dissolved O_2. Under the experimental conditions used, the reaction profile can be analysed satisfactorily in terms of first-order kinetics, at least over early stages (Table S1). That is to say that the two-step mechanism observed for bleaching of MB^+ in air-equilibrated solution is replaced by a single-step (i.e., first-order) reaction in the presence of modest concentrations of urea. This allows facile derivation of the corresponding first-order rate constant (k_U) for photobleaching of MB^+ (Table S1). Interestingly, the rate of bleaching is little affected by the presence of O_2; a typical example has k_U decreasing from 0.0049 ± 0.0005 min^{-1} to 0.0039 ± 0.0004 min^{-1} on removal of the dissolved O_2 (Table S1). Similar behaviour is seen in D_2O, where the corresponding k_U values are 0.0051 ± 0.0005 and 0.0040 ± 0.0004 min^{-1}, respectively, (Table S1). There is no indication for self-catalysis[43] at long illumination times in the presence of urea. Such events occur if a reactive product accumulates during the bleaching process and promotes further loss of chromophore.[39]

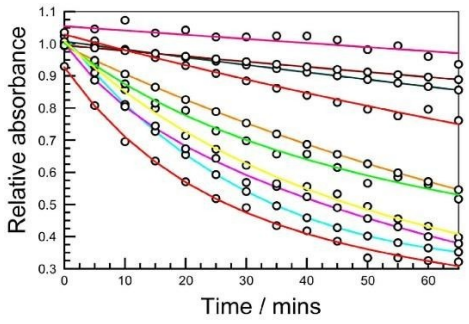

Figure 5. Plots of relative absorbance at the band maximum for MB^+ (ca. 3 μM) in aqueous solution at pH 7.4 under illumination with visible light. The solutions contained various amounts of urea (see Table S1 for composition) and were air-equilibrated before exposure to the light beam. The solid line drawn through each data set corresponds to a non-linear fit to a first-order reaction. The derived rate constants are included in Table S1. N.B. The reactions conditions, notably the light intensity, differ from those used for Figure 2 and direct comparison should not be attempted.

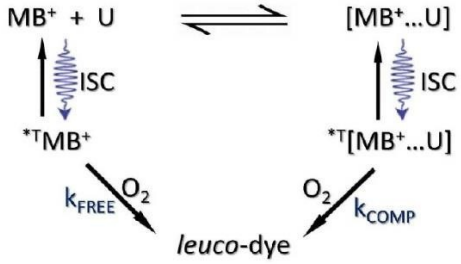

Scheme 3. Outline of reaction sequence proposed to account for the inhibition of MB^+ photobleaching exerted by urea in aqueous solution. The key step is the fast establishment of an equilibrium between free and complexed MB^+.

Although high solute concentrations are required, it is apparent that urea inhibits photobleaching of MB^+ in neutral aqueous solution. The effect of added urea on the rate constant (k_U) for bleaching of MB^+ can be expressed in terms of Equation (3) (Figure 6). This situation is shown pictorially by Scheme 3. Our understanding of this behaviour is that an equilibrium is established between free MB^+ and a complex formed with urea. Analysis of the spectroscopic data is consistent with formation of a 1:1 complex[44] but this might not be an adequate representation of the situation since binding has little effect on the measurable properties. From Equation (3),[45] it appears that the complexed dye does not undergo photo-bleaching on the relevant timescale. The derived rate constant ($k_{COMP} = 0.00012$ min^{-1}) is essentially zero. In contrast, the free dye bleaches with a global rate constant (k_{FREE}) of 0.021 ± 0.001 min^{-1} under these conditions (Figure 6). From the analysis, the equilibrium constant, K, has a value of 1.5 M^{-1}, in excellent agreement with that derived from the spectroscopic studies.

$$k_U = (1 - \sigma)k_{FREE} + \sigma k_{COMP} \quad (3a)$$

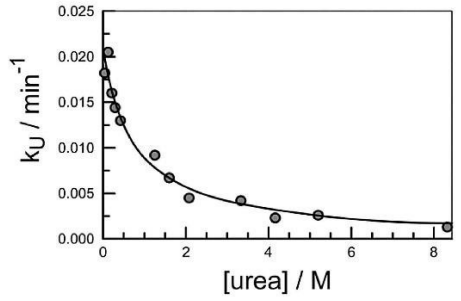

Figure 6. Effect of added urea on the derived first-order rate constant for photochemical bleaching of MB^+ in air-equilibrated water at pH 7.4. The solid line drawn through the data points is a non-linear least-squares fit to Equation (3) with the parameters reported in the text.

$$\sigma = \frac{1}{1 + 1/\{K[urea]\}} \quad (3b)$$

The presence of urea does not inhibit formation of the MB^+ triplet-excited state but high concentrations lead to an increased triplet lifetime in air-equilibrated solution (Figure S17). For example, laser flash photolysis studies indicate that τ_T increases from 3 μs in the absence of urea to 9±2 μs at a urea concentration of 4 M. In de-aerated solution, urea has no effect on τ_T at pH 7.4, which remains at 45±8 μs. Unlike thiourea,[46] native urea is not a quencher for singlet oxygen and does not compete with molecular O_2 for quenching the triplet-excited state. No information exists about the possible effect of urea on O_2 solubility in water. Since triplet sensitization[47] of singlet oxygen requires orbital contact between the reactants it is plausible to suggest that the urea-MB^+ complex partially restricts close proximity with O_2. This would explain the somewhat extended triplet lifetime. Furthermore, the same argument could be used to suggest that the route to formation of the O_2-adduct is blocked upon complexation. This situation would eliminate the main bleaching processes introduced to explain loss of MB^+ in aerobic conditions. Finally, the complex would also hinder close association of two or more MB^+ molecules and, if so, this would limit the efficacy of any anaerobic bleaching that requires bimolecular electron transfer.[48] Thus, formation of the weak complex at the ground state level appears to be instrumental in protecting the dye against adventitious photobleaching in solution.

3. Conclusions

The major finding reported herein concerns the observation that urea protects MB^+ against photochemical bleaching in neutral aqueous solution. Urea is a cheap and abundant reagent, generally regarded as waste material, which dissolves readily in water. It introduces no obvious source of excited-state quenching and, at least in the case of MB^+, increases both the molar absorptivity and the triplet lifetime in air-equilibrated solution. Our NMR spectroscopy studies do not indicate specific interactions between MB^+ and urea (Figure S11, S12), although the optical spectroscopy results could be analyzed satisfactorily in terms of 1:1 complexation. In reality, the effect of urea on the optical spectroscopic properties of MB^+ would pass without notice were it not for the observation that urea inhibits photobleaching of the dye. The effect is profound and, when associated with a urea molecule, MB^+ is effectively protected against photofading in solution. At much higher (i.e., >10 μM) concentrations of MB^+, where aggregation is an issue,[25] urea is expected[41] to help dissociate any dimers and in fact this effect has been seen but not yet examined in detail (see Supporting Information).

Urea is well known[49] as being a reagent that forms inclusion compounds, or clathrates, with certain substrates. This provides a simple means for separating mixtures or for purifying hydrocarbons.[50] Perhaps the same approach could be developed to construct highly stable artificial light-harvesting antennae by incorporating the chromophore into the porous ordered matrix. In this respect, urea would be a most convenient host. The key rationale for this approach is the acceptance that the multiple electron breakdown of large dye molecules involves some type of bimolecular interactions. Preventing these associations could result in greatly improved photochemical stability.

Experimental Section

Samples of MB^+ were obtained from Sigma-Aldrich and subjected to Soxhlet extraction with chloroform. A minor amount of a red coloured product was removed. Analysis by ^{1}H NMR spectroscopy of the residual dye, after drying in a vacuum oven, showed the presence of small amounts of one or more impurities. These were estimated to contribute less than 2% to the total dye concentration. Urea was recrystallized from warm water, the temperature being held at less than 50 °C to avoid contamination with ammonium cyanate,[51] on addition of ethanol. Water was deionised and then distilled. All solutions were prepared with freshly distilled water. The pH was adjusted by addition of phosphate buffer to give a final concentration of 5 mM. Where appropriate, the solution was purged for 15 minutes with O_2-free nitrogen.

Absorption spectra were recorded with a Hitachi U3310 spectrophotometer while emission spectra were recorded with a Hitachi F4500 spectrophotometer. All such studies were carried out at room temperature. ^{1}H NMR spectra were recorded in D_2O at 298 K on a Bruker 700 Avance III HD NMR spectrometer operating at 700.13 MHz. Chemical shifts are quoted in ppm relative to tetramethylsilane. Illumination studies were made with a 400 W HQI lamp filtered to remove IR and UV (λ<450 nm) radiation. The sample was contained in a 1 cm^2 cuvette held in a purpose-built holder and situated 30 cm from the source. The temperature was kept constant at 18 °C. The light intensity was controlled by insertion of suitable neutral density filters in front of the sample cuvette. Additional light intensity dependence studies were made by varying the distance between source and sample and invoking the inverse square law. The source was calibrated with a Thor Labs S140 C integrating power meter, using a quartz plate to deflect a small fraction of the total light intensity to the detector. In all cases, the course of reaction was followed by absorption spectrophotometry. Analysis of the kinetic data was made using standard analytical protocols[52] following least-squares fitting of the data. Global analysis[34] used the entire spectral window rather than rely on a single wavelength. Each experiment was repeated at least twice.

Laser flash photolysis studies were made with an Applied Photophysics LKS80 instrument delivering 4-ns pulses at 610 nm from a frequency-doubled Nd-YAG laser with optical parametric oscillator. Transient absorption spectra were compiled point-by-point, with five individual records being averaged at each wavelength. Kinetic measurements were made at fixed wavelength by averaging 50 individual records. Aqueous solutions of the dye were prepared in buffer and saturated with N_2 prior to recording spectra.

Acknowledgements

We thank Newcastle University for financial support of this work. SJMN thanks Umm Al-Qura University of Saudi Arabia for the award of a postgraduate scholarship.

Conflict of Interest

The authors declare no conflict of interest.

Keywords: complexation · dyes and pigments · kinetics · photostability · singlet oxygen

[1] *Industrial Dyes: Chemistry, Properties and Applications*, 1st Ed. (Ed.: K. Hunger) Wiley-VCH, Weinheim, **2003**.
[2] R. E. Blenkinsop, *Molecular Mechanisms of Photosynthesis*, 2nd Ed. John Wiley & Son, Chichester, **2014**.
[3] T. S. Mang, T. J. Dougherty, W. R. Potter, S. Somer, J. Moan, *Photochem. Photobiol.* **1987**, *45*, 501–506.
[4] a) L. Song, C. A. G. O. Varma, J. W. Verhoeven, H. J. Tanke, *Biophys. J.* **1996**, *70*, 2959–2968; b) J. Widengren, R. Rigler, *Bioimages* **1996**, *4*, 149–157; c) J. C. Finlay, S. Mitra, M. S. Patterson, T. H. Foster, *Phys. Med. Biol.* **2004**, *49*, 4837–4860; d) C. Tanielian, R. Mechin, M. Shakirullah, *J. Photochem. Photobiol. A* **1992**, *64*, 191–199; e) D. M. Beltukova, I. V. Semenova, A. G. Smolin, O. S. Vasyutinskii, *Chem. Phys. Lett.* **2016**, *662*, 127–131.
[5] a) K. Li, Y. Xiang, X. Wang, A. Tong, B. Z. Tang, *J. Am. Chem. Soc.* **2014**, *136*, 1643–1649; b) M. A. Van Dijk, L. C. Kapitein, J. Mameren, C. F. Schmidt, E. J. G. Peterman, *J. Phys. Chem. B* **2004**, *108*, 6479–6484; c) J. R. Saylor, *Exp. Fluids* **1995**, *18*, 445–447; d) N. A. George, B. Aneeshkumar, P. Radhakrishnan, C. P. G. Vallabhan, *J. Phys. D: Appl. Phys.* **1999**, *32*, 1745–1749.
[6] a) T. Bernas, M. Zarebski, R. R. Cook, J. W. Dobrucki, *J. Microsc.* **2004**, *215*, 281–296; b) S. Rajagopal, D. Joly, A. Gauthier, M. Beauregard, R. Carpentier, *FEBS J.* **2005**, *272*, 892–902.
[7] a) A. Harriman, P. Stachelek, A. Sutter, R. Ziessel, *Phys. Chem. Chem. Phys.* **2015**, *17*, 26175–26182; b) M. A. H. Alamiry, A. Harriman, A. Haefele, R. Ziessel, *ChemPhysChem* **2015**, *16*, 1867–1872.
[8] A. Harriman, P. Stachelek, A. Sutter, R. Ziessel, *Photochem. Photobiol. Sci.* **2015**, *14*, 1100–1109.
[9] a) R. B. Vegh, K. B. Bravaya, D. A. Bloch, A. I. Krylov, K. M. Solntsev, *J. Phys. Chem. B* **2014**, *118*, 4527–4534; b) C. Duan, V. Adam, M. Byrdin, I. Demachy, D. Bourgeois, *J. Am. Chem. Soc.* **2013**, *135*, 15841–15850; c) J. Li, Y. Hao, M. Zhong, J. Nie, X. Zhu, *Dyes Pigm.* **2019**, *165*, 467–473; d) L. Z. Zhang, G.-Q. Tang, *J. Photochem. Photobiol. B* **2004**, *74*, 119–125; e) Q. Lin, L. Yang, Z. Wang, X. Gong, L. Zhu, *Angew. Chem. Int. Ed.* **2018**, *57*, 3722–3726; *Angew. Chem.* **2018**, *130*, 3784–3788; f) V. Octeau, L. Cognet, L. Duchesne, D. G. Fernig, B. Lounis, *ACS Nano* **2009**, *3*, 345–350; g) K. Imura, H. Mizobata, Y. Makita, *Bull. Chem. Soc. Jpn.* **2016**, *89*, 1518–1522.
[10] a) M. P. Gordon, T. Ha, P. R. Selvin, *Proc. Natl. Acad. Sci. USA* **2004**, *101*, 6462–6465; b) C. Jung, B. K. Müller, D. C. Lamb, K. Müllen, C. Bräuchle, *J. Am. Chem. Soc.* **2006**, *128*, 5283–5291.
[11] a) C. Wang, M. Taki, Y. Sato, T. Higashiyama, S. Yamaguchi, *J. Am. Chem. Soc.* **2017**, *139*, 10374–10381; b) V. I. Sokolov, A. S. Akhmanov, I. M. Asharchuk, K. V. Khaydukov, M. M. Nazarov, *Opt. Spectrosc.* **2017**, *122*, 469–474; c) E. F. F. Da Silva, F. M. Pimenta, B. W. Pedersen, L. G. Arnaut, P. R. Ogilby, *Integr. Biol.* **2016**, *8*, 177–193; d) P. A. Dalgarno, C. A. Traina, J. C. Penedo, G. C. Barzan, I. D. W. Samuel, *J. Am. Chem. Soc.* **2013**, *135*, 7187–7193; e) D. Rhinow, M. Imhof, I. Chizhik, R.-P. Bauman, N. Hampp, *J. Phys. Chem. B* **2012**, *116*, 7455–7462.
[12] a) I. P. Kaminov, L. W. Stulz, E. A. Chandross, C. A. Pry, *Appl. Opt.* **1972**, 11, 1563–1567; b) C. M. Carbonaro, A. Anedda, S. Grandi, A. Magistris, *J. Phys. Chem. B* **2006**, *110*, 12932–12937; c) A. M. Weiss, E. Yariv, R. Reisfeld, *Opt. Mater.* **2003**, *24*, 31–34; d) C. Julien, A. Debarre, D. Nutarelli, A. Richard, P. Tchénio, *J. Phys. Chem. B* **2005**, *109*, 23145–34153.
[13] H. Nakamoto, N. Suzuki, S. K. Roy, *FEBS Lett.* **2000**, *483*, 169–174.
[14] a) T. Cordes, J. Vogelsang, P. Tinnefeld, *J. Am. Chem. Soc.* **2009**, *131*, 5018–5019; b) L. A. Campos, J. Liu, X. Wang, D. S. English, V. Muñoz, *Nat. Methods* **2011**, *8*, 143–146; c) J. Widengren, A. Chmyrov, C. Eggeling, P.-A. Löfdahl, C. A. M. Seidel, *J. Phys. Chem. A* **2007**, *111*, 429–440; d) T. J. Pintar, F. Lin, A. W. Girotti, *Free Radical Biol. Med.* **1994**, *16*, 603–612.
[15] a) G. T. Dempsey, J. C. Vaughan, K. H. Chen, M. Bates, X. Zhuang, *Nat. Methods* **2011**, *8*, 1027–1040; b) T. Ha, P. Tinnefeld, *Ann. Rev. Phys. Chem.* **2012**, *63*, 595–617.
[16] a) P. P. Lima, M. M. Nolasco, F. A. A. Paz, O. L. Malta, L. D. Carlos, *Chem. Mater.* **2013**, *25*, 586–598; b) V. Glembockyte, R. Lincoln, G. Cosa, *J. Am. Chem. Soc.* **2015**, *137*, 1116–1122; c) R. B. Altman, Q. Zheng, Z. Zhou, J. D. Watten, S. C. Blanchard, *Nat. Methods* **2012**, *9*, 428–429.
[17] a) M. Ballottari, M. J. P. Alcocer, C. D'Andrea, G. Cerullo, R. Bassi, *Proc. Natl. Acad. Sci. USA* **2014**, *111*, E2431–E2438; b) S. Takahashi, M. R. Badger, *Trends Plant Sci.* **2011**, *16*, 53–60.
[18] A. Nagarayan, R. L. Burnap, *Biochim. Biophys. Acta Bioenerg.* **2014**, *1837*, 1417–1426.
[19] M. Oz, D. E. Lorke, M. Hasan, G. A. Petroianu, *Med. Res. Rev.* **2011**, *31*, 93–117.
[20] H. Caro, *Engl. Pat.* **1877**, 3751.9/10.
[21] P. Ehrlich, *Dtsch. Med. Wochenschr.* **1886**, *12*, 49–52.
[22] a) E. M. Tuite, J. M. Kelly, *J. Photochem. Photobiol. B* **1993**, *21*, 103–124; b) R. Rohs, H. Sklenar, R. Lavery, B. Röder, *J. Am. Chem. Soc.* **2000**, *122*, 2860–2866; c) B. S. Fujimoto, J. B. Clendenning, J. J. Delrow, P. J. Heath, M. Schurr, *J. Phys. Chem.* **1994**, *98*, 6633–6643.
[23] a) M. Wainwright, K. B. Crossley, *J. Chemother.* **2002**, *14*, 431–443; b) K. Orth, G. Beck, F. Genze, A. Rück, *J. Photochem. Photobiol. B* **2000**, *57*, 186–192; c) Y. Lu, R. Jiao, X. Chen, A. Ji, P. Shen, *J. Cell. Biochem.* **2008**, *105*, 1451–1460.
[24] C. A. Parker, *J. Phys. Chem.* **1959**, *63*, 26–30.
[25] a) Z. Zhao, E. R. Malinowski, *J. Chemom.* **1999**, *13*, 83–94; b) J. B. Ghasemi, M. Miladi, *J. Chin. Chem. Soc.* **2009**, *56*, 459–468; c) J. Vara, C. S. Ortiz, *Spectrochim. Acta Part A Mol. Biomol. Spec.* **2016**, *166*, 112–120; d) A. Fernández-Pérez, T. Valdés-Solís, G. Marbán, *Dyes Pigm.* **2019**, *161*, 448–456.
[26] a) P. V. Kamat, N. N. Lichtin, *J. Phys. Chem.* **1981**, *85*, 814–818; b) R. Bonneau, R. Pottier, O. Bagno, J. Joussot-Dubien, *Photochem. Photobiol.* **1975**, *21*, 159–163.
[27] a) R. Nilsson, P. B. Merkel, D. R. Kearns, *Photochem. Photobiol.* **1972**, *16*, 109–116; b) R. H. Kayser, R. H. Young, *Photochem. Photobiol.* **1976**, *24*, 395–401; c) R. M. Danziger, *J. Phys. Chem.* **1967**, *71*, 2633–2640.
[28] a) S. Kato, M. Morita, M. Koizumi, *Bull. Chem. Soc. Jpn.* **1964**, *37*, 117–122; b) R. D. Lowe, R. D. Snook, *Analyst* **1993**, *118*, 613–616; c) C. Eggeling, J. Widengren, R. Rigler, C. A. M. Seidel, *Anal. Chem.* **1998**, *70*, 2651–2659.
[29] a) A. Mills, J. Wang, *J. Photochem. Photobiol. A* **1999**, *127*, 123–134; b) Y.-H. Xu, D.-H. Liang, M.-l. Liu, D.-Z. Liu, *Mater. Res. Bull.* **2008**, *43*, 3474–3482; c) E. L. Quitevis, J. Martorell, Y. Chang, T. W. Scott, *Chem. Phys. Lett.* **2000**, *319*, 138–144; d) J. W. Lekse, B. J. Haycock, J. P. Lewis, D. R. Kaufman, C. Matranga, *J. Mater. Chem. A* **2014**, *2*, 9331–9337; e) F. Fu, Y. Zhang, L. Yan, X. Gao, D. Wang, *J. Mater. Sci. Mater. Electronics* **2017**, *28*, 691–696.
[30] a) G. N. Lewis, O. Goldschmid, T. T. Magel, J. Bigeleisen, *J. Am. Chem. Soc.* **1943**, *65*, 1150–1154; b) G. N. Lewis, J. Bigeleisen, *J. Am. Chem. Soc.* **1943**, *65*, 2419–2423; c) G. Oster, N. Wotherspoon, *J. Am. Chem. Soc.* **1957**, *79*, 4836–4838.
[31] K. Bergmann, C. T. O'Konski, *J. Phys. Chem.* **1963**, *67*, 2169–2177.
[32] S. J. Atherton, A. Harriman, *J. Am. Chem. Soc.* **1993**, *115*, 1816–1822.
[33] S. J. Wagner, A. Skripchenko, D. Robinette, J. W. Foley, L. Cincotta, *Photochem. Photobiol.* **1998**, *67*, 343–349.
[34] A. de Juan, R. Tauler, R. Dyson, C. Marcolli, M. Rault, M. Maeder, *TrAC Trends Anal. Chem.* **2004**, *23*, 70–79.
[35] J. H. Espenson, *Chemical Kinetics and Reaction Mechanisms* 2nd Edition, Chap. 4, McGraw-Hill, New York, **2002**.
[36] a) D. Ball, *J. Chem. Educ.* **1998**, *75*, 917–919; b) T. A. Bak, P. Salaman, B. Andresen, *J. Phys. Chem. A* **2002**, *106*, 10961–10964.
[37] M. A. J. Rodgers, P. T. Snowden, *J. Am. Chem. Soc.* **1982**, *104*, 5541–5543.
[38] R. A. Floyd, M. S. West, K. L. Eneff, J. E. Schneider, *Arch. Biochem. Biophys.* **1989**, *273*, 106–111.
[39] J. K. G. Karlsson, O. J. Woodford, R. Al-Aqar, A. Harriman, *J. Phys. Chem. A* **2017**, *121*, 8569–8576.

[40] a) G. Terrones, A. J. Pearlstein, *Macromol.* **2001**, *34*, 8894–8906; b) A. Rück, C. Hildebrandt, T. Köllner, H. Schneckenburger, R. Steiner, *J. Photochem. Photobiol. B* **1990**, *5*, 311–319.
[41] a) K. Patil, R. Pawar, P. Talup, *Phys. Chem. Chem. Phys.* **2000**, *2*, 4313–4317; b) S. C. Nunez, T. M. Yoshimura, M. S. Ribeiro, H. C. Junqueira, C. Maciel, M. D. Coutinho-Neto, M. S. Baptista, *J. Photochem. Photobiol. B* **2015**, *150*, 31–37
[42] M. Levy, *Comptes Rendus des Travaux du Laboratoire Carlsberg, Ser. Chim.* **1958**, *30*, 291–300.
[43] S. Sirbu, O. J. Woodford, A. C. Benniston, A. Harriman, *Photochem. Photobiol. Sci.* **2018**, *17*, 750–762.
[44] T. L. Nemzek, W. R. Ware, *J. Chem. Phys.* **1975**, *62*, 477–489.
[45] A. Harriman, M. Hissler, A. Khatyr, R. Ziessel, *Chem. Commun.* **1999**, 735–736.
[46] G. Crank, A. Mursyidi, *J. Photochem. Photobiol. A* **1992**, *64*, 263–271.
[47] O. L. J. Gijzeman, F. Kaufman, G. Porter, *J. Chem. Soc. Faraday Trans. 2* **1973**, *69*, 727–737.
[48] A. Rosspeinter, D. R. Kattnig, G. Angulo, S. Landgruf, A. Grampp, *Chem. Eur. J.* **2008**, *14*, 6213–6221.
[49] J. Le Brumant, M. Jaffrain, G. Lacrampe, *J. Phys. Chem.* **1984**, *88*, 1548–1554.
[50] a) A. E. Tonelli, *Macromol.* **1991**, *24*, 275–278; b) A. E. Tonelli, *Macromol.* **1990**, *23*, 3134–3137.
[51] N. Wen, M. H. Brooker, *Can. J. Chem.* **1994**, *72*, 1099–1106.
[52] R. R. W. Ellerton, E. W. Mayne, *Anal. Chem.* **1980**, *52*, 773–774.

Manuscript received: May 12, 2019
Revised manuscript received: June 19, 2019
Accepted manuscript online: June 21, 2019
Version of record online: July 10, 2019